RETROFIT55

Ref. Ares(2025)1683759 - 03/03/2025

Funded by the European Union

Horizon Europe programme, grant agreement No. 101096068

RETROFIT SOLUTIONS TO ACHIEVE 55% GHG REDUCTION BY 2030

Integration of the ship model in weather routing tool

WP 3 – Operational Synthesis and Optimization
Task 3.2 – Integration of the ship model in the weather routing tool
D3.2 – Integration of the ship model in the weather routing tool
Partners involved: NTUA, CNR, SFD, AWS, FSYS, AALTO, B4B, AES
Authors: Nikos Themelis (NTUA), Aggeliki Kytariolou (NTUA), George Dafermos (NTUA)

Project details

Project Title	RETROFIT SOLUTIONS TO ACHIEVE 55% GHG REDUCTION BY 2030
Project Type	Innovation Action
Project Acronym	RETROFIT55
Grant Agreement No.	101096068
Duration	36 M
Project Start Date	01/01/2023

Deliverable information

Status (F: final; D: draft; RD: revised draft)	F
Planned delivery date	31/10/2024
Actual delivery date	03/03/2025
• **Dissemination level:** PU – Public, fully open, e.g. web (Deliverables flagged as public will be automatically published in CORDIS project's page) • SEN – Sensitive, limited under the conditions of the Grant Agreement • Classified R-UE/EU-R – EU RESTRICTED under the Commission Decision No2015/444 • Classified C-UE/EU-C – EU CONFIDENTIAL under the Commission Decision No2015/444 Classified S-UE/EU-S – EU SECRET under the Commission Decision No2015/444	
Type: Report, Website, Other, Ethics	Report

Document history

Version	Date	Created/Amended by	Changes
V1	9/12/2024	Nikos Themelis, Aggeliki Kytariolou (NTUA)	1st draft
V2	15/01/2025	Nikos Themelis, Aggeliki Kytariolou, George Dafermos (NTUA)	2nd draft, revision after comments received by the review process
Final	27/02/2025	Nikos Themelis, Aggeliki Kytariolou, George Dafermos (NTUA)	Final version

Quality check review

Reviewer (s)	Main changes / Actions
Emanuele Spinosa (CNR)	Technical review
Cecilia Leotardi (CNR)	Editorial revision
Cecilia Leotardi and Alessandro Iafrati (CNR)	Final review of contents and submission to EC.

Table of Contents

List of figures 6
List of tables 8
List of acronyms 9
Nomenclature 10
Executive Summary 15
1 Introduction 16
1.1 Aim of the work 16
1.2 Literature review 17
2 The weather routing optimization tool and the current ship model 19
2.1 Calm water resistance 21
2.2 Added wave resistance 21
2.3 Wind resistance 22
2.4 Propeller and main engine modelling 23
3 Modification of the ship model to account for retrofit options 24
3.1 Definitions of parameters introduced in the ship model 24
3.2 Ship model including transverse forces and yaw moments (3-d.o.f.) 25
3.3 WASP forces 28
4 Safety criteria 30
4.1 Seakeeping based criteria 30
4.1.1 Propeller emergence 30
4.1.2 Slamming occurrence 31
4.1.3 Deck wetness – Deck submergence 31
4.1.4 Bridge accelerations 32
4.1.5 Motion Sickness Incidence 32
4.1.6 Critical values of seakeeping-based criteria 32
4.2 Criteria for avoiding dangerous phenomena in adverse weather conditions 33
4.2.1 Surf-riding and Broaching-to 33
4.2.2 Successive high wave attack 33
4.2.3 Synchronous and parametric rolling 33
4.3 Course-keeping 34
5 Case study: modelling the existing ship 35

5.1 Calm water resistance 35
5.2 Propeller characteristics 36
5.3 Wind resistance 36
5.4 Added wave resistance 37
5.5 Power predictions for several drafts 39
5.6 Integration of retrofit options 40
5.6.1 WASP forces and configuration 42
5.6.2 WASP case study 45
6 Case study in specific route (1-d.o.f. ship model) 50
6.1 Examined route 50
6.2 Weather data comparison 50
6.3 Real voyage simulation and comparison with noon reports data 52
6.4 Examination of safety criteria 55
6.5 Route optimization of the initial design 57
6.6 Examined route with hydrodynamic related retrofit options 60
6.7 Examined route with WASP as retrofit option 61
6.7.1 Voyage simulation with WASP and optimization 61
7 Case study using the 3-d.o.f. ship model 65
7.1 Comparison of the results with the optimal route of 1-d.o.f. ship model 65
7.2 Comparison of previous results with the optimal route derived from the 3-d.o.f. ship model 67
8 Conclusions 74
References 76
Appendix A – Seakeeping 78
Appendix B – Regression analysis for safety criteria 85
Appendix C – Regression analysis for added wave resistance 88
Appendix D – Hydrodynamic transverse force and yaw moment 90

List of figures

Figure 1: Framework of the weather routing tool. 19
Figure 2: Random route generation 20
Figure 3: Ship model. 20
Figure 4: Calculation of apparent wind speed and direction. 22
Figure 5: Forces in the 3.d.o.f. ship model including WASP. 25
Figure 6: Dimensions of spade rudder [16]. 27
Figure 7: Effective draft and freeboard [12]. 30
Figure 8: Calm water resistance curves for different drafts. 35
Figure 9: Open water characteristics for the re-constructed propeller 36
Figure 10: Longitudinal and lateral wind resistance coefficients, and yaw moment coefficient. 37
Figure 11: Non-dimensional added wave resistance in regular waves for different heading angles. 38
Figure 12: Effect of vessel's speed on added wave resistance (scantling draft considered). 38
Figure 13: Effect of vessel's loading condition on added wave resistance for a ship's speed of 10 [kn]. 39
Figure 14: ME power for different drafts and speeds, using sea trials data and the respective calculations from the ship model. 39
Figure 15: SFOC map. 40
Figure 16: FOC vs. ship speed for different drafts, considering calm water resistance only. 40
Figure 17: Calm water resistance for the scantling draft for the initial design and for a fictitious one using ALS. 41
Figure 18: Open water characteristic curves for the real propeller and a fictitious one with improved efficiency. 41
Figure 19: Arrangement of the 4 eSAILs. 42
Figure 20: Regression model for the driving force. 43
Figure 21: Regression model for the heeling force. 44
Figure 22: Regression model for eSAIL required power. 44
Figure 23: Apparent wind speed for different apparent wind angles. 45
Figure 24: Drift and rudder angles vs. apparent wind and wave direction. 46
Figure 25: Transverse forces vs. relative wind direction. 46
Figure 26: Longitudinal forces vs. relative wind direction. 47
Figure 27: ME power for scenarios with/without WASP system and considering the 1-d.o.f. and 3-d.o.f. ship models. 47
Figure 28: ME FOC for scenarios with/without WASP system and considering the 1-d.o.f. and 3-d.o.f. ship models. 48
Figure 29: FOC savings when using WASP system for the 3-d.o.f. and the 1-d.o.f. ship models 48
Figure 30: Power savings for 1-d.o.f. model vs true wind speed direction (left) and apparent wind direction (right). 49
Figure 31: ME power savings for the 3-d.o.f. ship model vs the true wind speed direction (left) and apparent wind direction (right). 49
Figure 32: Trajectory from Port Louis to Singapore. 50
Figure 33: Significant Wave Height (SWH) values comparison between DTN and Copernicus data. 51
Figure 34: Wave peak period values comparison between DTN and Copernicus data. 51
Figure 35: Wave direction values comparison between DTN and Copernicus data. 52

Figure 36: Shaft horse power and speed through water along the route. 53
Figure 37: Added wave resistance and significant wave height along the route. 53
Figure 38: Resistance components along the route. 54
Figure 39: FOC for the real voyage using noon reports data and simulation results derived per day. 54
Figure 40: Different frameworks for SHP vs. RPM. 55
Figure 41: Vertical acceleration on bridge (rms) along the route. 56
Figure 42: Pitch rms along the route. 56
Figure 43: Deck wetness probability along the route. 57
Figure 44: Synchronous and parametric rolling along the route. 57
Figure 45: The main segment of the real voyage which has to be optimized. 58
Figure 46: Algorithm's evolution regarding the time travel focused on 10 to 13 days. 58
Figure 47: FOC for the optimal route vs. the original (real) one. 59
Figure 48: Real trajectory (red) along with potential optimal routes found by the genetic algorithm. 59
Figure 49: Added wave resistance along the real voyage and the optimal path. 60
Figure 50: Comparison of demanded power along the real voyage between the original and the improved hydrodynamic case. 61
Figure 51: Optimal route with WASP (black) and the real (red) route. 62
Figure 52: ME Power and RPM for the real voyage with and without (w/o) WASP system. 63
Figure 53: WASP longitudinal force, relative wind speed and direction for the real voyage. 63
Figure 54: DGs' demanded power for the real voyage with and without (w/o) WASP system. 64
Figure 55: DGs' demanded total power for the real voyage with and without (w/o) WASP system and for the optimal path. 64
Figure 56: ME power with and w/o WASP for 1-d.o.f. and 3-d.o.f. for the optimal path. 65
Figure 57: Prevailing wind conditions for the optimal path corresponding to 1-d.o.f. ship model. 66
Figure 58: Transverse forces along the optimal path. 66
Figure 59: Longitudinal forces along the optimal path. 67
Figure 60: Drift and rudder angles along the optimal route considering different scenarios. 67
Figure 61: Real voyage (red) and the optimal routes found with 3-d.o.f. and 1-d.o.f. Ship Models when WASP is considered. 68
Figure 62: Apparent wind speed and direction along the 3-d.o.f. optimal route. 69
Figure 63: Drift and rudder angles along the 3-d.o.f. and the1-d.o.f. optimal paths. 70
Figure 64: Longitudinal rudder forces along the 3-d.o.f. and 1-d.o.f. optimal paths. 70
Figure 65: Transverse WASP forces for the 3-d.o.f. and 1-d.o.f. optimal paths. 71
Figure 66: Longitudinal WASP forces for the 3-d.o.f. and 1-d.o.f. optimal paths. 71
Figure 67: ME power along the 3-d.o.f. and 1-d.o.f. optimal paths. 72
Figure 68: Typical RAO graphs with respect to centre of gravity and bridge. 79
Figure 69: Regression model for Heave (a) and Pitch (b) RMS. 86
Figure 70: Regression model for Bridge lateral (a) and vertical acceleration (b). 86
Figure 71: Regression model for added wave resistance at mean draft=13.1m. 88
Figure 72: Comparison between regression and direct from spectrum data. 89
Figure 73: Transverse force and yaw moment based on CFD results carried out in D2.2. 90

List of tables

Table 1: Ship models (1-d.o.f. and 3-d.o.f.) and the impact of retrofit measures. 24
Table 2: Limiting values of the seakeeping criteria [19]. 32
Table 3: MV Kastor main characteristics. 35
Table 4: Frontal and lateral areas of the vessel. 36
Table 5: Waterline entrance length and radius of gyration for different loading conditions. 37
Table 6: ME FOC for the as-built ship and the scenarios considered for hydrodynamic improvements. 42
Table 7: Validation metrics for regression models regarding the WASP. 43
Table 8: Weather and loading conditions for the case study. 45
Table 9: KASTOR Voyage on 22.05.2022. 50
Table 10: Statistical comparison of DTN's with Copernicus' Weather predictions (reference source: Copernicus). 52
Table 11: Total main engine fuel oil consumption. 54
Table 12: Details about the real trajectory and results from the optimization. 60
Table 13: Results for real voyage and optimal path considering retrofit options. 61
Table 14: Detailed information for the real and the optimal route (1-d.o.f. ship model). 62
Table 15: Mean values for resistance components and WASP force for the real voyage and the optimal route. 63
Table 16: Summary results for the examined routes using the 1d.o.f. and 3-d.o.f. models. 72
Table 17: Loading conditions considered for the safety criteria. 79
Table 18: Heave and Pitch RMS (Heading 180 [deg], V=11[kn]). 79
Table 19: Heave and Pitch RMS (Heading 180 [deg], V=14[kn]). 79
Table 20: Heave, Pitch, and Roll RMS (Heading 150 [deg], V=11[kn]). 79
Table 21: Propeller emergence (Heading 180 [deg], V=11[kn]). 80
Table 22: Propeller emergence (Heading 180 [deg], V=14[kn]). 80
Table 23: Propeller emergence (Heading 150 [deg], V=11[kn]). 81
Table 24: Slamming occurrence (Heading 180 [deg], V=11[kn]). 81
Table 25: Slamming occurrence (Heading 180 [deg], V=14[kn]). 81
Table 26: Slamming occurrence (Heading 150 [deg], V=11[kn]). 81
Table 27: Deck submergence (Heading 180 [deg], V=11[kn]). 82
Table 28: Deck submergence (Heading 180 [deg], V=14[kn]). 82
Table 29: Deck submergence (Heading 150 [deg], V=11[kn]). 82
Table 30: RMS values of bridge accelerations (Heading 180 [deg], V=11[kn]). 83
Table 31: RMS values of bridge accelerations (Heading 150 [deg], V=11[kn]). 83
Table 32: MSI (Heading 180 [deg], V=11[kn]). 84
Table 33: MSI (Heading 150 [deg], V=11[kn]). 84
Table 34: Data used for safety regression analysis. 85
Table 35: Neural network validation for all regression models used for safety calculations. 86
Table 36: Data for added resistance regression analysis. 88

List of acronyms

ALS	Air Lubrication System
AWD	Apparent Wind Direction
AWS	Apparent Wind Speed
B4B	Bound 4 Blue
CFD	Computational Fluid Dynamics
CMEMS	Copernicus Marine Environment Monitoring Service
DG	Diesel Generator
DG1	Diesel Generator 1
DG2	Diesel Generator 2
DTN	Data Transmission Network
DWL	Draught Water Line
DWT	DeadWeight Tonnage
FOC	Fuel Oil Consumption
KG	Vertical center of gravity
LCG	Longitudinal Centre of Gravity
MAE	Mean Absolute Error
MCR	Maximum Continuous Rating
ME	Main Engine
MII	Motion Induced Interruption
MSE	Mean Squared Error
MSI	Motion Sickness Incidence
NTUA	National Technical University of Athens
RAO	Response Amplitude Operator
RMS	Root Mean Square
RMSE	Root Mean Square Error
RPM	Revolutions Per Minute
SFOC	Specific Fuel Oil Consumption
SHP	Shaft Horse Power
SOG	Speed Over Ground
STW	Speed Through Water
SWH	Significant Wave Height
UW	Under Water
VCG	Vertical Centre of Gravity
WASP	Wind Assisted Ship Propulsion
VLCC	Very Large Crude Carrier

Nomenclature

Symbol [Unit]	Explanation
A [m²]	Wing sail projected area
A_F [m²]	Frontal projected area of the ship
A_L [m²]	Lateral projected area of the ship
AR_h [–]	Effective aspect ratio of the underwater part of the hull
AR_r [–]	Effective aspect ratio of the rudder
A_r [m²]	Rudder area
B [m]	Breadth of the ship
C_D [–]	Drag coefficient of the wing sail
C_L [–]	Lift coefficient of the wing sail
C_X [–]	Longitudinal thrust coefficient
C_Y [–]	Lateral thrust coefficient
C_s [–]	Swell-up coefficient
c [–]	Constant to determine T_R
c_B [–]	Block coefficient
c_L [–]	Specific geometry factor for certain wind propulsion systems
c_N [–]	Yawing-moment coefficient
c_R [–]	Specific geometry factor for certain wind propulsion systems
c_X [–]	Longitudinal wind force coefficient
c_{XD} [–]	Non-dimensional added resistance factor due to drift
c_Y [–]	Lateral wind force coefficient
D [N]	Wing sail model drag
D_p [m]	Distance between waterline and the tips of the propeller's upper blade.
D_{pe} [m]	Effective depth of the tips of the upper propeller blades
D_{pr} [m]	Propeller's diameter
d [m]	Draught at the forward perpendicular
F [m]	Freeboard

F_e [m]	Effective freeboard
F_N [kN]	Normal rudder force
GM [m]	Metacentric height
g [m/s^2]	Acceleration due to gravity
H_s [m]	Significant wave height
J [–]	Advance coefficient
K_{yy} [–]	Yaw radius of gyration
k [–]	Number of propellers
k_Q [–]	Torque coefficient
k_T [–]	Thrust coefficient
L_l [N]	Wing sail model lift
L_{OA} [m]	Overall length of the ship
L_{WL} [m]	Waterline length
L_{bp} , L [m]	Length between the perpendiculars
Le_{aft} [m]	Entrance length afterwards
Le_{fore} [m]	Entrance length forward
m_0 [m^2]	Variance of the relative motion
m_2 [m^2/s^2]	Variance of the relative motion velocity
m_4 [m^2/s^4]	Variance of the relative motion acceleration
N_h [kN·m]	Moment generated by hydrodynamic forces
N_H [kN·m]	Yaw moment
N_R [kN·m]	Rudder-induced moment
N_{ds} [–]	Average number of deck submergences per hour
N_{pe} [–]	Average number of propeller emergencies per hour
N_{sl} [–]	Average number of slamming occurrences per hour
N_{wasp} [kN·m]	Moment generated by the WASP system
N_{wind} [kN·m]	Moment generated by wind
n [rpm]	Propeller's revolutions
P_B [kW]	Brake power
P_{ds} [–]	Probability of deck submergence
P_{pe} [–]	Probability of propeller emergence

P_{sl} [–]	Probability of slamming occurrence
q [Pa]	Dynamic pressure of the apparent wind
R_{AWM} [kN]	Added resistance due to ship motions
R_{AWR} [kN]	Added resistance due to wave reflection
R_{WAVE} [kN]	Wave added resistance in regular waves
R_{tot} [kN]	Total resistance
r_3 [m]	Vertical relative motion
$\ddot{r}_3$ [m/s^2]	Vertical relative acceleration
S_z [m^2/(rad/s)]	Motion energy spectrum
S_ζ [m^2/(rad/s)]	Sea wave spectrum
s_3 [m]	Absolute vertical motion
$\ddot{s}_3$ [m/s^2]	Absolute vertical acceleration
T [m]	Draft of the ship
T_A [m]	Draught at aft end
T_E [s]	Encounter period
T_F [m]	Draught at fore end
Th [kN]	Thrust
T_R [s]	Natural rolling period of the ship
T_W [s]	Wave period
T_p [s]	Wave peak period
T_{p_av} [s]	Average peak period of the motion energy spectrum
t [–]	Thrust deduction coefficient
u [m/s]	Ship speed in x-direction
V' [–]	Dimensionless drift speed
V_{AW} [m/s]	Apparent wind speed
V_S [m/s]	Ship's speed
V_{ad} [m/s]	Advance speed of the propeller
V_r [m/s]	Inflow speed to the rudder
V_{tw} [m/s]	True wind speed
v [m/s]	Ship speed in y-direction
v_{cr} [m/s]	Critical velocity
w [–]	Wake coefficient

X_D [kN]	Added resistance due to drift
X_R [kN]	Added resistance due to rudder
X_c [kN]	Calm water resistance component
X_{wasp} [kN]	Longitudinal force generated by the WASP system
X_{wind} [kN]	Wind resistance component / longitudinal wind force
X_{wv} [kN]	Mean added wave resistance component in irregular waves
x_3 [m]	Rudder span
x_R [m]	Lever arm distance from the rudder's pressure point to the midship
x_s [m]	Longitudinal distance from the point where Y_{wasp} acts to the center of gravity of the ship
Y_H [kN]	Hydrodynamic side force
Y_R [kN]	Lateral rudder force
Y'_V , Y'_{VV} [–]	Hydrodynamic derivatives of the lateral force
Y_{m0} [–]	Additional factor
Y_{wasp} [kN]	Lateral (heeling) force generated by the WASP system
Y_{wind} [kN]	Lateral wind force
z_0 [m]	Heave motion amplitude
a [deg]	Relative wave heading
a_H [–]	Hydrodynamic force factor
a_r [deg]	Arbitrary angle inflow angle
β [deg]	Drift angle
δ [deg]	Rudder angle
ε [–]	Small constant
ζ_α [–]	Wave amplitude
η_0 [–]	Propeller's open water efficiency
η_{Did} [–]	Propulsive efficiency
η_R [–]	Propeller's total rotational coefficient
η_s [–]	Shaft efficiency

η_H [–]	Hull efficiency
Θ [deg]	Angle between V_S and V_t
λ [m]	Wavelength
μ_{MSI} [%]	Mean Motion Sickness Incidence
ρ [kg/m³]	Air density
ρ_w [kg/m³]	Water density
Φ [–]	Cumulative normal distribution function
φ [deg]	Angle between the apparent wind and the ship course
ω [rad/s]	Wave frequency
ω_e [rad/s]	Encounter frequency

Executive Summary

The enhancement of the ship model of NTUA's weather routing tool to account for RETROFIT55's measures is presented. The developed tool can be used for the assessment of retrofit measures along specific routes with and without enabling route optimization. Firstly, the current tool is presented with emphasis on the underlying physics-based ship model used for the calculation of the Main Engine's Fuel Oil Consumption corresponding to a set of navigation and weather parameters. Based on the retrofit measure(s) to be considered, the necessary modifications and additions needed to the ship model to appropriately account for the impact of the measures are analyzed. Especially for the case of Wind Assisted Ship Propulsion (WASP), two versions of the ship model were developed: a 1-d.o.f. model considering only the longitudinal forces, and a 3-d.o.f. model that further accounts for the wind and sail transverse (sway) forces and yaw, which result in drifting forces as well as the necessary rudder forces to counterbalance these effects.

The bulk-carrier MV Kastor was used as a case study for the application, and the initial design was set up in the ship model. The suitability of the setting was tested using sea trials results and operational data of a real route. Then, the calculation of the fuel savings achieved by fictitious hydrodynamic improvements related to propeller improvements and calm water resistance reduction is presented. A more detailed analysis of the case of the eSAILs of B4B was carried out. Specifically, the specific Wind Assisted Ship Propulsion (WASP) configuration for MV Kastor was examined for several operational and weather scenarios using both versions of ship model. When the 1-d.o.f. ship model is considered, fuel reductions up to 28% were derived for the examined range of apparent wind headings. The 3-d.o.f. ship model considers the side effects that reduce the potential benefits of the Wind Assisted Ship Propulsion (WASP) system by approximately 7.5%..

Furthermore, the developed tool was benchmarked against real data available for a past voyage of MV Kastor. In that case the comparison with the initial design was performed both when retrofit measures are considered introduced and when route optimization is enabled. The Wind Assisted Ship Propulsion (WASP) case was extensively studied, taking into consideration the auxiliary power needs of the system for the analysis. The results of the 1-d.o.f. ship model favor the utilization of the system, as total fuel savings of 10 % compared to the initial design were calculated corresponding to the examined past voyage. In addition, the optimal route derived enhances the potential fuel savings by an additional 3%. Similarly, when the 3-d.o.f. model is considered, the WASP resulted in 3.65% less fuel oil consumption for the examined past voyage, while when also route optimization is performed, improvements up to 8.32% have been achieved.

The weather routing system entails also safety criteria related to unacceptable ship responses, which are monitored along the route. Specifically, the criteria are based on the seakeeping analysis as well as on identifying critical combinations of navigational and weather parameters that could lead to dangerous instabilities. In Appendix A, B, and C, a detailed analysis of the safety criteria incorporation is provided, and the application of safety criteria has been demonstrated in the examination of the initial ship design and the existing route.

1 Introduction

1.1 Aim of the work

The aim of Task 3.2 is to develop a framework for the incorporation of retrofit measures in the ship model and its integration into the current NTUA's weather routing tool. More specifically, the retrofit options that shall be considered are the hydrodynamic optimization of the ship (e.g. bulbous bow installation, propeller improvement), the utilization of Wind-Assisted Ship Propulsion (WASP) and the usage of Air Lubrication System (ALS). The exact performance of each retrofit measure will be examined in the respective WPs. The main purpose of the current task is the development of a suitable framework that will receive the appropriate input concerning each retrofit measure and will quantify its impact. Therefore, this task will examine the effect of a (combination of) retrofit option(s)by assessing the fuel reduction achieved compared to the initial design, under a specific scenario defined by a set of navigational and weather parameters. The development will be carried out using the NTUA's weather routing tool. For demonstration, a specific route, considering the navigational parameters characterising the specific voyage and the weather conditions encountered will be examined, while the assessment can be performed with and without the selection of the route optimization.

The weather routing tool which has been developed by NTUA, is based on a physics-based model, referred to as the ship model, for the prediction of the required main engine's power and fuel oil consumption (FOC) under the examination of a specific scenario defined by a set of navigational and weather parameters. The current ship model entails the calculation of each component of the total ship resistance, assuming a constant, specific speed, while considering the characteristics of the propeller and the main engine. Moreover, safety criteria are applied to ensure safe passage. This concept allows the incorporation of the impact of retrofit options examined in the project, as it will be carried out by modifying the appropriate modules of the ship model that are affected by the introduction of a retrofit measure. Furthermore, the current (initial) ship model considers only the longitudinal components of the forces and thus is characterized as a 1 degree of freedom ship model (1-d.o.f.). However, at least for the examination of the WASP system it is necessary to expand it to consider also the transverse forces and yaw moments, as they are anticipated to have a significant role in the calculation procedure. Therefore, during this task, the enhancement of the initial ship model is carried out by introducing the sway (transverse) motion and yaw moment to derive a 3-d.o.f. ship model. This enhancement entails also the inclusion of rudder and drift forces in the ship model and thus the differences derived by the application of the two versions of the ship model (1-d.o.f. and 3-d.o.f.) are considered one of the key targets of this task.

As the issue is significant, the next sub-section is devoted to the review of studies related to the examination of weather routing when a WASP is installed in the examined ship, whereas focus is given on the type of mathematical model used. Section 2 provides a comprehensive description of the weather routing tool emphasizing the role of its initial ship model version. Section 3 analyses the modifications needed to be implemented in the ship model to account for the effect of the retrofit measures and thus defining the data needed from the retrofit developers. Moreover the 3-d.o.f ship model is presented. Section 4 presents the definition of the safety criteria to be considered along the examined route, which are based on seakeeping performance, the avoidance of ship instabilities and adequacy of course-keeping. Section 5 refers to the case study of the initial design of the examined ship in the ship model in order to validate its suitability by comparing the main calculated outcome (shaft power and FOC) against available sea trials data. In the same section the results

obtained by the developed ship model regarding fuel savings achieved by different retrofit options, are also presented. Section 6 corresponds to the examination of a real voyage by comparing the initial design ship model's predictions with operational data and examining the safety performance along the route. Then, route optimization is enabled to derive potential savings for the initial design, while assessments of several retrofit options are calculated. Emphasis is given to the case of WASP, where optimization resulted in a different optimal route to maximize both measures (WASP and routing). The WASP examined is eSAILs of B4B. In Section 7 the results of assessment of the same voyage, using the 3-d.o.f. ship model either considering or not the route optimization procedure is presented, revealing significant differences from the previous 1-d.o.f. ship model predictions. Finally, key conclusions are summarized in Section 8. In the Appendixes several sub-models of the ship model and details of the safety calculation procedure are presented.

1.2 Literature review

WASP technologies have been in the spotlight since the last decade and several works have been published examining their significance and impact on ships' operation. In [1] the evaluation of the WASP systems was conducted through a comprehensive approach, integrating theoretical modelling and on-board measurements. In this work, a routing optimization tool is developed, utilizing data collected from specific ships equipped with various measuring instruments. By simulating different WASP technologies, the potential contributions to energy savings are estimated, and the WASP can be integrated into the optimal route selection process. The significance of energy savings by taking advantage of wind forces is also presented in [2]. That study analyses the power generation of a cylindrical Flettner rotor without endplates, focusing on ship speeds of 15 and 20 knots and wind speeds of 5 - 20 [m/s], across various wind angles. Results show maximum net power outputs of 386.7 [kW] and 575.2 [kW] at 15 and 20 knots, respectively, under 20 m/s wind. Higher coefficients of rotation reduce net power due to increased rotor energy consumption. The study highlights the Flettner rotors' potential for sustainable maritime propulsion, with a performance increase under stronger wind and higher ship speeds. A novel energy-saving evaluation approach based on wind resource analysis along typical shipping routes is proposed by [3]. The method incorporates a 3-d.o.f. model for sail-assisted ships, considering balancing between wing sail forces and rudder forces. Wind field characteristics are analysed to calculate wind energy availability. By combining wind data with ship sailing conditions, a thrust matrix is developed, to estimate energy savings. A case study is also demonstrated for a VLCC achieving annual energy savings about 5.5%. Moreover, the work presented in [4] introduces a comprehensive numerical simulation tool for evaluating the performance of wind-assisted container ships in actual shipping routes. The model incorporates the dynamics of the ship hull, rudder, controllable pitch propeller (CPP), main propulsion diesel engine fuel consumption, and the force profile generated by suction sails. High fidelity to real-world operations is achieved by using data from short sea trials and long-distance voyages. The results highlight that maintaining a constant ship's speed, while wind-generated assisting power is varying, significantly enhances energy savings compared to simply increasing ship's speed by using this assisting power.

In [5] a simulation model for predicting ship FOC under real sea conditions while accounting for surge, sway, yaw and roll is presented. The model considers also engine limitations except from environmental sea and weather conditions, in order to capture involuntary speed losses. The simulations performed using 1-d.o.f. and 4-d.o.f. modelling demonstrate significant differences, especially when WASP system is in use. The results highlight the importance of considering the yaw moments and rudder angle, particularly for wind assisted propulsion. In addition, [6] evaluates

various methods for calculating drift angles, rudder angles and added resistance by comparing Skogman's, Wagner's, and the DST formulas against model tests. In this work it is highlighted how these different methods perform for different ship designs and speeds. It is also emphasized that even though rudder angle and the associated resistance increase are key contributors to overall ship performance, most methods underestimate them, and it is necessary to select a method that aligns with ship design specifics, as no single method is universally accurate for all ship types.

2 The weather routing optimization tool and the current ship model

A weather routing tool that has been developed by NTUA is utilized in the current Work-Package of RETROFIT55. The tool is developed in the MATLAB environment, making use of numerous available functions and toolboxes (e.g. mapping toolbox, regression toolbox, etc.). The tool can be considered as a decision support tool for the Master, aiming to reduce FOC and improve safety and efficiency. Figure 1 presents the respective calculation framework, denoting the modularity of the whole application. The tool can generate random routes (Figure 2) from a port of departure to a given port of arrival. For each one of these routes, the FOC can be calculated considering the ship's characteristics and the prevailing weather conditions. In addition, constraints concerning the minimum depth, the entrance in forbidden areas or ECA zones, etc. can be integrated in the process and therefore a suitable algorithm differentiates the feasibility of the generated routes.

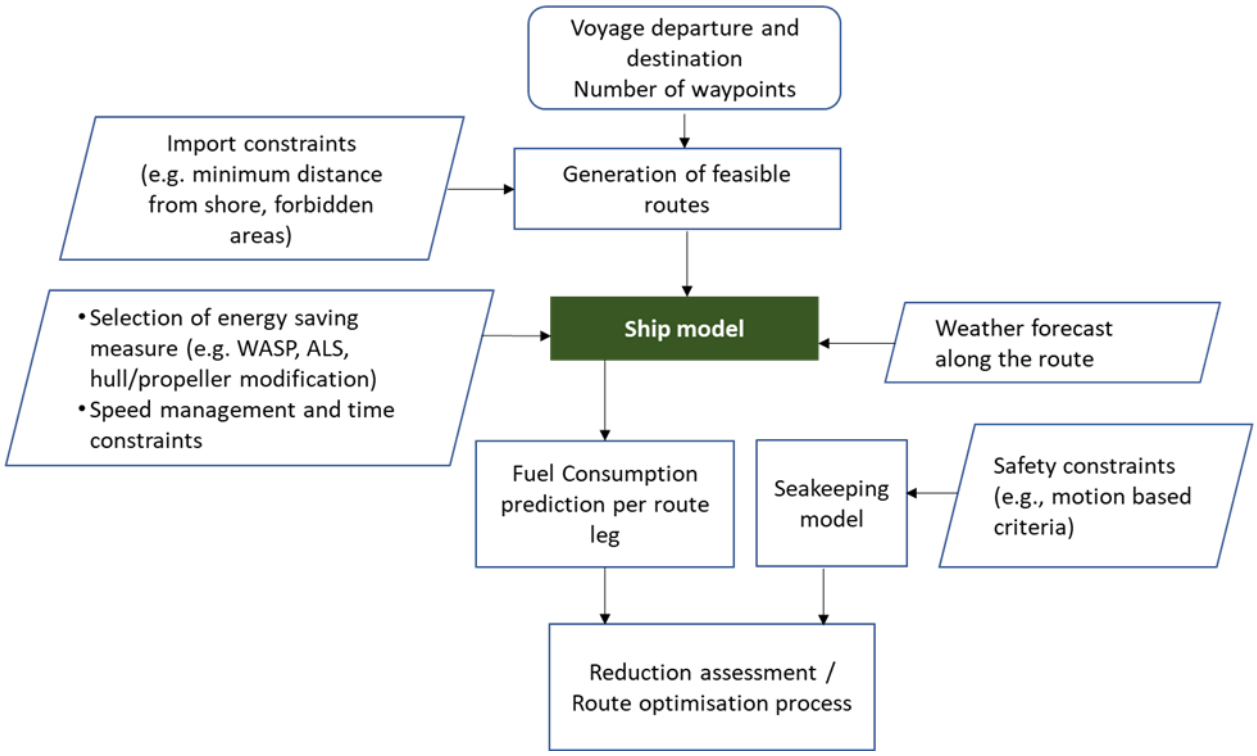

Figure 1: Framework of the weather routing tool.

Except from the two main points indicating the port of departure and the port of arrival, n-waypoints are selected each time either randomly or by preference forming n+1 legs. Between every two of these points the vessel is following a thumb line (a loxodromic path), meaning that its course is constant. Moreover, each one of these sub-segment routes is divided into equidistance points with respective coordinates. For any of these points a series of calculations using the ship model is performed, while between every two of them weather conditions and ship speed are assumed constant.

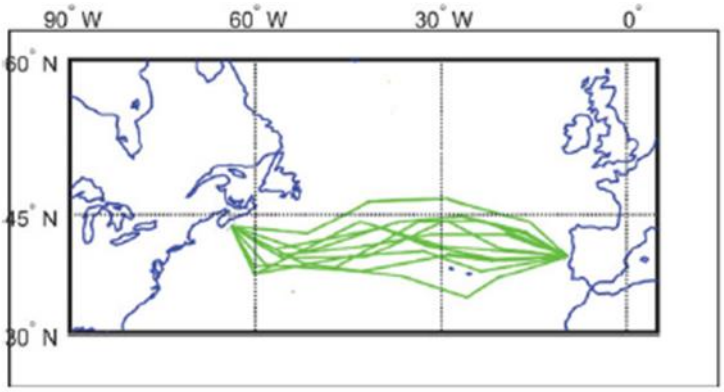

Figure 2: Random route generation.

As shown in Figure 1, the ship model is the key element in the calculation procedure. The ship model utilizes data concerning total resistance, the main engine and the propeller of a specific vessel. As shown in Figure 3, the different components of resistance are calculated in this section by providing specific data such as the vessel's speed, the prevailing weather conditions, etc. Instructions and data provided by the engine's manufacturer, are processed properly to determine the specific fuel oil consumption (SFOC) of the engine under varying load. Moreover, the open water characteristics of the propeller under examination are also incorporated in the ship model, in order to calculate the required propeller revolutions. Finally, FOC is estimated for any requested operating time interval.

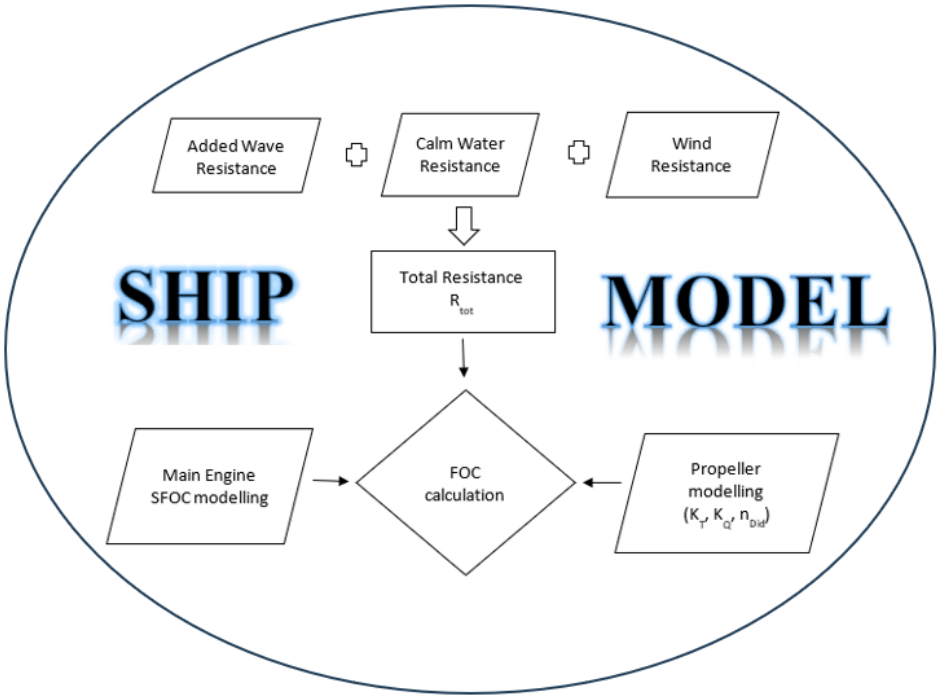

Figure 3: Ship model.

As already mentioned, weather data are provided to the ship model for essential calculations to be performed.

Weather data concerning waves, wind and currents can be obtained from any available weather provider (e.g. Copernicus). The spatial resolution of these data may not coincide with the points of interest (xi) mentioned in [7], so it is necessary to get the information by assuming that the desired value coincides with the nearest respective value. At each one of these points (xi) the total resistance is calculated, and the required ME power and propeller's revolutions are estimated using the propeller's open water characteristics. Then the SFOC (at each operating point at the Main Engine loading diagram is calculated. Based on the SFOC and the ME power, the FOC of the main engine over the voyage can therefore be derived as the summation of the FOC between every two of the points mentioned above (FOC_i).

Using the total FOC of any route as the objective function, optimization can be performed for several random generated routes. In addition, optimisation can be performed through the optimisation toolbox available in MATLAB [8]. A genetic algorithm is employed for solving this optimization problem by evolving the population towards the optimal solution over successive generations. The minimization of the FOC is the objective function of the optimisation as shown in the following equation:

$$FOC = min \sum FOC_i \quad \text{Eq. 1}$$

All necessary calculations are presented below.

2.1 Calm water resistance

Calm water resistance refers to the resistance a vessel encounters while travelling through the water with a constant forward speed, assuming that wind and waves do not influence its motion. This type of resistance is determined by the vessel's submerged volume, shape and speed. The hull's cleanliness significantly impacts calm water resistance, as the frictional resistance increases due to the accumulation of biofouling on the hull's surface. Calm water resistance is one of the major components of the total resistance that a vessel will experience in real sea conditions. It can be calculated using resistance curves obtained from towing-tank experiments, semi-empirical formulas (such as [1]), or computational fluid dynamics (CFD) simulations.

2.2 Added wave resistance

When operating in real sea environment, the attainable speed for the same engine power will be decreased due to added wave resistance. Especially in severe weather conditions, this resistance component can be significantly increased, and safety issues might rise. In these cases, speed reduction is required, or route change can also be a choice. To estimate the impact of waves, many studies are available proposing empirical or semi-empirical methods (such as [10], STAWAVE, etc).

The analysis presented in the following are based on the empirical formula from [11] and [10], where wave added resistance (R_{WAVE}) in regular waves is defined as:

$$R_{WAVE}(\omega; V_S) = R_{AWM} + R_{AWR} \quad \text{Eq. 2}$$

Where R_{AWM} is the added resistance due to ship motions and R_{AWR} is due to wave reflection in regular waves of frequency ω, under the assumption of a constant ship forward speed *Vs*. The mean added wave resistance (X_{wv}) in random seas for a given wave direction, is calculated by linear superposition of the wave spectral components (S_ζ) and the added resistance in regular waves (R_{WAVE}) [12]:

$$X_{wv} = 2\int_0^{\infty} \frac{R_{WAVE}(\omega;V_S)}{\zeta_a^2} S_\zeta(\omega)d\omega \quad \text{Eq. 3}$$

2.3 Wind resistance

The wind exerts an external force on the vessel, generating wind resistance. The following equations (Eq. 4, Eq. 5, and Eq. 6) represent the longitudinal (X_{wind}) and lateral (Y_{wind}) forces generated by wind and the respective yaw moment (N_{wind}):

$$X_{wind} = c_X q A_F \quad \text{Eq. 4}$$

$$Y_{wind} = c_Y q A_L \quad \text{Eq. 5}$$

$$N_{wind} = c_N q A_L L_{OA} \quad \text{Eq. 6}$$

where:

- c_X is the longitudinal wind force coefficient,
- c_Y is the lateral wind force coefficient,
- c_N is the yawing-moment coefficient,
- $q = \rho/2{V_{AW}}^2$ is the dynamic pressure of the apparent wind (apparent wind speed V_{AW}, air density $\rho \approx 1.23$ kg/m^3),
- A_F is the frontal projected area of the ship,
- A_L is the lateral projected area of the ship,
- L_{OA} is the overall length of the ship.

The wind force and moment coefficients can be calculated using various methods, including semi-empirical formulas, experimental results from wind tunnel tests, and computational fluid dynamics (CFD) simulations. It is important to note that the transverse component can cause drift, potentially increasing the resistance and/or affecting the vessel's manoeuvrability, which is examined in the next sections. The wind speed experienced by a moving vessel at sea is called apparent wind speed and differs from the true wind speed that the weather forecasts provide. So, it is necessary to calculate the apparent wind speed V_{AW} and direction φ, where according to Figure 4, V_S is the ship's speed, V_t is the true wind speed, and Θ is the angle formed between the two vectors, $Y = 90 - \Theta$.

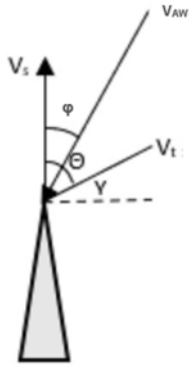

Figure 4: Calculation of apparent wind speed and direction.

Apparent wind speed and its direction are two major parameters to estimate wind resistance. In the presented cases, the wind resistance was determined by using the Blendermann's method [13], which uses a semi-empirical loading function based on wind tunnel tests.

2.4 Propeller and main engine modelling

With all the above calculations, the total resistance R_{tot} can be determined and summed up as follows:

$$R_{tot} = X_c + X_{wv} + X_{wind} \quad \text{Eq. 7}$$

where X_c, X_{wv} and X_{wind} refer to calm water, added wave and wind components of the resistance, respectively. Having determined the ship's total resistance, the brake power can be calculated (e.g. [7]):

$$P_B = \frac{R_{tot} V_S}{k \eta_s \eta_0 \eta_H \eta_R} \quad \text{Eq. 8}$$

where V_S is the ship's speed, k corresponds to the number of the propellers, η_s corresponds to the shaft efficiency, η_0 refers to the propeller's open water efficiency which is equal to ($k_T J$ /($k_Q 2\pi$), η_H refers to the hull efficiency equals to (1– t)/(1– w), J is the advance coefficient, and t and w are the trust deduction and wake coefficient, respectively, while η_R corresponds to the propeller's total rotational coefficient. When a propeller's characteristics (diameter, pitch ratio, number of blades and the ratio of the expanded blade area) are known, and thrust and torque coefficient curves are provided, then the quantities k_T, k_Q, J, n can be determined from a propeller's open water diagram, which corresponds to calm water conditions. First, the following quantity is calculated:

$$\frac{k_T}{J^2} = \frac{Th/(\rho_w n^2 D^4)}{(\frac{V}{nD_{pr}})^2} = \frac{Th}{\rho_w V^2 D^2} = CC \quad \text{Eq. 9}$$

where ρ_w is the water density, n is the propeller's revolutions, D_{pr} is the propeller's diameter and Th is the thrust ($Th = R_{tot}/(1-t)$). From the intersection of the curve $k_T = CCJ^2$ with the curve ($k_T - J$) of the open water diagram of the propeller, the values of J, k_T, k_Q and η_0 can be determined. Then,

$$n = \frac{V_{ad}}{J D_{pr}} \quad \text{Eq. 10}$$

where $V_{ad} = V_S\,(1 - w)$ is the advance speed of the propeller when operating in the ship's wake.

Finally, the power required from the main engine and the number of revolutions of the propeller have been estimated. This is the main engine's revolutions when no gearbox is installed. For any pair of brake power-revolutions (P_B, n) the SFOC is to be estimated based on the manufacturer's manual and the given instructions. Specifically, the SFOC for an arbitrary load within the loading diagram is needed. Knowing the SFOC value for the nominal Maximum Continuous Rating (MCR) L_1[1] rating, the reduction rates are provided in the manual for the propeller curve and the constant speed curve for a range of loads. Then, for the operating points that lie between these curves, interpolation is carried out, while for the others, extrapolation. Then between every two points of interest (named x_i and x_{i+1}), the corresponding FOC can be derived (FOC_i):

$$FOC_i = t_i SFOC(P_i, n_i) P_{Bi} \quad \text{Eq. 11}$$

where t_i is the sailing time from x_i to x_{i+1} while assuming constant weather conditions and ship speed.

[1] Engine layout point, designating nominal maximum continuous rating, at 100% engine power and 100% engine speed.

3 Modification of the ship model to account for retrofit options

3.1 Definitions of parameters introduced in the ship model

The ship model presented in the previous sections contains forces only in the longitudinal direction (1-d.o.f.). However, especially when a WASP system is considered side forces and yaw moments will have to be accounted due to the drift motion resulting in a drift angle and the subsequent rudder action to balance the developed yaw moments. Therefore, a three degree of freedom model (3-d.o.f.) is needed, which considers longitudinal and transverse forces as well as yaw moments. Nevertheless, the 3-d.o.f. ship model can be also used when a WASP is not installed. In this case the side force and yaw moment are produced by the wind on ship's lateral windage areas.

Table 1 presents the parameters in each type of ship model (1-d.o.f. and 3-d.o.f.) as well as the additional parameters introduced by the retrofit options. In each case and depending on the retrofit option, the total resistance (Eq. 7) is derived using the respective longitudinal forces. Next a detailed analysis of the 3-d.o.f. ship model is presented, which includes the presence of a WASP.

Table 1: Ship models (1-d.o.f. and 3-d.o.f.) and the impact of retrofit measures.

Ship model component	Parameter in the ship model (1-d.o.f.)	Parameter in the ship model (3-d.o.f.)	Explanation
Calm water resistance	X_c	X_c	Resistance values for a range of speeds, mean drafts and trims
Wind forces	X_{wind}	$X_{wind}, Y_{wind}, N_{wind}$	Transverse force /Yaw moment due to superstructures. Based on semi-empirical coefficients
Added wave resistance	X_{wv}	X_{wv}	Longitudinal component based on semi-empirical methods
Effect of drift (transverse) motion	-	X_D, Y_H, N_H	Drift resistance in longitudinal direction, transverse force and yaw moment due to drift motion
Effect of rudder	-	X_R, Y_R, N_R	Rudder force (resistance) in the longitudinal direction, transverse force and yaw moment due to rudder action
WASP forces	X_{wasp}	$X_{wasp}, Y_{wasp}, N_{wasp}$	Longitudinal and heeling (transverse) forces, as well as yaw moment of the system for a range of apparent wind speeds and directions
Propeller retrofit (tip rake, cavitation)	$K_{Q(\text{new})}, K_{T(\text{new})}$	$K_{Q(\text{new})}, K_{T(\text{new})}$	New propeller open water characteristics

Bulbous bow or/and trim optimisation	$X_{c(\text{bow})}$	$X_{c(\text{bow})}$	New calm water resistance curves for a range of speeds, mean drafts, trims
ALS: effect on resistance	$X_{c(\text{ALS})}$	$X_{c(\text{ALS})}$	New calm water resistance when ALS works
ALS: effect on propeller efficiency	$K_{Q(\text{ALS})}$, $K_{T(\text{ALS})}$	$K_{Q(\text{ALS})}$, $K_{T(\text{ALS})}$	New propeller open water characteristics considering the effect of ALS

3.2 Ship model including transverse forces and yaw moments (3-d.o.f.)

As previously mentioned, the ship model is expanded to also consider the transverse forces and yaw moments exerted by the WASP system and by the wind. These forces result in drifting and thus to rudder angle deviations. There are many methods in literature to calculate the drift (β) and rudder (δ) angles. The methodology presented in the following, is based on the method derived from [14] which uses equations originally presented in [15]. The Skogman's equations [14] are modified to provide the angles (drift and rudder) as output in [6]. These expressions are based on the equilibrium of moments around the centre of gravity, assuming steady-state conditions (Figure 5).

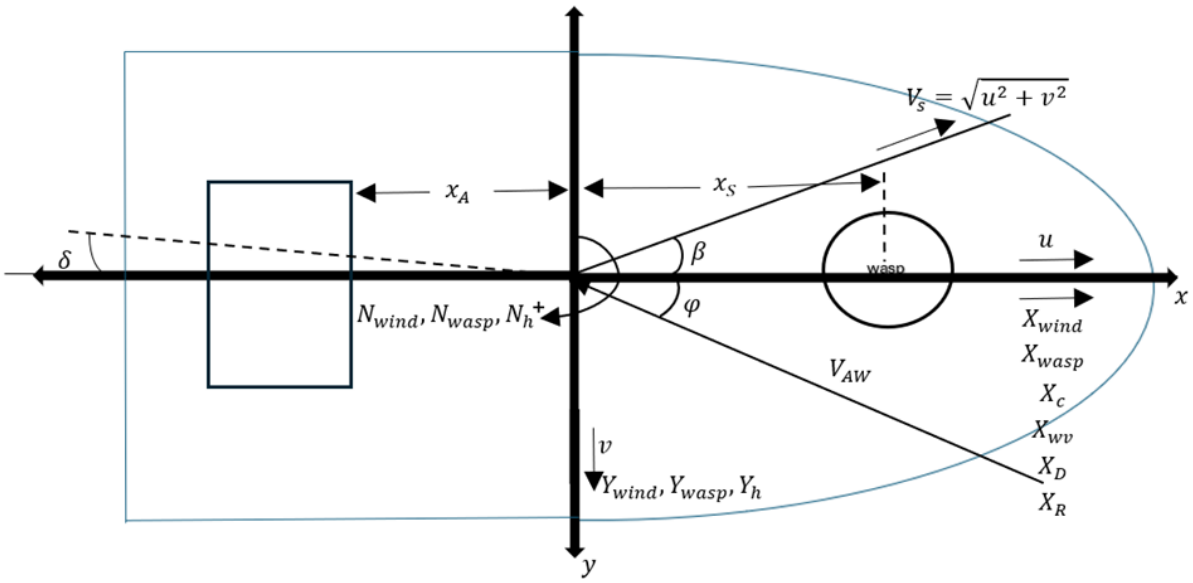

Figure 5: Forces in the 3.d.o.f. ship model including WASP.

To simplify calculations, the centre of gravity is placed at the midship section. In the coordinate system used, the x-axis points forward along the ship's length, and the y-axis is positive towards the starboard side. The moments from the superstructure's aerodynamic forces N_{wind} , from the WASP system N_{wasp}, and from hydrodynamic forces N_h must be in balance, leading to the equation:

$$N_{wind} + N_{wasp} + N_h = 0 \quad \text{Eq. 12}$$

More specifically, N_{wasp} is calculated according to:

$$N_{wasp} = Y_{wasp} x_s \quad \text{Eq. 13}$$

while Y_{wasp} is the transverse force created by the wind due to the WASP system and should be taken as negative when comes from starboard, and x_s is the longitudinal distance from the point where Y_{wasp} acts to the center of gravity of the ship. In addition, Eq. 6 is transformed as follows to be in accordance with the coordinate system:

$$N_{wind} = -0.5\rho A_L {V_{AW}}^2 c_N L_{OA} \quad \text{Eq. 14}$$

and

$$N_h = N_H + N_R \quad \text{Eq. 15}$$

where, N_H and N_R are the yaw moment and the rudder-induced moment.

The aerodynamic transverse force (Eq. 5) is also transformed as follows:

$$Y_{wind} = -0.5\rho A_L {V_{AW}}^2 c_Y \quad \text{Eq. 16}$$

Next, an additional factor is determined using x_R as the lever arm distance from the rudder's pressure point to the midship:

$$Y_{m0} = \frac{1}{0.5\rho_w T L_{WL} V_S^2}\left(Y_{wind} + Y_{wasp} - \frac{1}{x_R}\left(N_{wind} + N_{wasp}\right)\right) \quad \text{Eq. 17}$$

The effective AR_h aspect ratio of the underwater part of the hull:

$$AR_h = 2T/L_{WL} \quad \text{Eq. 18}$$

The hydrodynamic transverse force is determined as:

$$Y_H = 0.5\rho_w T L_{WL} V_S^2 (Y'_V V' + Y'_{VV} V'|V'|) \quad \text{Eq. 19}$$

Also, the derivatives of the transverse force are:

$$Y'_V = 0.5\pi AR_h - 1.4 c_B B_{WL}/L_{WL} \quad \text{Eq. 20}$$

$$Y'_{VV} = -6.6(1 - c_B)T/B_{WL} + 0.08 \quad \text{Eq. 21}$$

The dimensionless drift speed is:

$$V' = \frac{\left(Y'_V + \frac{AR_h L_{WL}}{x_R}\right) \pm \left(\sqrt{(Y'_V + \frac{AR_h L_{WL}}{x_R})^2 + 4Y'_{VV} Y_{m0}}\right.}{2Y'_{VV}} \quad \text{Eq. 22}$$

Then the drift angle can be obtained as:

$$\beta = arc \sin V' \quad \text{Eq. 23}$$

The ship's speed in the y-direction is:

$$v = V' V_S \quad \text{Eq. 24}$$

and that in the x-direction is:

$$u = \sqrt{V_S^2 - v^2} \quad \text{Eq. 25}$$

Finally, the non-dimensional added resistance factor due to drift is:

$$c_{XD} = 0.0833\beta - 0.1\beta^2 + 0.0041667\beta^3 \quad \text{Eq. 26}$$

which is a third-degree curve regression derived from model tests of different vessel types([6]), where β is in degrees. The added resistance due to drift can be derived from the formula:

$$X_D = c_{XD} 0.5 \rho_w u^2 L_{WL} T * 10^{-3} \quad \text{Eq. 27}$$

The yaw moment is:

$$N_H = 0.5 \rho_w {L_{WL}}^2 T V_S^2 (-AR_h V') \quad \text{Eq. 28}$$

The geometric effective aspect ratio of the rudder is:

$$c_{mean} = [(x_1 + x_2) + x_5]/2 \quad \text{Eq. 29}$$

$$AR_{r\_geo} = x_3 / c_{mean} \quad \text{Eq. 30}$$

Whereas the effective aspect ratio is:

$$AR_r = 2AR_{r\_geo} \quad \text{Eq. 31}$$

Where x_1, x_2, x_3 and x_5 are calculated according to Figure 6:

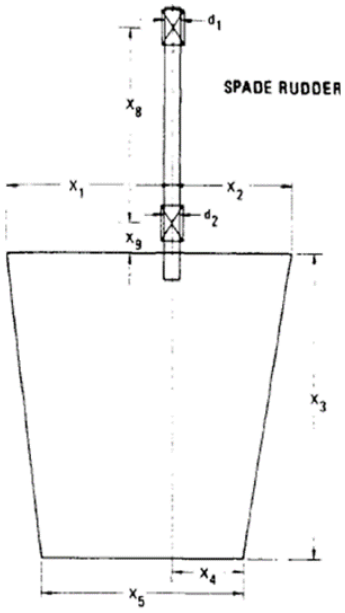

Figure 6: Dimensions of spade rudder [16][16].

The inflow speed to the rudder V_r is reduced by the wake w:

$$V_r = V_S(1 - w) \quad \text{Eq. 32}$$

To calculate the normal rudder force, an arbitrary angle inflow angle a_r is used (5º):

$$F_N = 0.5\rho_w \frac{6.13AR_r}{2.25+AR_r} A_r {V_r}^2 \sin a_r \quad \text{Eq. 33}$$

A force factor a_H is applied to represent the hydrodynamic force exerted on the ship's hull due to rudder action. a_H is defined as the ratio of the hull force generated by the rudder to the rudder force itself and is derived through regression analysis from model testing [17].

$$a_H = 0.64c_B - 0.154 \quad \text{Eq. 34}$$

The rudder angle can be derived as:

$$\delta = 0.5arc\sin\left(\frac{2}{-\frac{(1-a_H)x_R F_N}{\sin a_r}}(0.5\rho_w AR_h {L_{WL}}^2 T {V_s}^2 V' - N_{wind} - N_{wasp})\right) \quad \text{Eq. 35}$$

Then,

$$a_r = \arcsin\left(\frac{N_{wind}+N_{wasp}+N_H}{(1+a_H)x_R 0.5\rho_w 6.13AR_r/(2.25+AR_r)A_r {V_r}^2 \cos\delta}\right) \quad \text{Eq. 36}$$

The added resistance due to rudder and the lateral rudder force are:

$$X_R = -F_N \sin\delta \quad \text{Eq. 37}$$

$$Y_R = -(1 - a_H)F_N \cos\delta \quad \text{Eq. 38}$$

And the rudder moment is:

$$N_R = -(1 - a_H)x_R F_N \cos\delta \quad \text{Eq. 39}$$

Finally, Eq. 18 can be re-written as follows, also considering the drift and rudder resistance components:

$$R_{tot} = X_c + X_{wv} + X_{wind} - X_{wasp} + X_R + X_D \quad \text{Eq. 40}$$

In the case of the 1-d.o.f. model, the total resistance would be:

$$R_{tot} = X_c + X_{wv} + X_{wind} - X_{wasp} \quad \text{Eq. 41}$$

3.3 WASP forces

Wind assisted propulsion systems are also under investigation in WP4. Alternative supportive propulsion systems are to be integrated into the current ship model to examine their impact on FOC and on the ship's total efficiency. The aim is to calculate the main engine's FOC under specific weather (wave, wind) and navigational (ship speed, loading) conditions. When the WASP system is operational on a vessel, the basic equation used to model the resulting force is typically of the following form [1]:

$$F_{wasp} = \frac{\rho}{2} V_{AW}^2 A f(c_R, c_L, \varphi) \quad \text{Eq. 42}$$

where

- V_{AW} is the apparent wind speed,
- φ is the angle between the apparent wind and the ship course,
- A is scaling parameter for the size of the wind propulsion system, in case of wind sail system, A is the wing sail projected area.
- c_R and c_L are specific geometry factors for the examined wind propulsion system.

The term $f(c_R, c_L, \varphi)$ according to [1] describes the angle dependence of the wind propulsion system, which is a distinctive feature of the system examined.

Assuming a sails system installed on a vessel as supportive propulsion system, Eq. 42 can be re-written as:

$$X_{wasp} = \frac{\rho}{2} V_{AW}^2 A C_X \quad \text{Eq. 43}$$

$$Y_{wasp} = \frac{\rho}{2} V_{AW}^2 A C_Y \quad \text{Eq. 44}$$

where

- X_{wasp} is the longitudinal force generated by the WASP system,
- Y_{wasp} is the lateral (heeling) force generated by the WASP system,
- C_X and C_Y are the longitudinal and lateral thrust coefficients,
- ρ is the air density.

The above coefficients can be calculated as follows:

$$C_X = C_L \sin\varphi - C_D \cos\varphi \quad \text{Eq. 45}$$

$$C_Y = C_L \cos\varphi + C_D \sin\varphi \quad \text{Eq. 46}$$

where C_L and C_D are the lift and drag coefficients of the wing sail:

$$C_L = L_l / \frac{\rho}{2} V_{AW}^2 A \quad \text{Eq. 47}$$

$$C_D = D / \frac{\rho}{2} V_{AW}^2 A \quad \text{Eq. 48}$$

and L and D are the wing-sail model lift and drag.

In addition, it is assumed that the required power for the WASP system to operate is provided by a diesel generator that is already in use to cover the vessel's electrical needs. When the WASP system does not positively contribute to the propulsion, it is turned off and is considered as an additional superstructure, adding extra wind resistance due to its projected area.

4 Safety criteria

Safety restrictions are also considered in the optimization process, to ensure a safe passage for the crew, the cargo, and the ship itself. These restrictions are incorporated as constraints by a given maximum allowable value that cannot be exceeded during a feasible transit. The first category of safety criteria is based on hazards related to ship motions, while the second is related to ship instabilities in adverse weather conditions.

4.1 Seakeeping based criteria

The next seakeeping criteria are considered:

- slamming of bulbous bow,
- deck wetness,
- propeller immersion,
- excessive acceleration in critical locations (bridge).

For more information, please see Appendix **Error! Reference source not found.**, B, and C.

4.1.1 Propeller emergence

According to [12] the calculation of the propeller emergence is described below:

$$D_{pe} = D_p + r_3 \qquad \text{Eq. 49}$$

Where,

- D_{pe} is the effective depth of the tips of the upper propeller blades,
- D_p is defined in Figure 7,
- $r_3 = s_3 - \zeta_\alpha$ is the vertical relative motion determined at the appropriate location on the ship as shown in Figure 7, representing the vertical displacement of the propeller relative to the calm waterline due to the ship's motion in waves.
- s_3 is the absolute vertical motion and ζ_α is the wave amplitude.

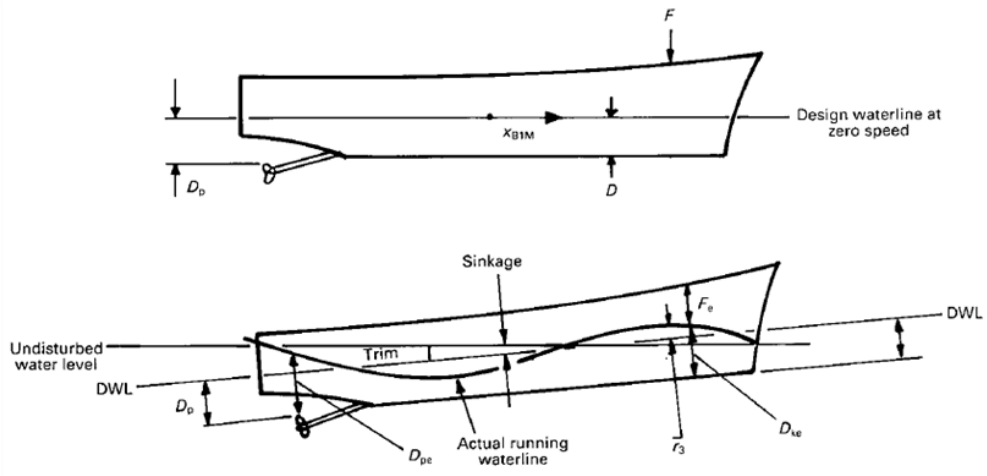

Figure 7: Effective draft and freeboard [12].

In addition, the probability of propeller emergence is:

$$P_{pe} = \exp\left(-\frac{1}{2}\frac{D_{pe}^2}{C_s^2 m_0}\right) \quad \text{Eq. 50}$$

where

- C_s is a swell up coefficient, selected equal to 1 for Froude numbers up to 0.30, since in this range the effect of swell up is minimal, and the additional resistance due to generated waves is negligible,
- m_0 is the variance of the amplitude of the relative motion at the appropriate location on the ship.

Lastly, the average number of propeller emergencies per hour are:

$$N_{pe} = \frac{3600 P_{pe}}{T_{p\_av}} \quad \text{Eq. 51}$$

Where $T_{p\_av} = 2\pi\sqrt{\frac{m_2}{m_4}}$ is the average period of the peaks of the relative motion at the appropriate location on the ship, and m_2, m_4 are the variances of the relative motion velocity and acceleration (see Appendix A).

4.1.2 Slamming occurrence

Also, according to [12] the calculation for the slamming occurrence can be evaluated using the relationship:

$$P_{sl} = \exp\left(-\frac{v_{cr}^2}{2C_s^2 m_2} - \frac{d^2}{2C_s^2 m_0}\right) \quad \text{Eq. 52}$$

where

- $v_{cr} = 0.093\sqrt{(gL_{bp})}$,
- $g = 9.81$ m/s^2,
- L_{bp} is the ship's length
- d is the draught at the forward perpendicular at the appropriate location on the ship.

The average number of slamming occurrences per hour are:

$$N_{sl} = \frac{3600 P_{sl}}{T_{p\_av}} \quad \text{Eq. 53}$$

4.1.3 Deck wetness – Deck submergence

The probability of deck submergence is:

$$P_{ds} = \exp\left(-\frac{1}{2}\frac{F_e^2}{C_s^2 m_0}\right) \quad \text{Eq. 54}$$

where

- $F_e = F - r_3$ is the effective freeboard,
- F is calculated according to **Error! Reference source not found.**.

The average number of deck submergences per hour are:

$$N_{ds} = \frac{3600 P_{ds}}{T_{p\_av}} \quad \text{Eq. 55}$$

4.1.4 Bridge accelerations

Bridge accelerations are also an important criterion for safe and convenient voyage for the crew members. Lateral and vertical accelerations are to be estimated at an appropriate location on the bridge deck.

4.1.5 Motion Sickness Incidence

Motion Sickness Incidence (MSI) is a key criterion in ship design, measuring the likelihood of crew members to experience motion sickness. MSI depends on factors like roll, pitch, heave motions, and the duration of exposure. In [12] the motion sickness incidence derives from the formulation of [18] as follows:

$$MSI\% = 100\Phi\left(\frac{\log\left(\frac{\ddot{s}_3}{g}\right) - \mu_{MSI}}{0.4}\right) \quad \text{Eq. 56}$$

Where Φ is the cumulative normal distribution function up to x for a normal distribution with zero mean and unity standard deviation. The factor $\mu_{MSI} = -0.819 + 2.32(log_{\omega_e})^2$ with ω_e in radians/s: $\omega_e = \sqrt{\frac{m_4}{m_2}}$ and absolute acceleration $\ddot{s}_3 = 0.798\sqrt{m_4}$.

4.1.6 Critical values of seakeeping-based criteria

Ship responses can be calculated and compared against seakeeping criteria requirements, based on hydrodynamic analysis such as strip theory (see Appendix A). Moreover, Table 2 presents limiting values of the presented criteria, based on available information from **Error! Reference source not found.**.

Table 2: Limiting values of the seakeeping criteria [19]**Error! Reference source not found.**.

Criterion	NATO STANAG 4154	NORDFORSK 1987 (Merchant ships)
Vertical acceleration at forward perpendicular	0.2g RMS	0.275g (L≤100 m) or 0.05g (L≥330m)
Vertical acceleration at bridge	0.1g RMS	0.15g
Lateral acceleration at bridge	0.10g RMS	0.10g for light manual work
Motion Sickness Incidence (MSI)	20% of crew in 4 hours	6.0° for light manual work
Motion Induced Interruption (MII)	1 tip per minute	
Roll amplitude	4.0° RMS	6.0° for light manual work
Pitch amplitude	1.5° RMS	
Slamming (probability)		0.03 (L≤100 m) or 0.01 (L≥300 m)
Deck wetness (probability)		0.05

where RMS= Root Mean Square.

4.2 Criteria for avoiding dangerous phenomena in adverse weather conditions

When sailing in adverse weather, ships may face dangerous conditions that can lead to capsizing or severe rolling, causing damage to cargo, equipment, and crew. A ship's vulnerability to these risks depends on its stability, hull shape, size, and speed. Therefore, the likelihood of dangerous events, including capsizing, is dependent on the specific ship and the specific sea state. The IMO [20] has introduced specific guidelines for shipmasters to avoid navigation in adverse weather and sea conditions, as some combinations of wave length and wave height under certain operation conditions may lead to dangerous situations.

4.2.1 Surf-riding and Broaching-to

Following and quartering seas may result in the ship to be accelerated to ride on the wave (surf-riding) which may further result to sudden change vessel's heading and loss of maneuverability leading to capsize (broaching to). To prevent this situation, the vessel should avoid entering areas where:

$$135^0 < a < 225^0 \quad \text{Eq. 57}$$

$$V_S > \frac{1.8\sqrt{L_{bp}}}{\cos(180^0 - a)} \quad \text{Eq. 58}$$

where

- a is the relative wave heading (0 degrees correspond to head waves),
- V_S in knots is the speed of the vessel,
- L_{bp} is the length of the vessel between perpendiculars.

4.2.2 Successive high wave attack

Successive high waves attack may occur when:

$$1.8T_W < T_E < 1.8T_W \quad \text{Eq. 59}$$

$$T_E = \frac{3T_W^2}{3T_W + V_S cos(180^0 - a)} \quad \text{Eq. 60}$$

where

- T_E the encounter period,
- T_W is the wave period.

4.2.3 Synchronous and parametric rolling

Both synchronous and parametric rolling are dangerous phenomena that can lead to potential cargo or structural damage and loss of stability. Synchronous rolling can occur when a ship's natural roll period aligns with the wave encounter period (often in beam seas), leading to dangerous roll motions. On the other hand, parametric rolling happens mostly in head or following seas causing increasingly severe rolling. The dangerous areas where synchronous and parametric rolling may occur are identified by the following equations and such conditions should be avoided:

$$| T_R - T_E | = \varepsilon T_E \quad \text{Eq. 61}$$

$$| T_R - 2T_E | = \varepsilon T_E \ \ \& \ \ | a | \leq 30^0 \quad \text{Eq. 62}$$

$$T_R = \frac{2cB}{\sqrt{GM}} \quad \text{Eq. 63}$$

$$c = 0.373 + 0.023\frac{B}{T} - 0.043\frac{L_{bp}}{100} \quad \text{Eq. 64}$$

where

- T_R is the natural rolling period of the ship,
- ε is a small constant to stipulate the width of the zone,
- GM is the metacentric height,
- B is the breadth of the ship,
- L_{bp} is the length between the perpendiculars and
- T is the draft.

4.3 Course-keeping

In addition to calculating the side forces due to the WASP system in use (Section 3.2), the drift angle (β) and rudder angle (δ) have also been estimated. Based on the rudder angle, another criterion related to course-keeping can be introduced. When the rudder angle exceeds 35°, the vessel loses its steering ability, resulting in a loss of course:

$$\delta \leq 35^0 \quad \text{Eq. 65}$$

5 Case study: modelling the existing ship

The ship examined for the analysis above and the upcoming results is a bulk carrier (MV Kastor) with the main characteristics shown in Table 3.

Table 3: MV Kastor main characteristics.

Parameter ID	Value
Length B.P. [m]	225.50
Breadth [m]	32.26
Depth [m]	20.05
Scantling Draft [m]	14.45
Design Draft [m]	12.20
Ballast Draft (mean) [m]	6.38
DWT [t]	81600
Main Engine MCR [kW]	9930
Service Speed [kn]	14.3

5.1 Calm water resistance

It is essential to calculate the resistance of calm water, as this is a key component in the subsequent stages of the process. For the vessel under investigation, the documentation concerning towing tank tests is available at different drafts. Resistance and power tests data are available for a speed range from 10 to 16 [kn].

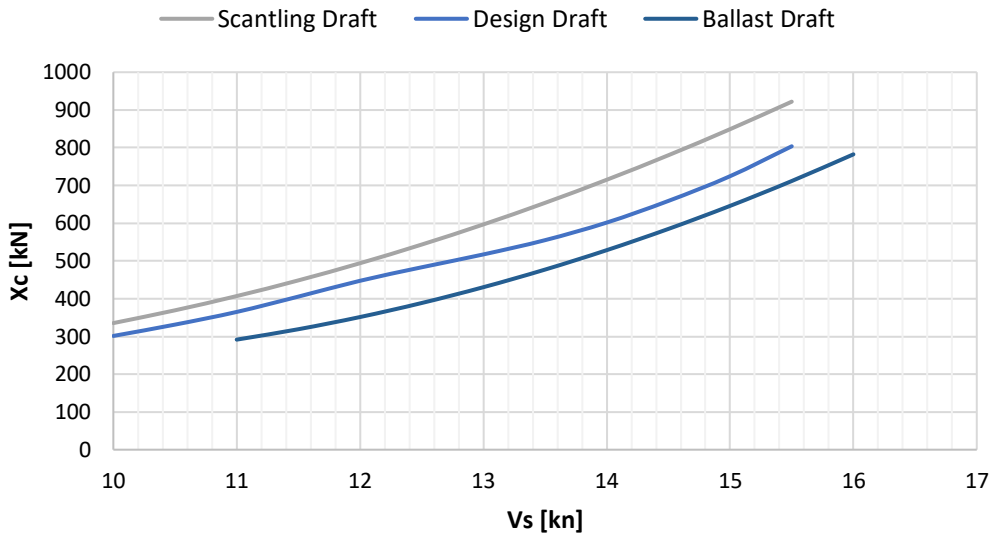

Figure 8: Calm water resistance curves for different drafts.

Calm water resistance data for scantling, design, and ballast draft are presented in Figure 8. In cases where further information is required for a different draft, interpolation between the two nearest curves can be performed.

5.2 Propeller characteristics

In addition, based on the analysis carried out in WP2, due to insufficient data from propeller documentation, a "new" propeller has been created based on the original one. The open water characteristics (i.e., thrust coefficient k_T, torque coefficient k_Q, and propulsion efficiency η_{Did}, versus the advance coefficient J) of the propeller are presented in Figure 9.

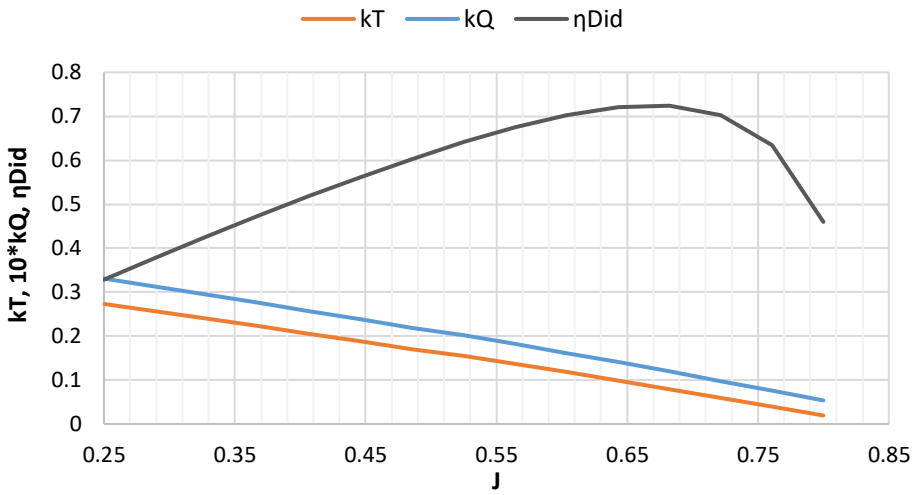

Figure 9: Open water characteristics for the re-constructed propeller.

5.3 Wind resistance

As previously stated, wind resistance is a significant contributing factor to the total resistance of the vessel. For the studies presented in the following, the Blendermann's coefficients method [13] has been used to estimate the longitudinal-force coefficient c_X and the lateral-force coefficient c_Y. The frontal projected area A_F and the lateral plane area A_L needed to be estimated for the calculations. The results are shown in Table 4 for different drafts.

Table 4: Frontal and lateral areas of the vessel.

ID	Scantling Draft	Design Draft	Ballast Draft
A_F [m^2]	637	710	836
A_L [m^2]	2034	2550	3438

Figure 10 represents the coefficients of longitudinal and lateral wind resistance c_X, c_Y, along with the yaw moment coefficient c_N, estimated with the Blendermann's coefficients method (180 deg. corresponds to head wind).

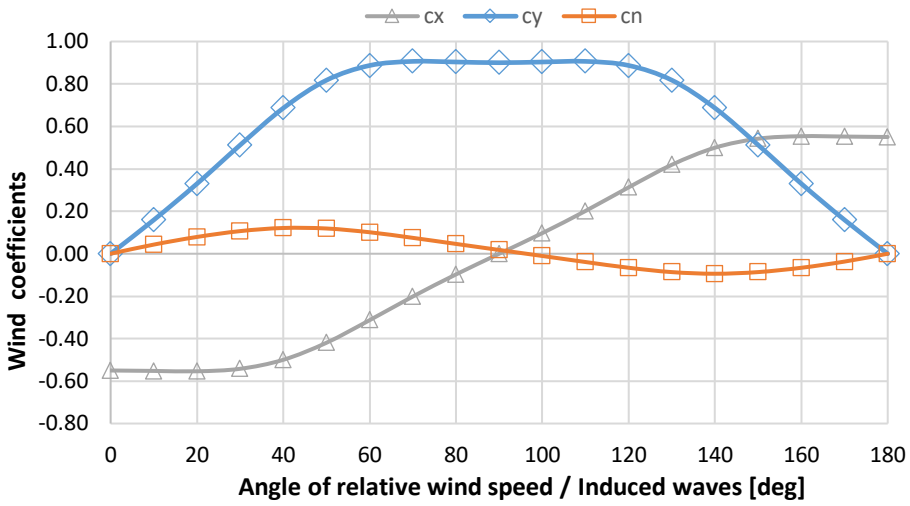

Figure 10: Longitudinal and lateral wind resistance coefficients, and yaw moment coefficient.

5.4 Added wave resistance

Added wave resistance X_{WV} has been estimated using the Liu-Papanikolaou method [10] calculating the relative responses due to regular waves. In Figure 11 the added wave resistance in non-dimensional form is presented for different heading angles[2] corresponding to the scantling draft at a vessel's speed of 10 [kn]. In addition, Figure 12 and Figure 13 show how vessel's speed and loading condition affect the added wave resistance. Table 5 summarized the parameters used for the calculations. The calculation of the mean added wave resistance in a random sea has been described in Section 2.2, while the JONSWAP wave spectrum was used.

For the weather routing application, it is essential to reduce the computational cost, especially when estimating the added wave resistance, since spectrum analysis calculations require a significant amount of time. Therefore, a regression model to estimate the added wave resistance has been developed. Further details about the regression model can be found in the Appendix C.

Table 5: Waterline entrance length and radius of gyration for different loading conditions.

Loading Condition	Le_{fore} ($L_{waterline\ entrance}$) [m]	Le_{aft} ($L_{waterline\ entrance}$) [m]	K_{yy} [%L_{bp}]
Scantling Draft	35.5	30	0.22
Design Draft	35.5	30	0.22
Ballast Draft	35.5	35	0.24

[2] It must be noted that 180 deg. correspond to head seas.

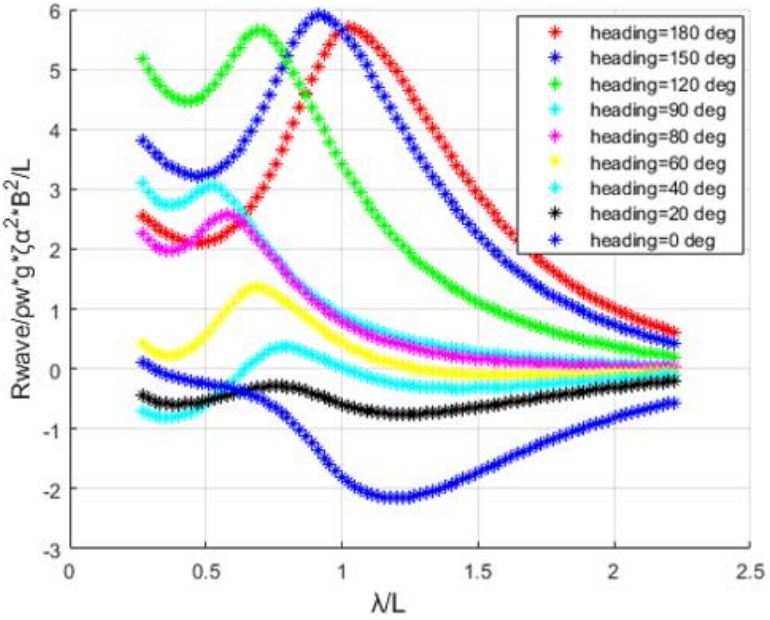

Figure 11: Non-dimensional added wave resistance in regular waves for different heading angles.

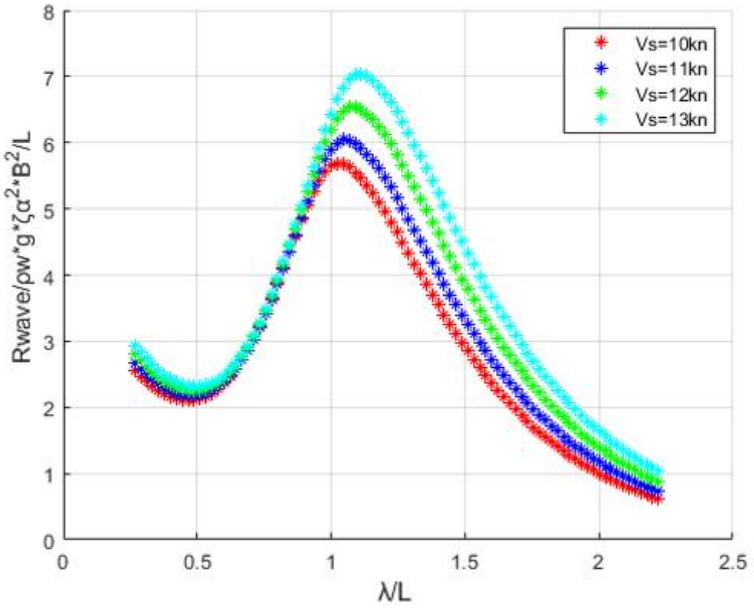

Figure 12: Effect of vessel's speed on added wave resistance (scantling draft considered).

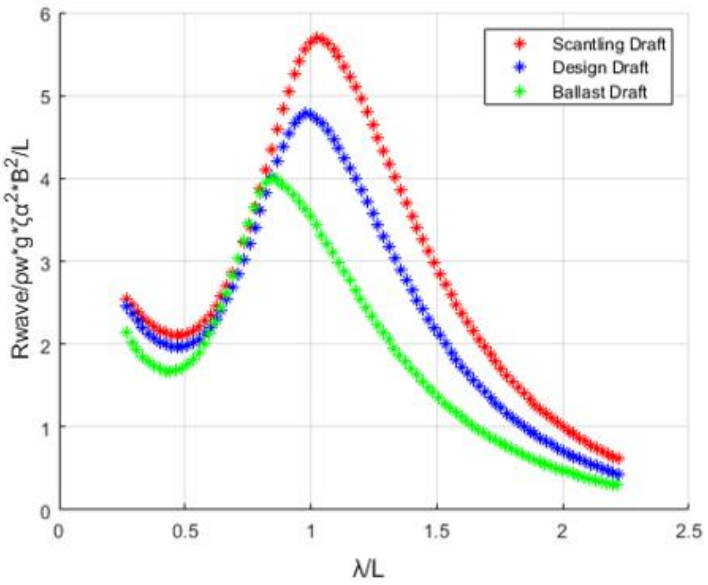

Figure 13: Effect of vessel's loading condition on added wave resistance for a ship's speed of 10 [kn].

5.5 Power predictions for several drafts

Among the data received, power results for scantling, design and ballast drafts for a range of vessel speeds were made available. Therefore, respective power demands were also calculated using all methods and tools described in the ship model section. The comparisons between the real power demands in sea trials and the calculated ones are presented in Figure 14.

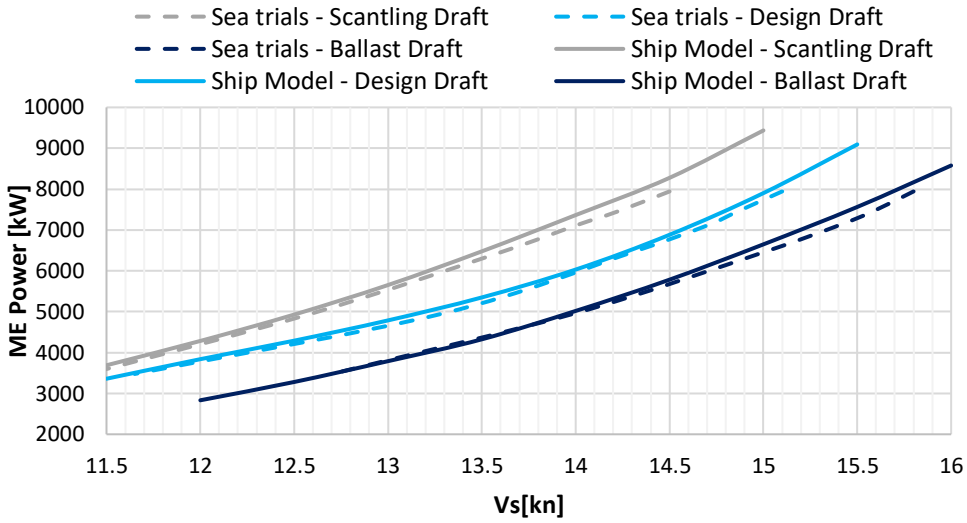

Figure 14: ME power for different drafts and speeds, using sea trials data and the respective calculations from the ship model.

As described in the previous sections of this report, based on main engine manufacturer's manual the SFOC is estimated for any pair of power-revolutions of the engine (Figure 15) and consequently the required FOC, when the engine is running under specific load for a particular period of time.

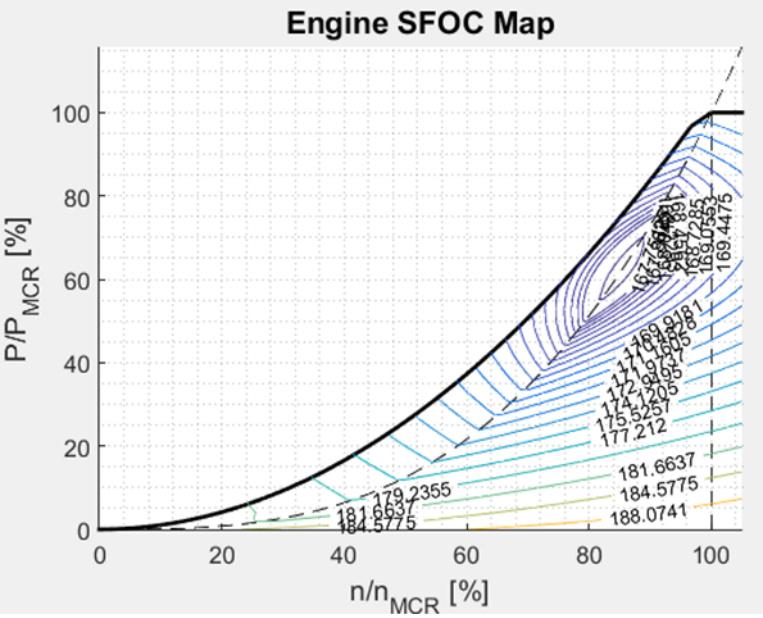

Figure 15: SFOC map.

In Figure 16 the estimated FOC for the three different drafts is presented for a range of vessel's speed.

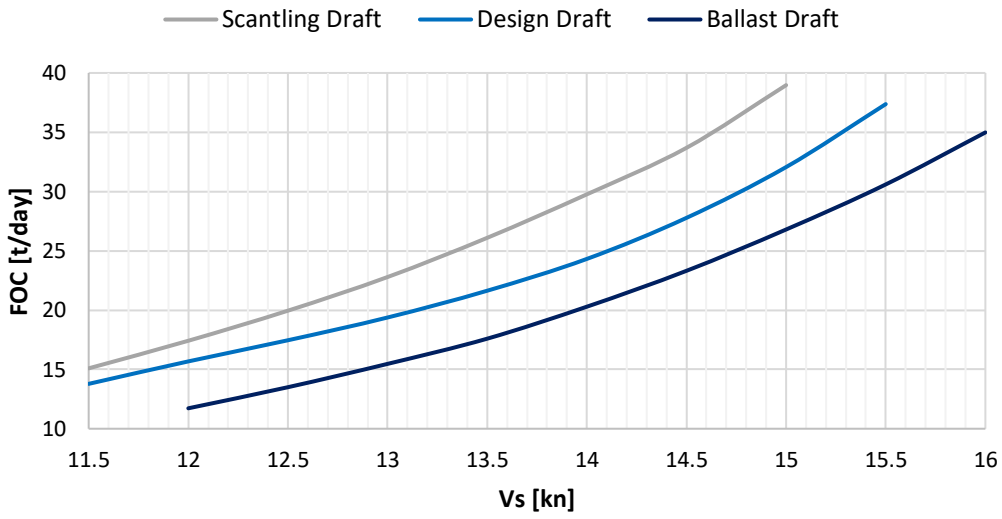

Figure 16: FOC vs. ship speed for different drafts, considering calm water resistance only.

5.6 Integration of retrofit options

The ship model can incorporate retrofit measures such as hydrodynamic improvements. To demonstrate the capability of the ship model to account for such improvements, a fictitious reduction (about 5%) of the calm water resistance is assumed (Figure 17), which could represent the utilisation of an ALS. Moreover, the consideration of a fictitious propeller efficiency improvement (about 3% of the propulsive efficiency n_{Did}) is also considered (Figure 18). More specific results from the

incorporation of such retrofit measures will be studied in WP2 and WP5. In Table 6 results from the above-mentioned fictitious retrofits are presented for a series of speed values, while the weather effect is neglected, and scantling draft is assumed.

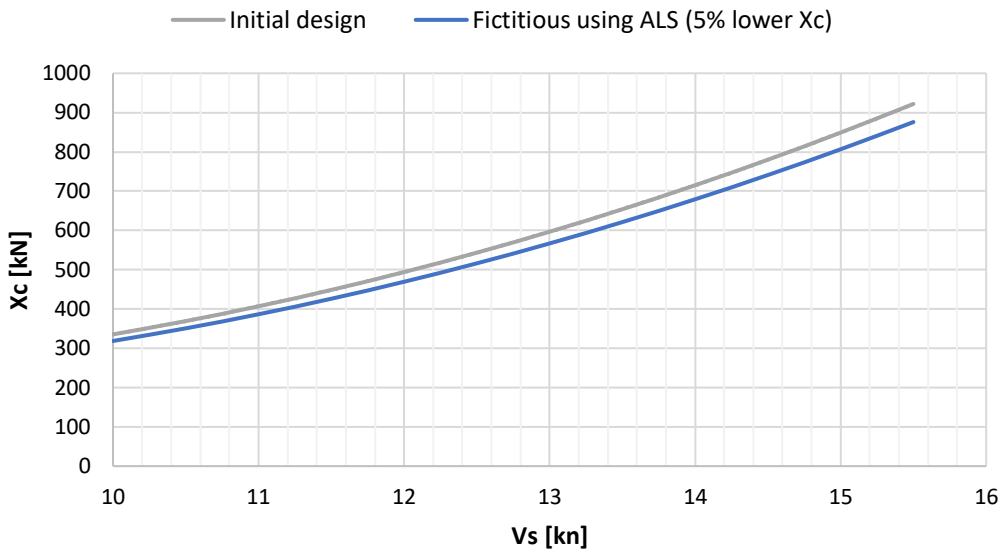

Figure 17: Calm water resistance for the scantling draft for the initial design and for a fictitious one using ALS.

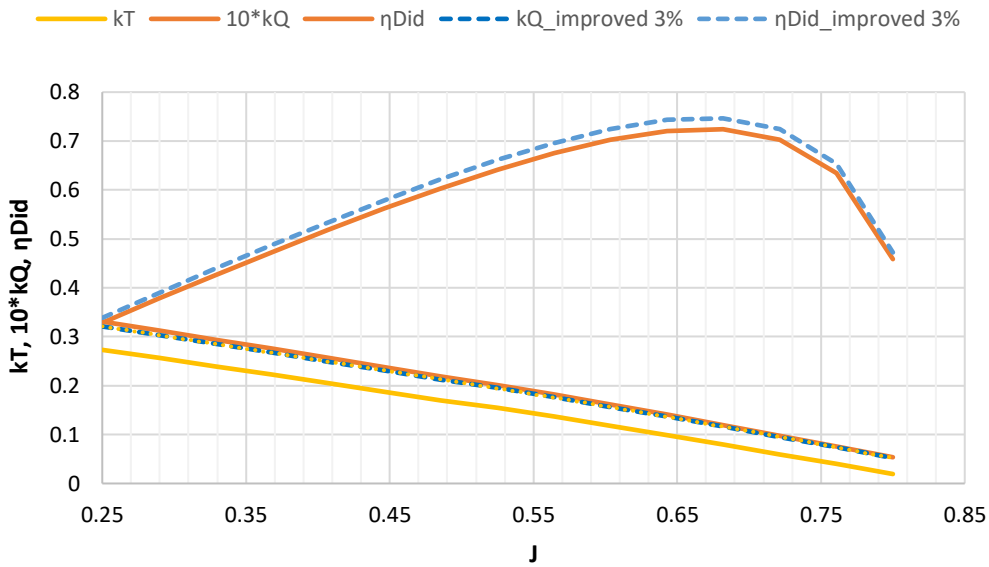

Figure 18: Open water characteristic curves for the real propeller and a fictitious one with improved efficiency.

Table 6: ME FOC for the as-built ship and the scenarios considered for hydrodynamic improvements.

ID	Main engine fuel oil consumption [t/day]		
	V_s = 13.25 [kn] (speed condition corresponding to the average value of the speed range)	**V_s = 12 [kn]** (speed condition corresponding to the lower bound of the speed range)	**V_s = 14.5 [kn]** (speed condition corresponding to the upper bound of the speed range)
As-built ship	25.47	17.42	33.69
Propeller improvement by 3% increased η_{Did}	24.69 (-3.08%)	16.90 (-3.00%)	32.64 (-3.12%)
Reducing calm water resistance by 5%	23.82 (-6.47%)	16.35 (-6.09%)	31.42 (-6.72%)
Combined effect	23.12 (-9.24%)	15.92 (-8.57%)	30.46 (-9.56%)

5.6.1 WASP forces and configuration

A WASP system from B4B is integrated into the weather routing tool and its impact on route selection and ship's efficiency will be examined. The WASP system consists of 4 eSAILs as shown in Figure 19.

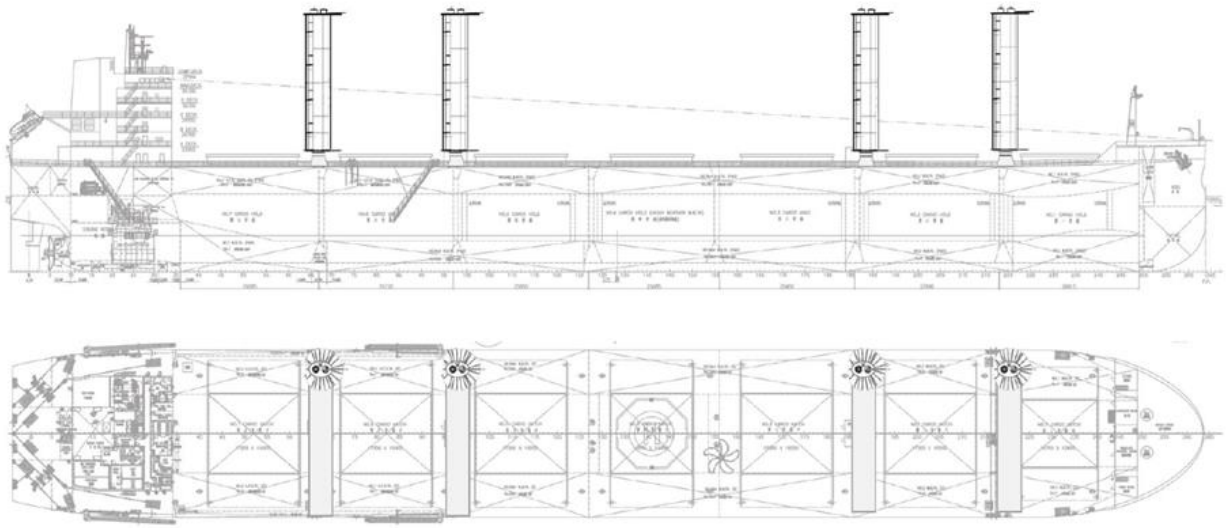

Figure 19: Arrangement of the 4 eSAILs.

Available data from B4B regarding WASP forces (driving and transverse) are used to train a regression model for a range of apparent wind speed and direction to decrease the computational time for the required calculations. Information about the required power for an eSAIL to operate is also provided.

The developed regression model, which predicts the driving force generated by a single eSAIL, has been trained using a neural network and validated with a Root Mean Square Error (RMSE) of 0.77716 (Figure 20).

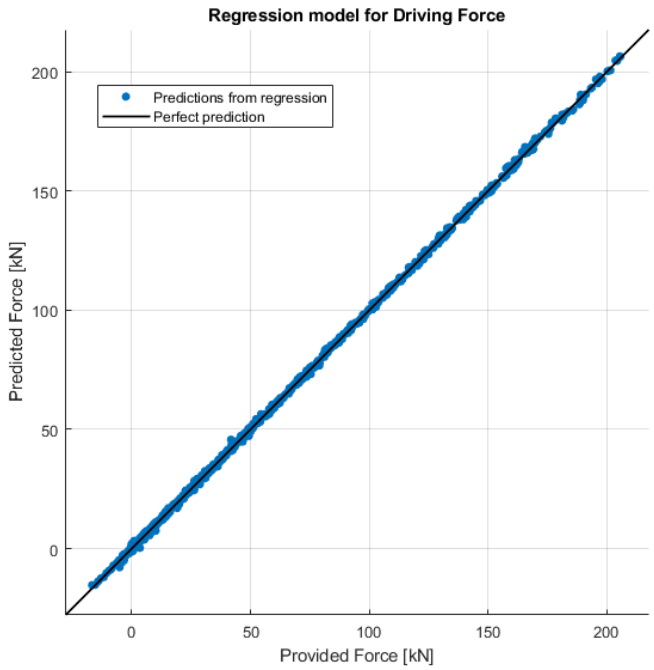

Figure 20: Regression model for the driving force.

A similar regression has been performed for the transverse force (Figure 21) and the auxiliary power (Figure 22) needed by the system. Their validation metrics are summed up in Table 7.

Table 7: Validation metrics for regression models regarding the WASP.

Regression model for	**RMSE**	**R^2**
Driving force - X_{wasp}	0.77716 [kN]	0.99981
Heeling force - Y_{wasp}	3.1727 [kN]	0.998
Required auxiliary power	1.0385 [kW]	0.99949

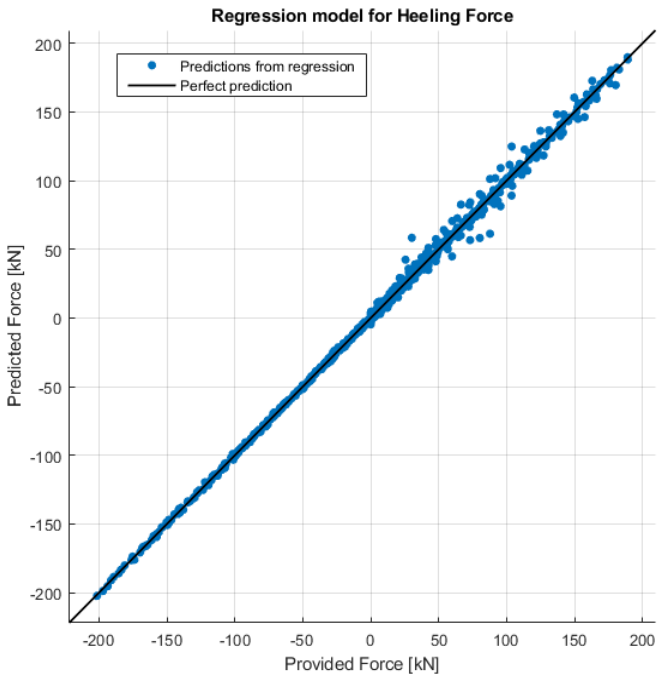

Figure 21: Regression model for the heeling force.

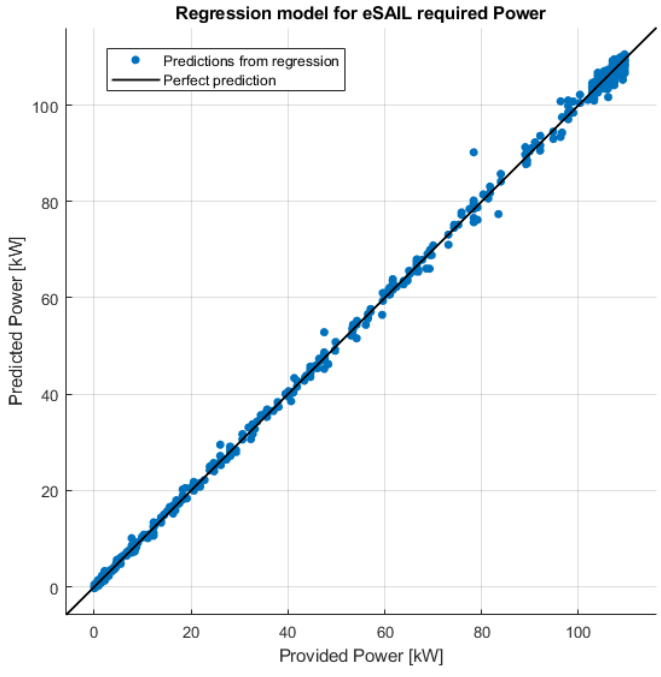

Figure 22: Regression model for eSAIL required power.

5.6.2 WASP case study

In this case study, the vessel is assumed to travel at a speed of 11 knots with a loading condition at the scantling draft of T = 14.45 meters. The weather conditions correspond to a significant wave height (H_s) of 2 meters and a peak wave period (T_p) of 10 seconds, while the true wind speed (V_{tw}) is 7.5 m/s (Table 8). For the purpose of this analysis, it is assumed that the wind and waves are coming from the same direction. The ship model is used to account for the added resistance due to wind and waves, as detailed in previous sections of this report.

Table 8: Weather and loading conditions for the case study.

Parameter	Value
Scantling draft [m]	14.45
Ship speed [kn]	11
Wave height [m]	2
Wave peak period [s]	10
True wind speed [m/s]	7.5

As mentioned in the previous section, when a WASP system is in operation on a vessel, side forces must also be taken into account. Drift and rudder angles should be monitored to ensure they do not exceed their limitations, allowing the ship to maintain its course. Additionally, the added resistance caused by drift and rudder should be considered in the total resistance, since it affects the required power from the main engine.

This study demonstrates how the 1-d.o.f. and 3-d.o.f. ship models provide different results regarding the ship's overall performance and operability. Various scenarios have been analyzed regarding the use of the WASP system with the four eSAILs, as discussed in the previous sections, which include or neglect the side forces. It shall be noted that the specific study considers CFD results (Appendix D) for the transverse hydrodynamic force Y_H and the yaw moment N_H instead of the semi-empirical formulas of Eq. 19 and Eq. 28 respectively.

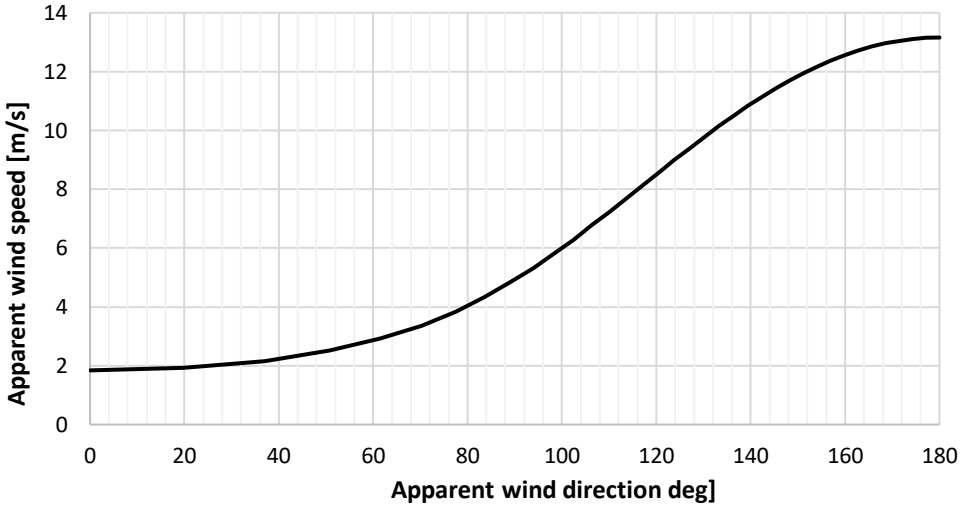

Figure 23: Apparent wind speed for different apparent wind angles.

In Figure 23, the apparent wind speed is presented along the angles of apparent wind from stern to bow, and in Figure 24 the generated drift and rudder angles are compared for different angles of

relative wind, both with and without WASP. As shown, their peaks are found around 140 degrees of relative wind, where the transverse forces are significantly high (Figure 25). As expected, the longitudinal component of the rudder resistance is also high at the same wind angles.

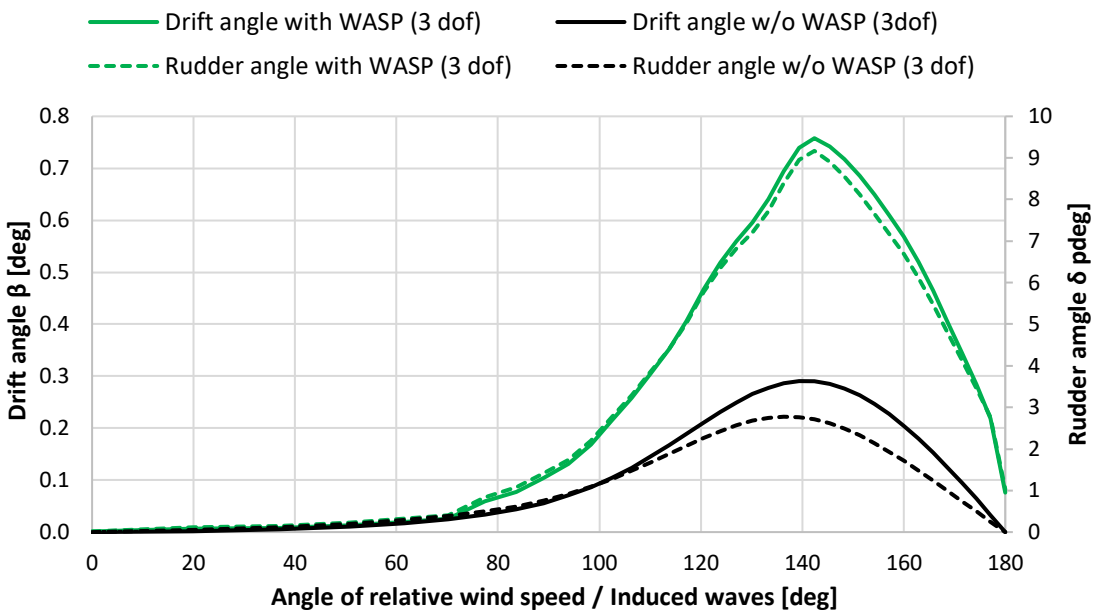

Figure 24: Drift and rudder angles vs. apparent wind and wave direction.

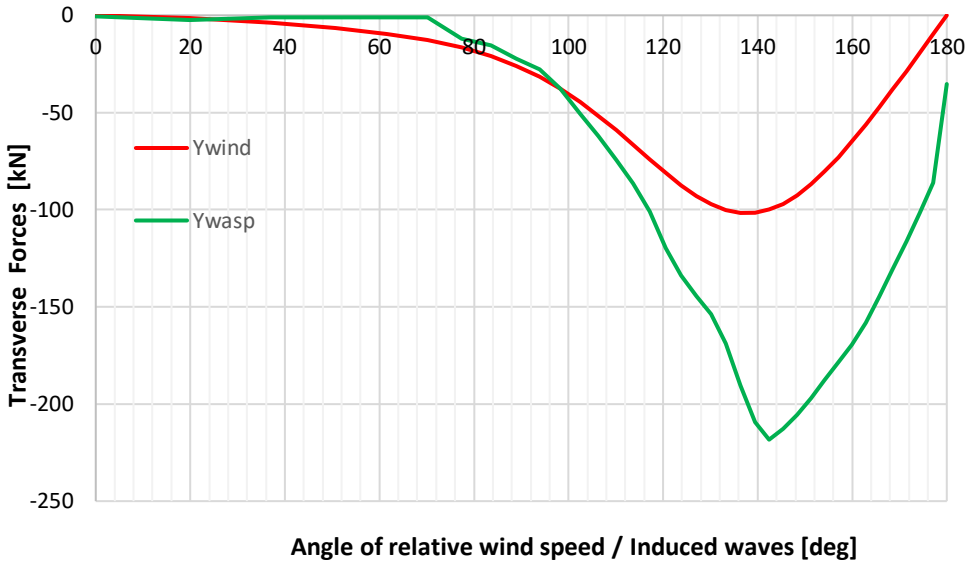

Figure 25: Transverse forces vs. relative wind direction.

All the longitudinal forces are presented in Figure 26. Calm water resistance X_c is steady and equals 406.93 [kN], but it is not included in Figure 26, to maintain the clarity in the graph.

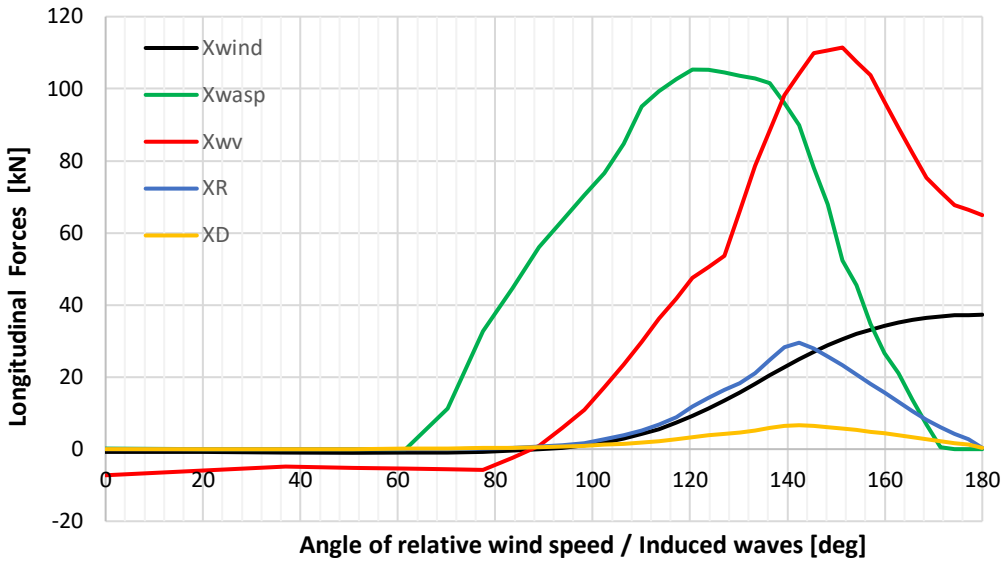

Figure 26: Longitudinal forces vs. relative wind direction.

Figure 27 and Figure 28 show the main engine power and ME FOC required respectively, comparing cases where the WASP system is installed versus not installed, as well as scenarios with and without the consideration of side forces in both cases. Moreover, in Figure 29 the FOC savings when using WASP with the 3-d.o.f. and the 1-d.o.f. ship model are shown.

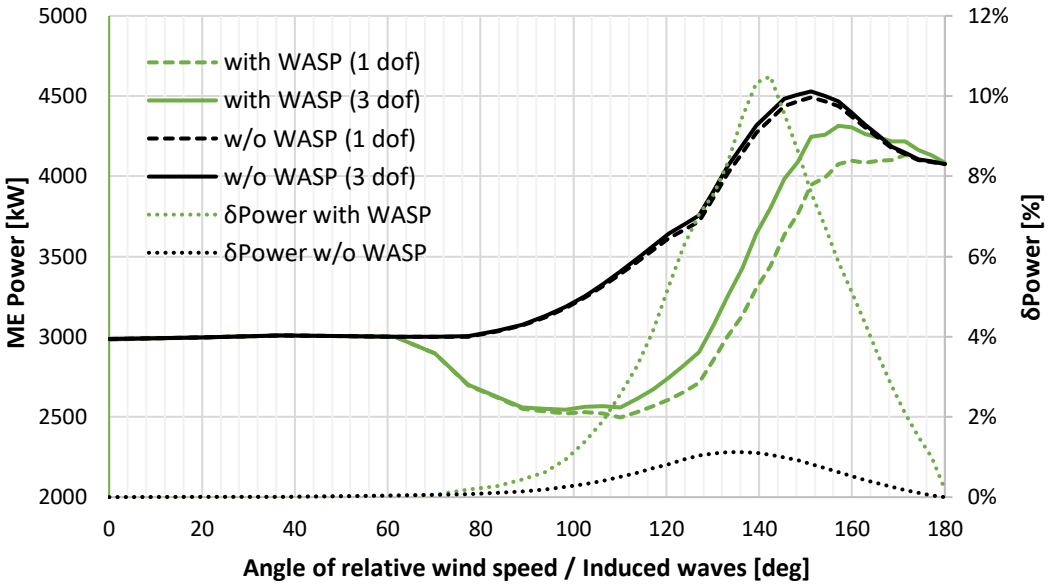

Figure 27: ME power for scenarios with/without WASP system and considering the 1-d.o.f. and 3-d.o.f. ship models.

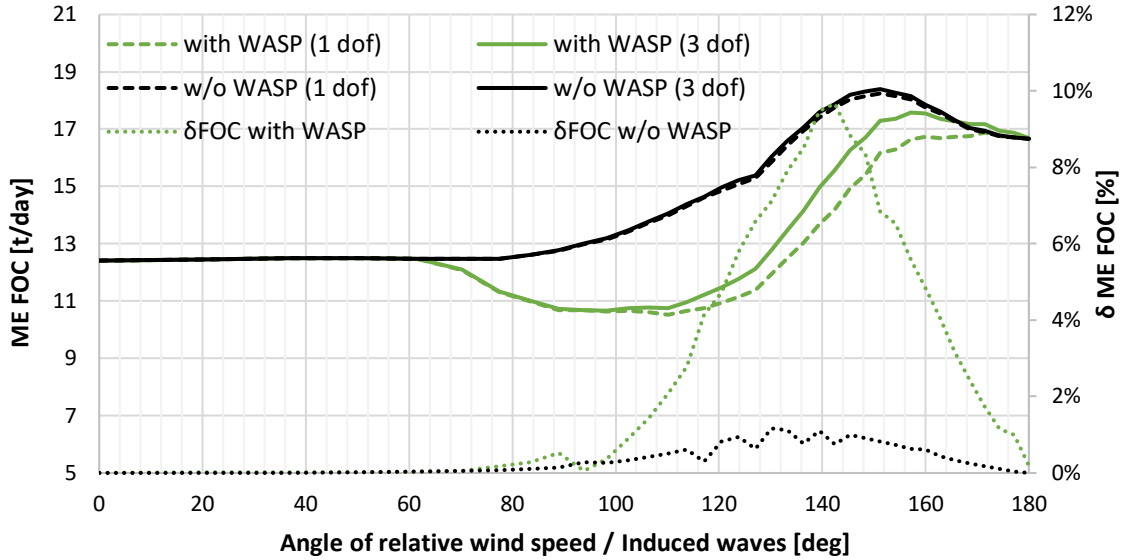

Figure 28: ME FOC for scenarios with/without WASP system and considering the 1-d.o.f. and 3-d.o.f. ship models.

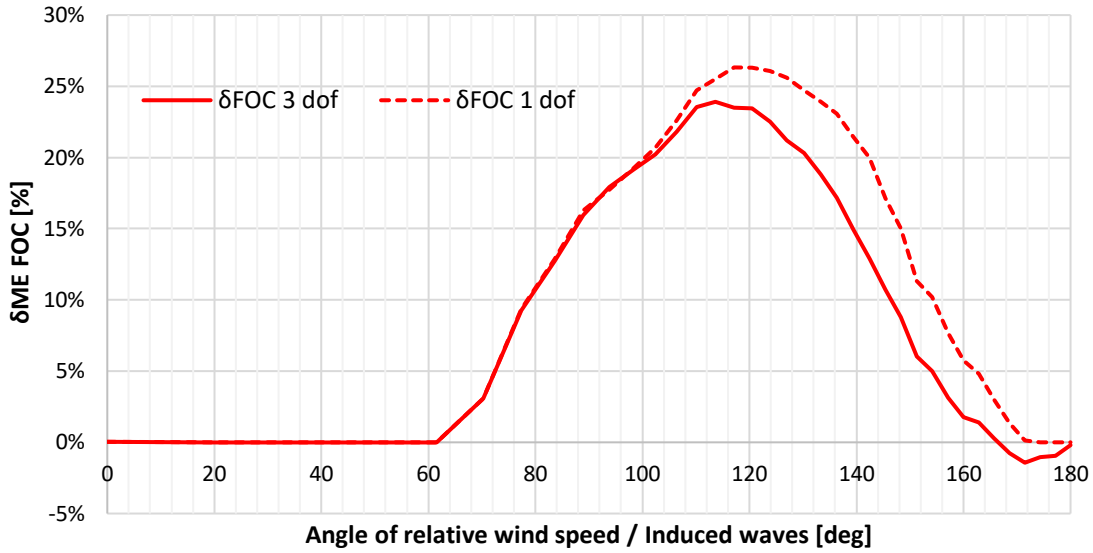

Figure 29: FOC savings when using WASP system for the 3-d.o.f. and the 1-d.o.f. ship models.

In addition, polar graphs have been created, considering the same ship speed and loading condition, showing the ME power savings when using the WASP system, both when considering 1-d.o.f. (Figure 30) and the 3-d.o.f. (Figure 31) ship models. Calculations were performed considering

various true wind directions within a 0–180-degree range for several values of true wind speeds, and the results are plotted against this range and alongside with the corresponding apparent wind direction. The wave conditions are same as mentioned in Table 8.

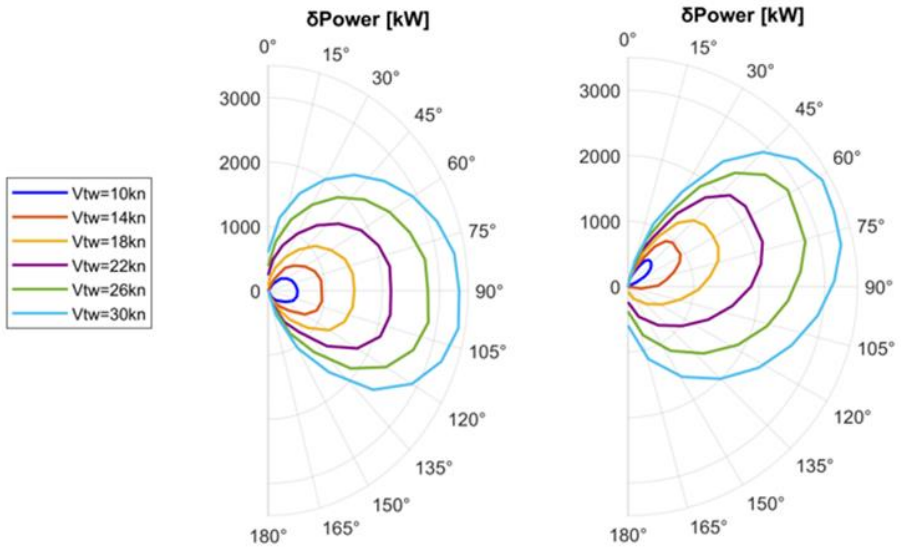

Figure 30: Power savings for 1-d.o.f. model vs true wind speed direction (left) and apparent wind direction (right).

In Figure 31, the results of the 1-d.o.f. ship model for the examined true wind speeds are also included as dotted lines.

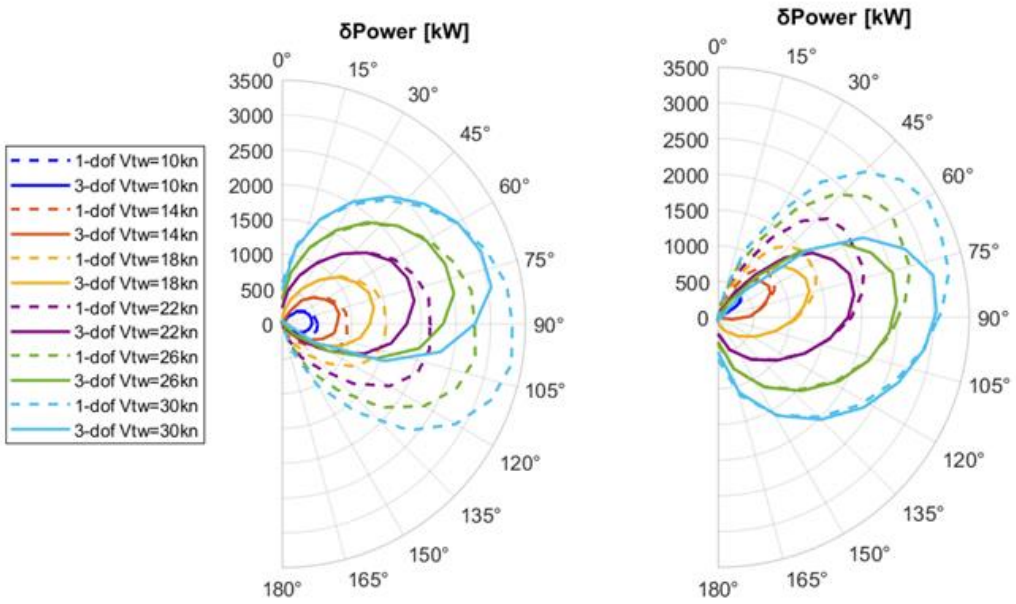

Figure 31: ME power savings for the 3-d.o.f. ship model vs the true wind speed direction (left) and apparent wind direction (right).

6 Case study in specific route (1-d.o.f. ship model)

In this section a representation of a historical voyage and an optimization demonstration is presented.

6.1 Examined route

All calculations and route optimization concern the voyage of KASTOR on 22.05.2022, whose main characteristics are reported in Table 9.

The voyage is from Port Luis (Mauritius) to Singapore (Figure 32). The specific voyage is selected since it was carried out right after Under Water (UW) hull cleaning, while the exact loading condition (KG, LCG) was considered. In addition, high frequency and noon reports data are used at 30-minute intervals for comparison with ship model's predictions. It should be also noted that in this case study, the 1-d.o.f. ship model has been used.

Table 9: KASTOR Voyage on 22.05.2022.

Parameter	Value
Voyage duration [days]	12.42
FOC (noon reports) [t]	259.33
Average speed over ground [kn]	11.13
Distance travelled [nm]	3322
Mean draft [m]	13.1

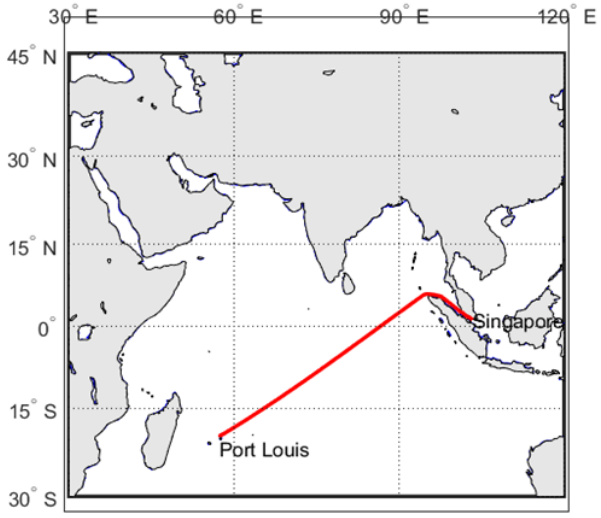

Figure 32: Trajectory from Port Louis to Singapore.

6.2 Weather data comparison

Based on high-frequency data available, for a specific voyage, we were able to compare the weather forecast data available in the ship's database with the data used in the weather routing tool from the Copernicus Marine Environment Monitoring Service (CMEMS). It should be noted that Data Transmission Network (DTN) is the weather provider and the comparison between the two providers is presented below for the basic wave parameters. In addition, the selected voyage for the

comparison is identical to the voyage simulation and route optimisation mentioned previously. Figure 33, Figure 34, and Figure 35 present a statistical comparison between the two weather providers. Data are summarised in Table 10.

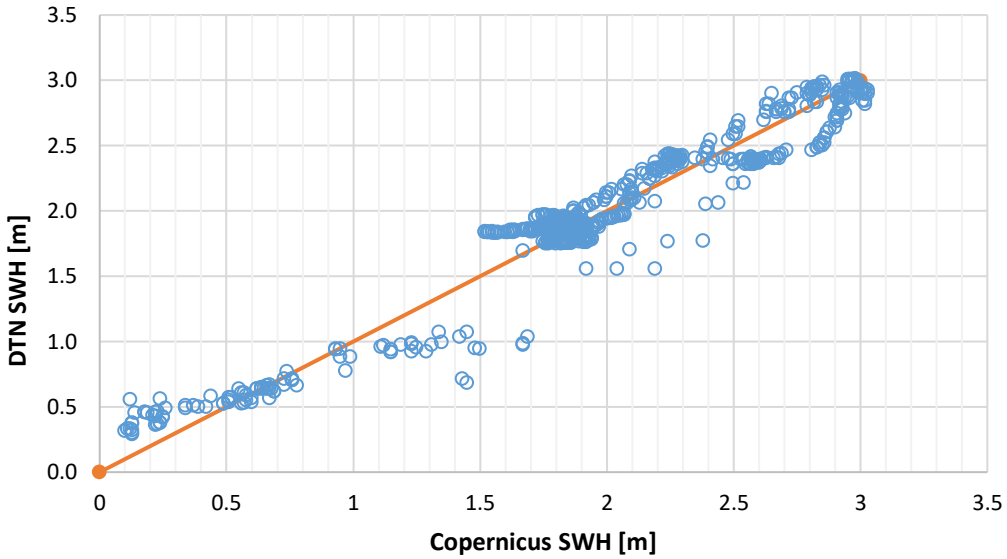

Figure 33: Significant Wave Height (SWH) values comparison between DTN and Copernicus data.

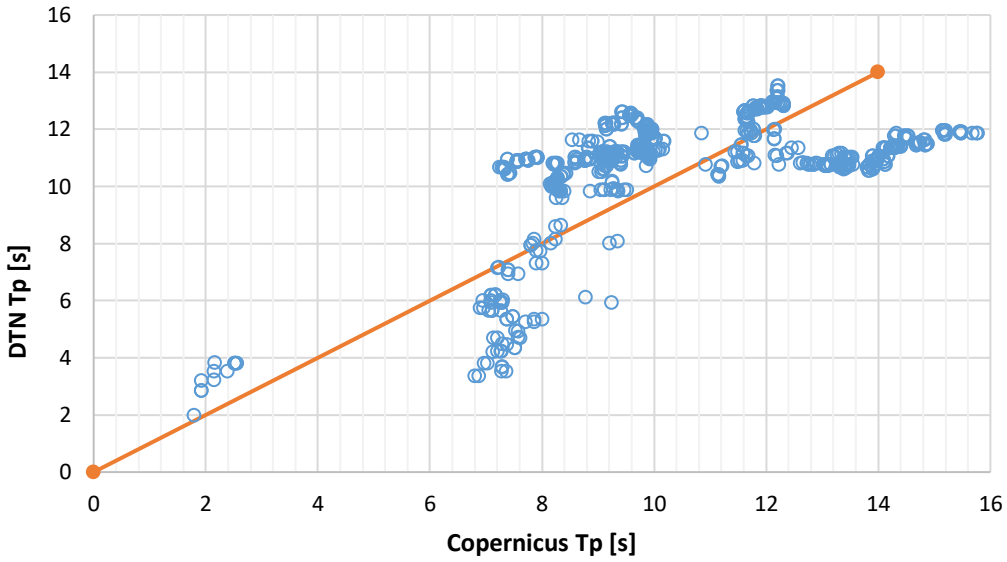

Figure 34: Wave peak period values comparison between DTN and Copernicus data.

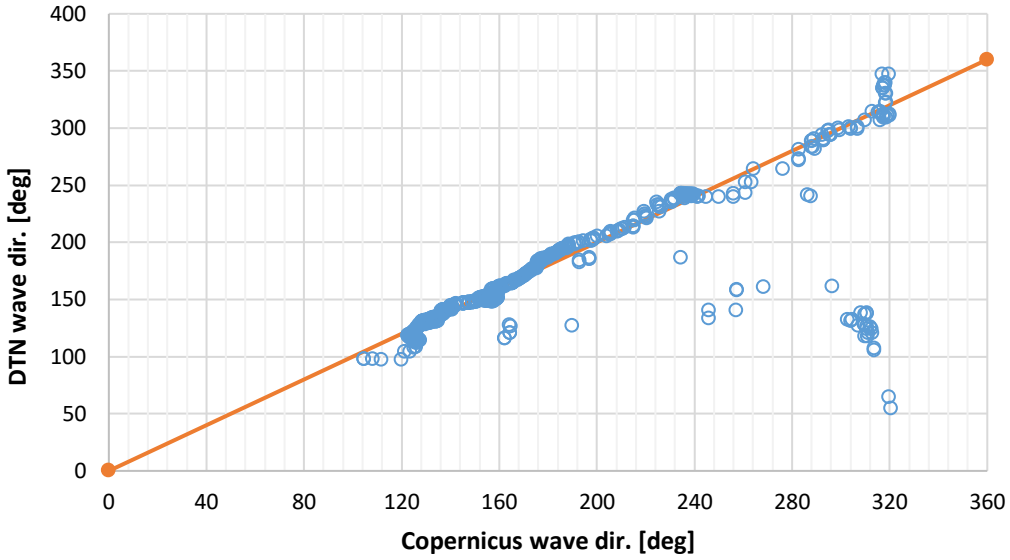

Figure 35: Wave direction values comparison between DTN and Copernicus data.

Table 10: Statistical comparison of DTN's with Copernicus' Weather predictions (reference source: Copernicus).

Parameter	Pearson correction coefficient	R^2	Mean error	Standard deviation
SWH [m]	0.969	0.938	0.002	0.173
T_p [s]	0.616	0.378	0.120	2.196
Mean wave direction [deg]	0.759	0.579	-9.258	40.245

6.3 Real voyage simulation and comparison with noon reports data

As already mentioned, the voyage on 22.05.2022 is selected taking advantage of the recent UW hull cleaning. Such a choice facilitates in minimizing estimation errors on calm water resistance, since the available data from tank tests refer to clean hull conditions. In high frequency data, speed through water (STW) and speed over ground (SOG) are available. The STW values were used to estimate the calm water resistance, excluding a few cases where erroneous STW measurements were identified. In these cases, the SOG values were used and corrected by the longitudinal current speed component. For the simulation the given DTN weather data used in the required calculations.

In Figure 36, the demanded shaft horse power in accordance with the STW values along the route is presented. As expected, an increase in the STW corresponds to a respective increase in the shaft horsepower (SHP) values. Similarly, in Figure 37 the added wave resistance and the respective significant wave height values along the route are shown. Beyond the significant wave height, the relative wave direction also impacts the added wave resistance. Waves originating from beam to stern can result in reduced added resistance, which may even become negligible. Moreover, in Figure 38 all three resistance components are presented along the trajectory, clearly illustrating the magnitude of each component to the total resistance.

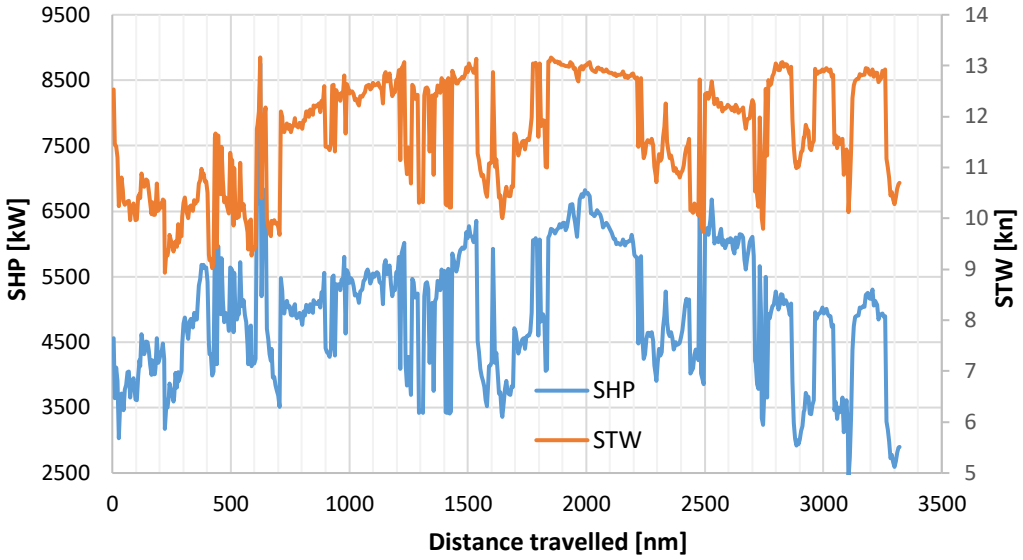

Figure 36: Shaft horse power and speed through water along the route.

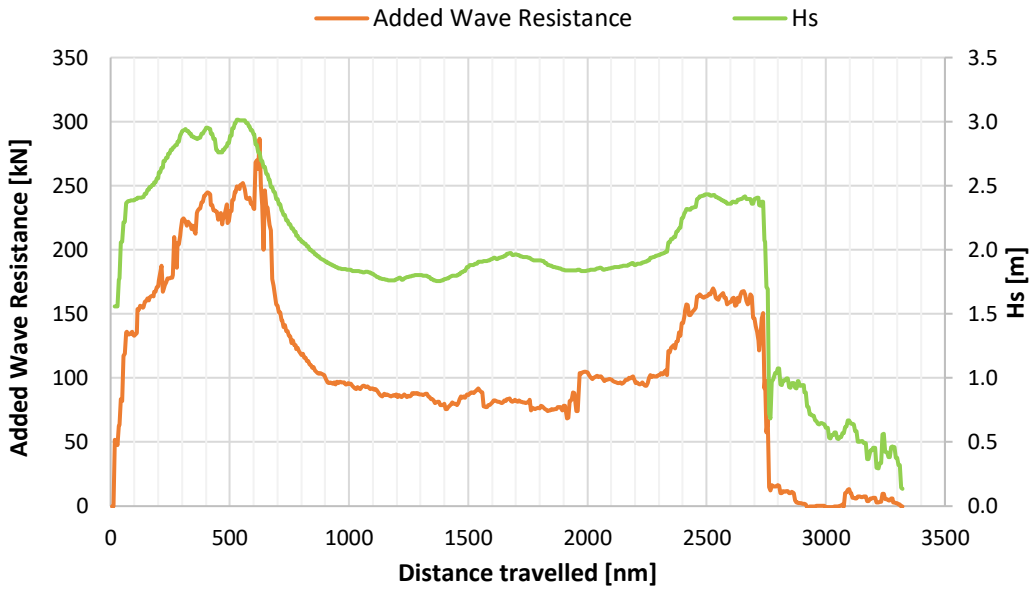

Figure 37: Added wave resistance and significant wave height along the route.

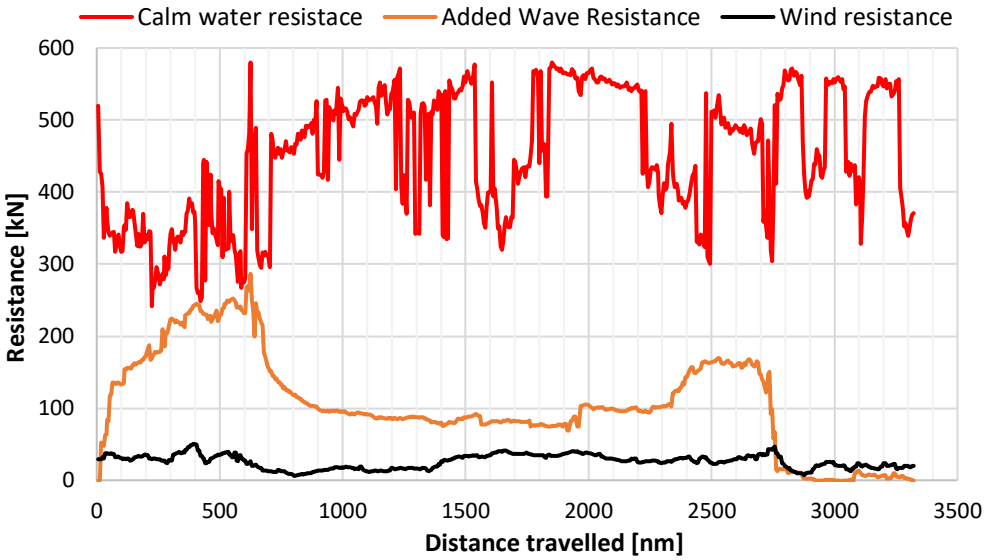

Figure 38: Resistance components along the route.

As indicated by the available noon reports, the real voyage required 259.33 [t] of fuel oil, whereas the simulated voyage resulted in the total FOC specified in Table 11.

Table 11: Total main engine fuel oil consumption.

	Simulation	Noon Reports	Difference
Total ME FOC	246.81 [tn]	259.33 [tn]	4.83 [%]

This comparison along the examined route is also shown in Figure 39.

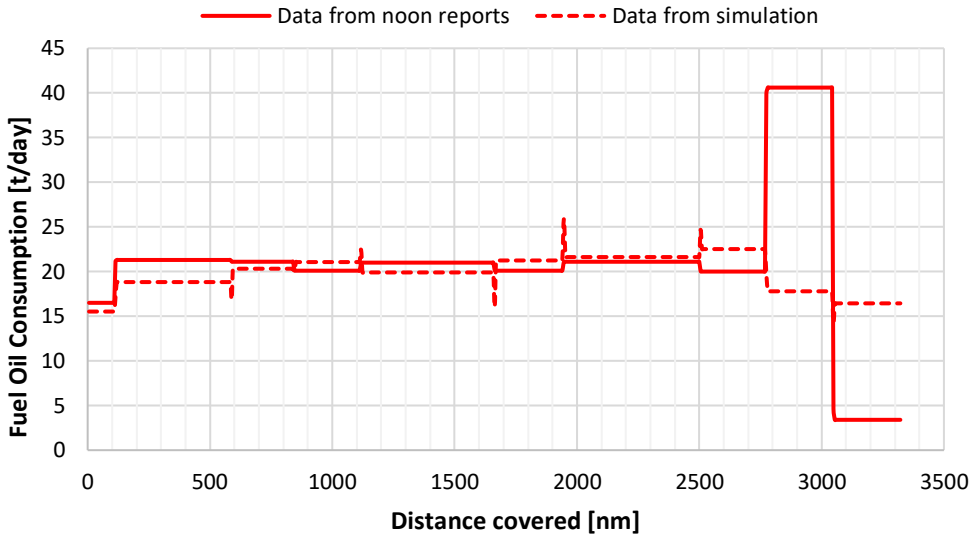

Figure 39: FOC for the real voyage using noon reports data and simulation results derived per day.

In Figure 40 the shaft power from the main engine as a function of rotational speed is shown according to three different sources. Blue points represent data from noon reports, the orange ones show the results from the ship model, and the black line is the theoretical curve as derived from calculations using the reconstructed propeller in the ship model.

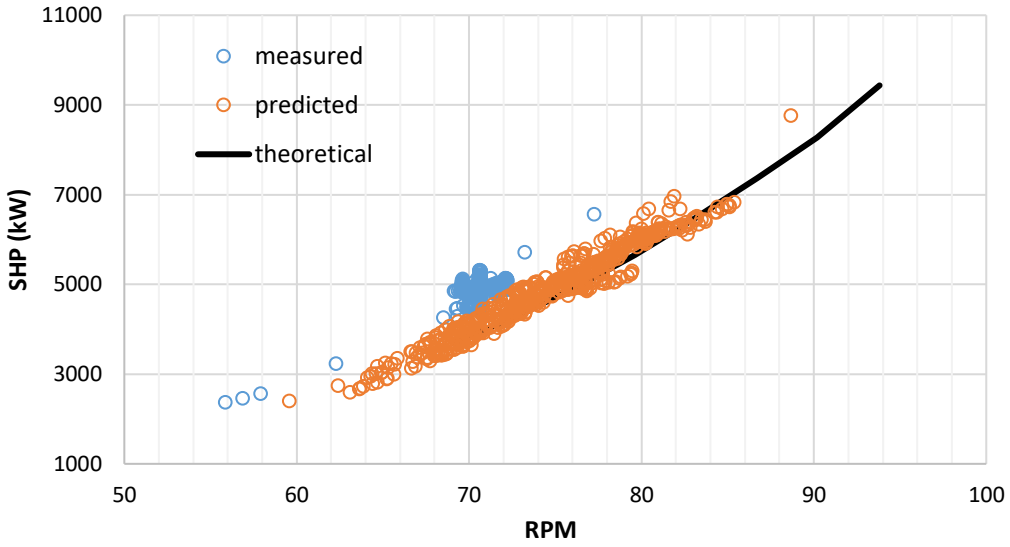

Figure 40: Different frameworks for SHP vs. RPM.

6.4 Examination of safety criteria

A special case regarding all safety criteria mentioned in Section 4 is presented in this section. Along the real voyage presented in the previous, all criteria have been considered and their probability of exceeding the limit values has been determined. Figure 41 shows the bridge accelerations during transit, along with the limits from NORDFORSK (1987) and NATO STANAG 4154. For a short period of time, the second, stricter criterion is slightly exceeded. In addition, Figure 42 presents the pitch RMS values along the route, as well as the limit value based on the NATO STANAG 4154 criterion. The values obtained during transit are significantly lower than the criterion. Meanwhile, Figure 43 shows the respective values for deck wetness probability, which approach the NORDFORSK 1987 criterion but never exceed it.

Figure 44 illustrates the limits of encounter frequency, where parametric and synchronous rolling may occur, and neither limit is reached. The calculations have been performed using Eq. 61 and Eq. 62, assuming ε=±0.025. The natural roll period has been calculated using Eq. 63 and Eq. 64 ($T_R = 14\ s$).

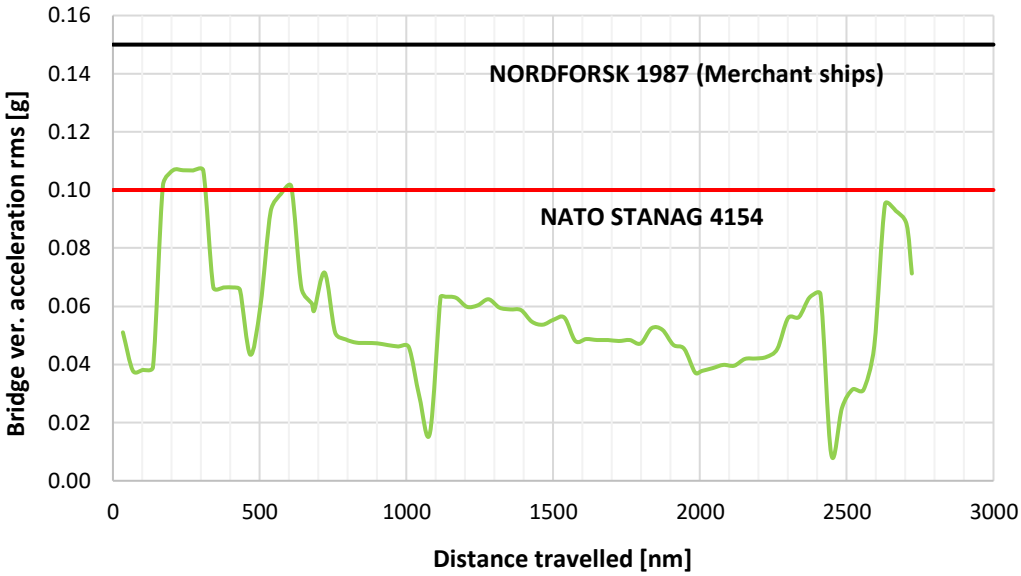

Figure 41: Vertical acceleration on bridge (rms) along the route.

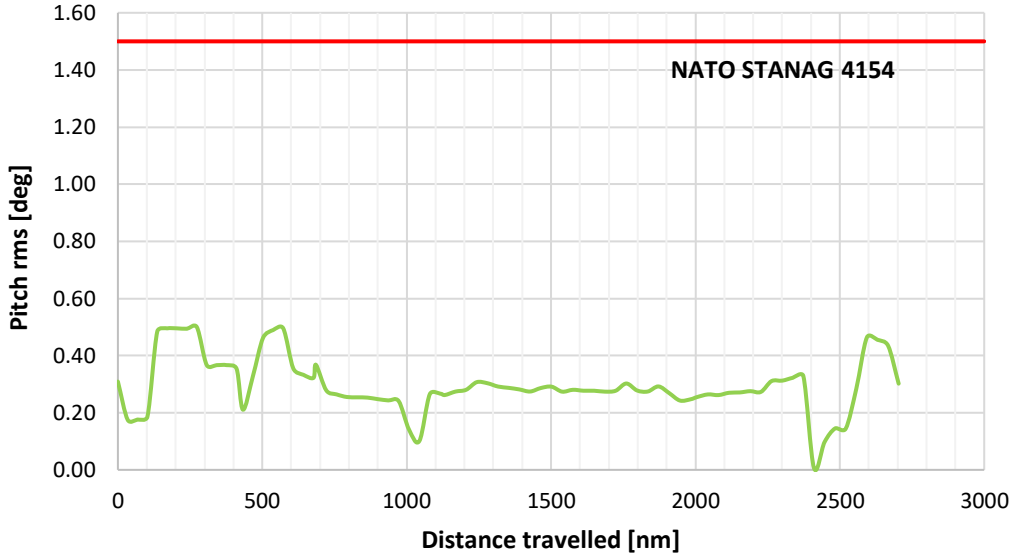

Figure 42: Pitch rms along the route.

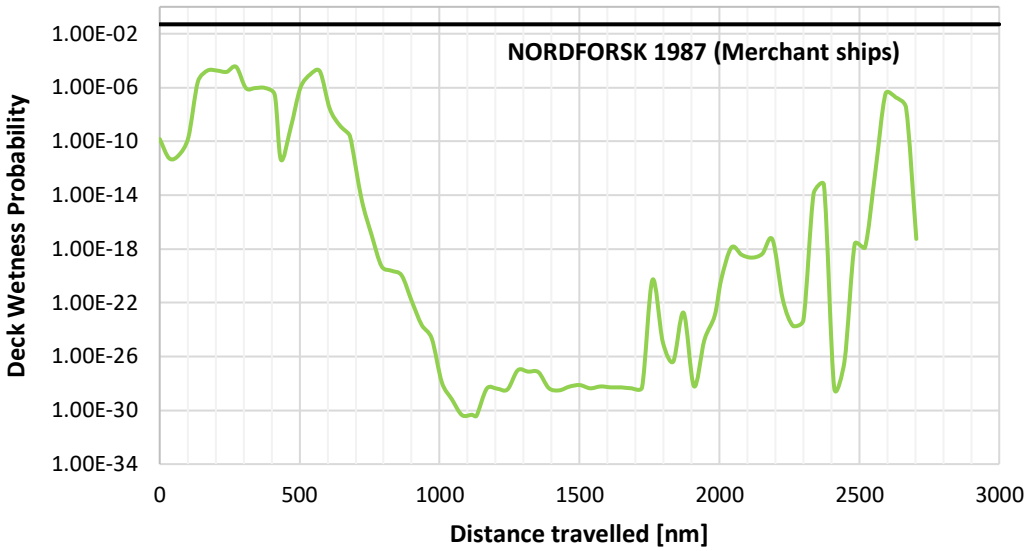

Figure 43: Deck wetness probability along the route.

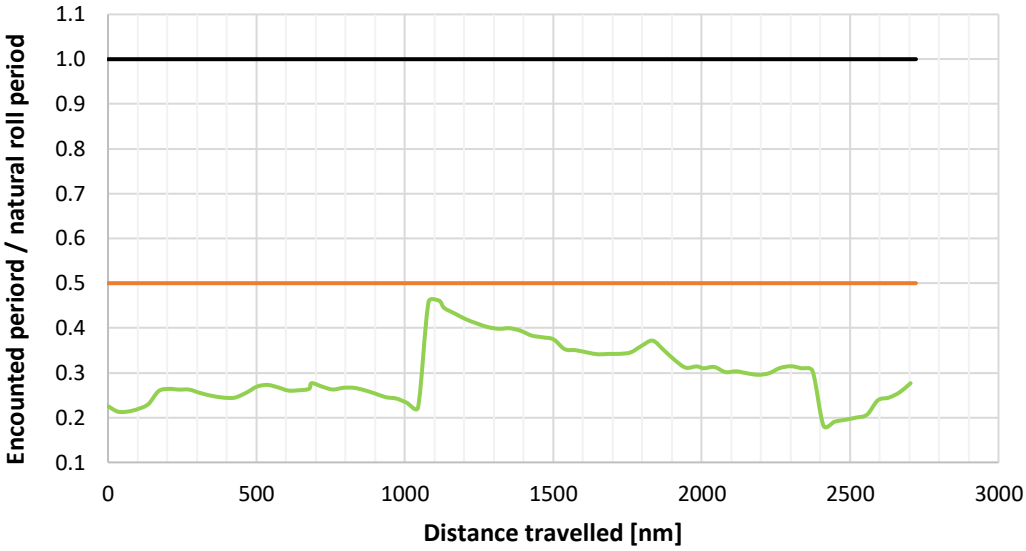

Figure 44: Synchronous and parametric rolling along the route.

6.5 Route optimization of the initial design

Aside from a specific voyage simulation using the weather routing tool described earlier, a relative route optimization has been conducted. This optimization focused on the voyage segment between Port Louis (Mauritius) and north of Banda Aceh (Indonesia). The remaining part of the voyage was not relevant to the route optimization and was therefore excluded from the process (Figure 45).

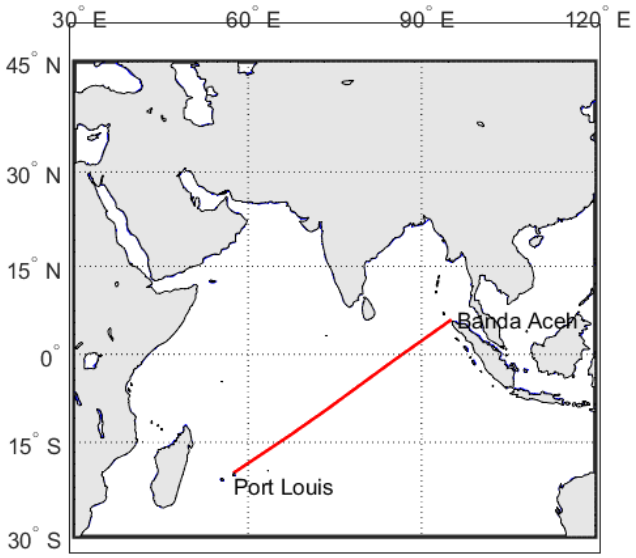

Figure 45: The main segment of the real voyage which has to be optimized.

For the optimization, a constant ship speed (about 11kn) is assumed, which is the average speed of the SOG calculated from the noon reports for that specific part of the voyage. The optimization was conducted using a genetic algorithm [8], set with 100 generations and a population size of 100 individuals per generation. The necessary weather data has been obtained from Copernicus database, while the objective function of the optimization is the minimization of fuel oil consumption (Eq. 1).

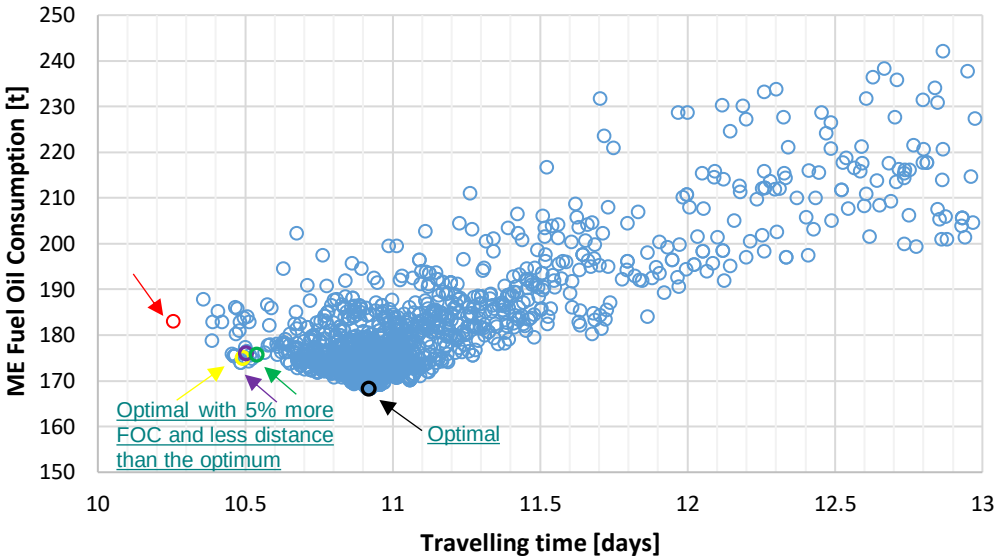

Figure 46: Algorithm's evolution regarding the time travel focused on 10 to 13 days.

Part of the optimization algorithm's evolution is presented in Figure 46, where the ME FOC versus the time duration of each candidate route is shown. The coloured circles represent specific routes mentioned in

Table 12. All calculations have been performed using the ship model.

Results showed that the "real" route follows the orthodromic path, which is the shortest path. However, the algorithm's optimal path requires 15 more hours of travel and 8% less FOC (Figure 47). More details as well as information about the "real – simulated" voyage and three more additional cases (with 5% more FOC than the optimal but with less distance required) are shown in

Table 12 and in Figure 48.

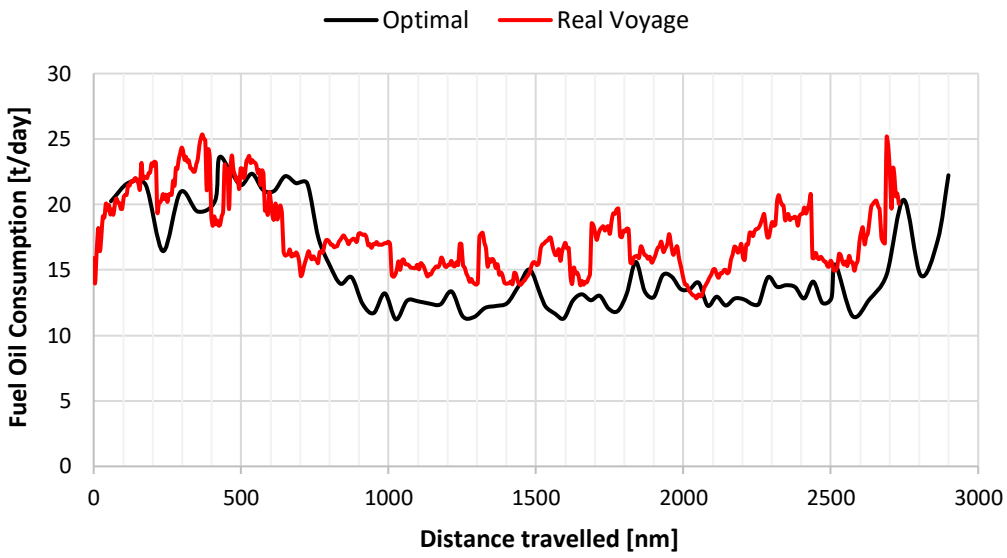

Figure 47: FOC for the optimal route vs. the original (real) one.

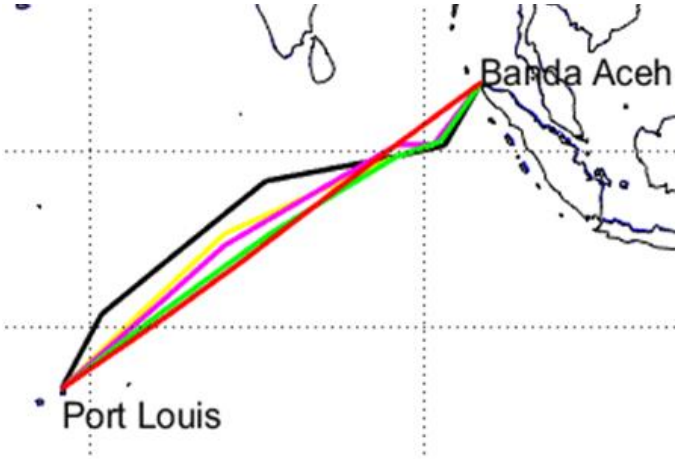

Figure 48: Real trajectory (red) along with potential optimal routes found by the genetic algorithm.

Table 12: Details about the real trajectory and results from the optimization.

	ME FOC		Total distance		ME FOC/distance travelled		Voyage duration
	[t]	[%]	[nm]	[%]	[t]	[%]	[days]
"Real" Voyage [red]	182.96	-	2731	-	0.067	-	10.26
Optimal [black]	168.24	-8.04	2899.01	+6.15	0.058	-13.37	10.92
Optimal [yellow]	174.97	-4.36	2785.44	+1.99	0.062	-6.23	10.49
Optimal [magenta]	175.94	-3.83	2788.24	+2.09	0.063	-5.80	10.50
Optimal [green]	178.78	-2.28	2757.83	+0.98	0.064	-3.23	10.39

The algorithm searches for routes where the added wave resistance is kept as low as possible, therefore following paths with lower significant wave height values and avoiding head seas (180^0).

Figure 49 shows the added wave resistance evaluated on the "real" and optimal routes.

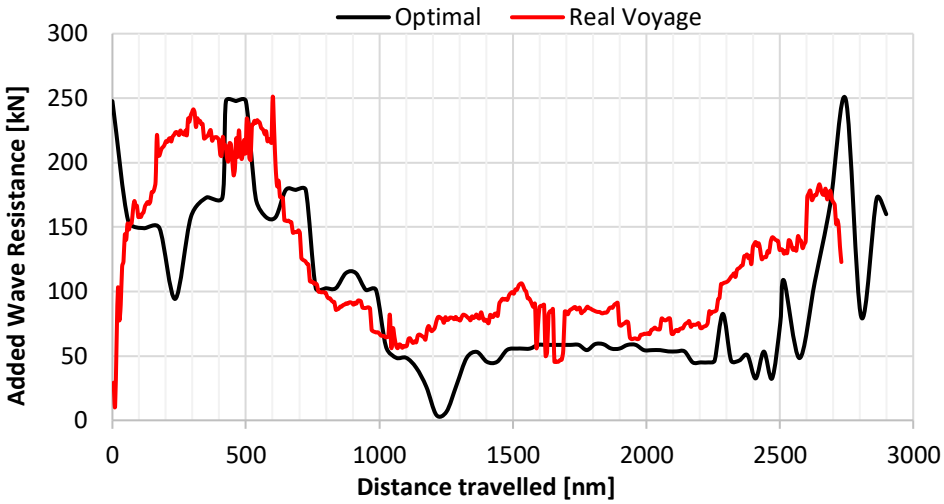

Figure 49: Added wave resistance along the real voyage and the optimal path.

6.6 Examined route with hydrodynamic related retrofit options

The “real” route and the optimal one are examined also with a fictitious 3% reduced calm water resistance and 1.5% better propeller performance (Figure 17 and Figure 18). In Figure 50 the differences in demanded power are presented for the real voyage, when improved performance has been assumed. In addition, Table 13 **Error! Reference source not found.**sums up all information about this scenario, in which the optimal route found on previous case is applied.

Table 13: Results for real voyage and optimal path considering retrofit options.

	ME FOC		Total distance		ME FOC/distance travelled		Voyage duration
	[t]	[%]	[nm]	[%]	[t]	[%]	[days]
“Real” Voyage [red] -Improved hydrodynamic case	175.69	-3.97	2731	-	0.064	-	10.26
Optimal [black] – Improved hydrodynamic case)	161.48	-11.74	2899.01	6.15	0.056	-16.85	10.92

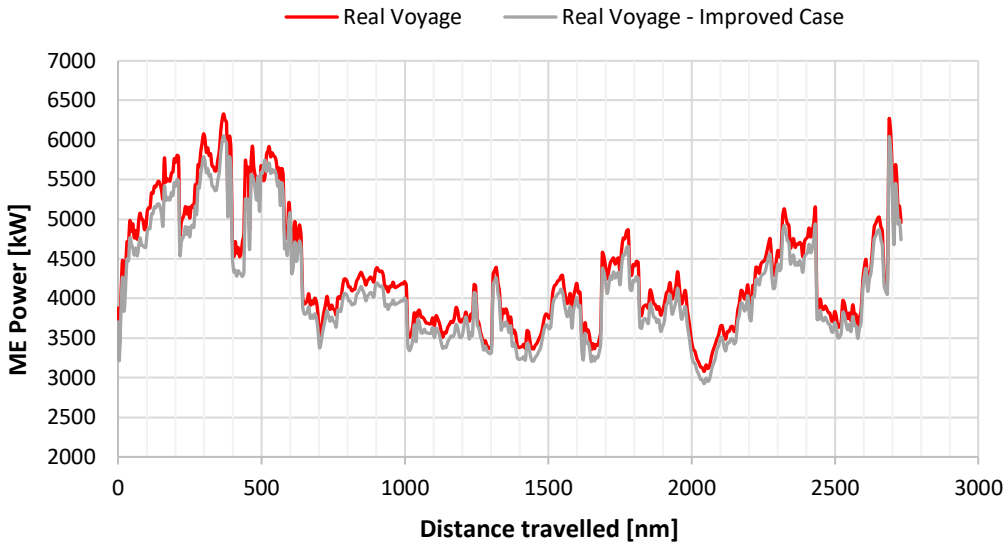

Figure 50: Comparison of demanded power along the real voyage between the original and the improved hydrodynamic case.

6.7 Examined route with WASP as retrofit option

6.7.1 Voyage simulation with WASP and optimization

In Section 6.3, the simulation of the "real" voyage has been presented using the 1-d.o.f. ship model for the required calculations. Here, the same voyage utilizing the WASP system using again the 1-d.o.f. ship model is analysed. This system consists of four eSAILs working together on board and powered by the ship's diesel generators, as presented in the previous section. When the WASP system does not positively contribute to propulsion, it is turned off. Regarding auxiliary power management, two diesel generators (DGs) are available during the voyage. The first generator (DG1) operates at 400 kW, when the eSAILs are not in use (as determined from the mean value in Task 6.1, where also the SFOC values of the DGs are presented). DG1 can handle up to 600 kW when the eSAILs are activated, with the remaining load distributed to DG2. In addition to the simulation, the optimization was performed for the voyage with the WASP system installed, having the objective of minimizing the fuel oil consumption. Figure 51 shows the optimal route on a typical map compared to the real route.

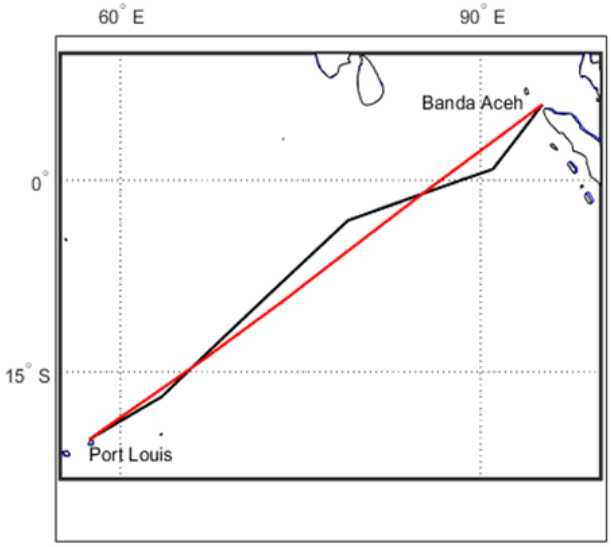

Figure 51: Optimal route with WASP (black) and the real (red) route.

Table 14 provides detailed information for both routes.

Table 14: Detailed information for the real and the optimal route (1-d.o.f. ship model).

	Total FOC	ME FOC	DG1 FOC	DG2 FOC	Distance	Voyage duration	δtotal FOC [%]	δME FOC [%]	δDG FOC [%]	ME FOC / distance
	[t]	[t]	[t]	[t]	[nm]	[days]				[ton/nm]
Real Voyage w/o WASP [red]	201.41	181.19	20.22	-	2721.88	10.26	-	-	-	0.067
Real Voyage with WASP [red]	181.14	155.01	22.60	3.52	2721.88	10.26	-10.06	-14.45	29.18	0.057
Optimal [black with WASP]	175.33	148.93	22.40	4.00	2781.29	10.48	-12.95	-17.80	30.56	0.054

The results demonstrate that for this examined route the installation of WASP reduces fuel oil consumption by approximately 10%. The impact of the WASP system is especially noticeable when the route is also optimized, resulting in additional fuel oil consumption savings of around 3%. Furthermore, the system led to a voyage length of an additional 60 nautical miles, which corresponds to approximately five more hours of travel.

In Figure 52 the variance of the ME power and its RPM is shown along the route of the real voyage, when WASP is operational or not. In Figure 53 the longitudinal force from the four eSAILs in comparison with the prevailing wind conditions along the real voyage is presented. As expected, the presence of the WASP reduces the main engine's power and RPM, and the major decreases occur in presence of side winds (near 90º) of large intensity and consequently increased sails' forces. The optimization algorithm seeks for a balance between the benefits of the WASP system and the selection of favorable routes, considering sea currents and waves, ultimately reducing fuel oil consumption.

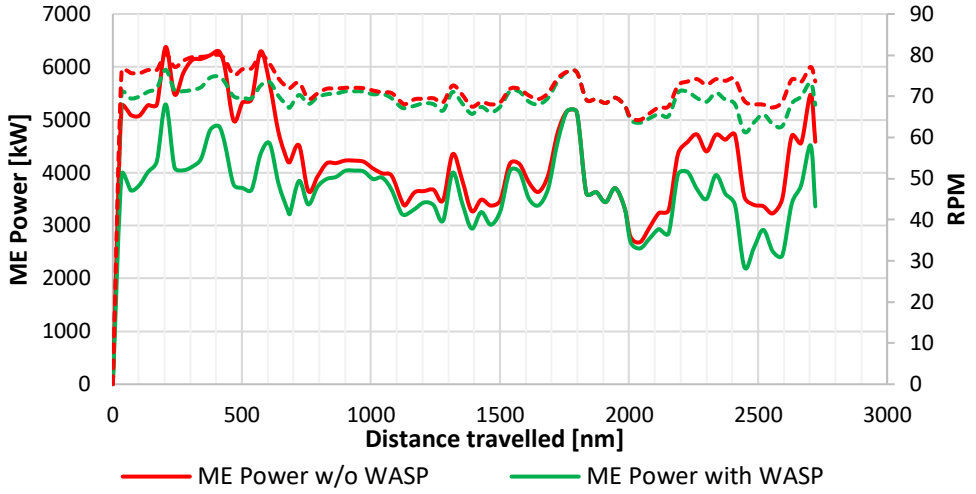

Figure 52: ME Power and RPM for the real voyage with and without (w/o) WASP system.

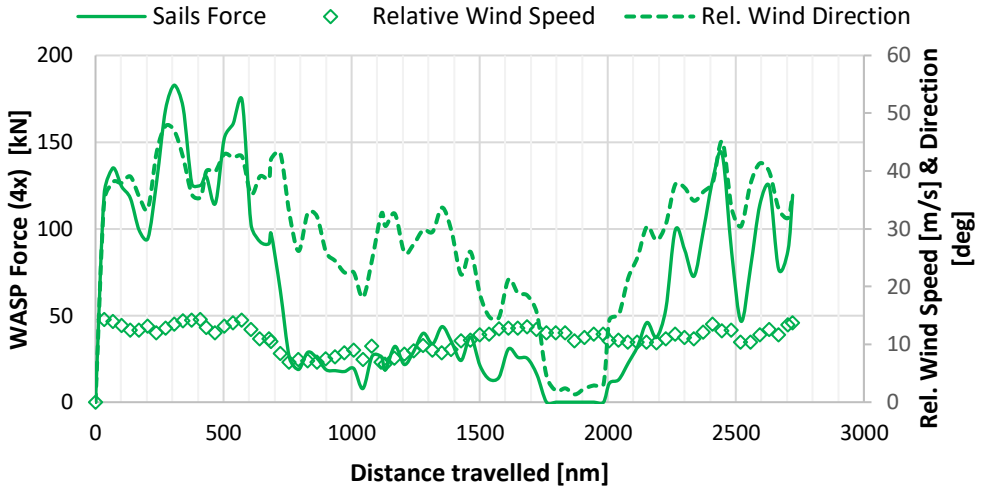

Figure 53: WASP longitudinal force, relative wind speed and direction for the real voyage.

In Table 15 the mean values of all resistance components and the longitudinal WASP force are presented for the real voyage and the optimal route.

Table 15: Mean values for resistance components and WASP force for the real voyage and the optimal route.

	Optimal route	Real voyage
Calm Water Resistance [kN]	365.84	375.91
Wave Resistance [kN]	105.45	121.93
Wind Resistance [kN]	27.08	27.71
WASP force [kN]	57.78	63.84

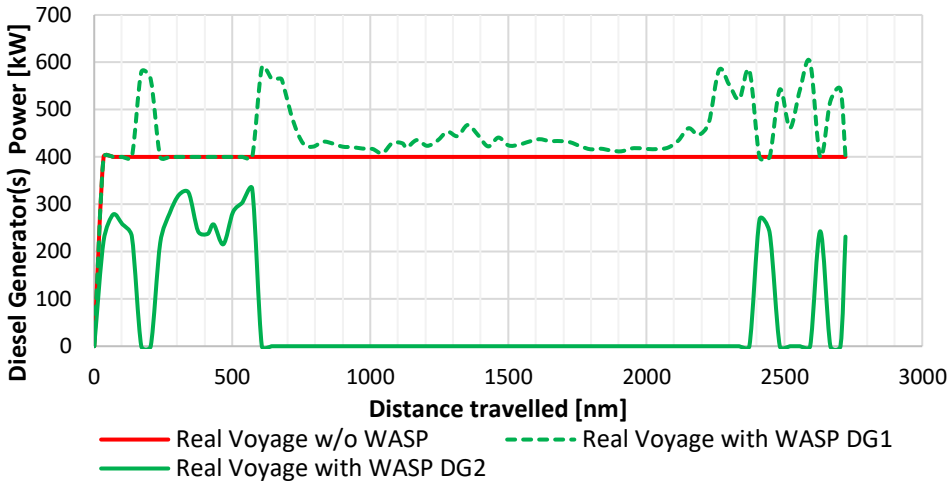

Figure 54: DGs' demanded power for the real voyage with and without (w/o) WASP system.

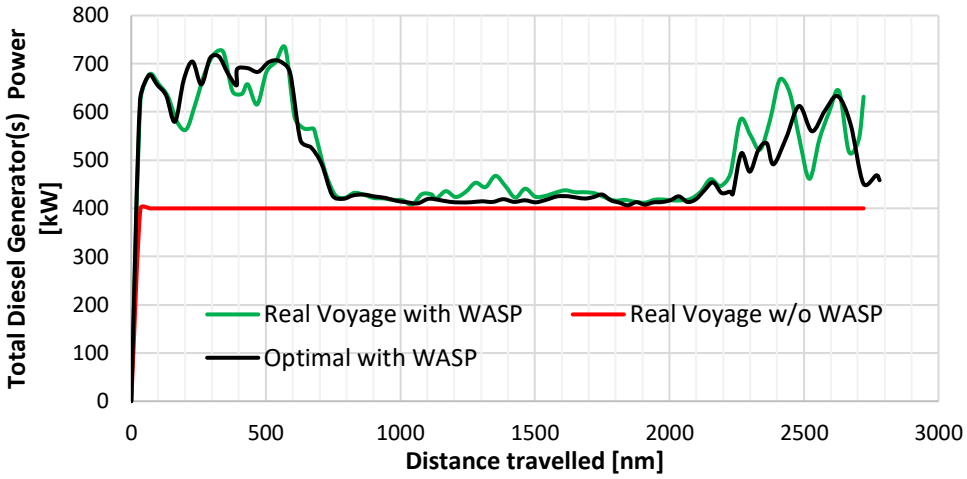

Figure 55: DGs' demanded total power for the real voyage with and without (w/o) WASP system and for the optimal path.

Moreover, the power required by the WASP system, as already mentioned, is generated by the auxiliary system of the ship. One or two diesel generators supply the system with the power needed, which fluctuates depending on the prevailing conditions. When there is no WASP system the generator operates only for the ship's electrical needs assuming a constant supply of 400 kW (Figure 54 and Figure 55).

7 Case study using the 3-d.o.f. ship model

7.1 Comparison of the results with the optimal route of 1-d.o.f. ship model

All the above results 6.7.1(Section 6.7.1) refer to 1 degree of freedom ship model (1-d.o.f.). However, to gain a clearer understanding and more accurate evaluation of the impact of the WASP system on the ship's operation, the 3-d.o.f. ship model is also employed to examine the ship's behaviour and its interaction with the WASP system. The optimal route found when the WASP is installed (1-d.o.f. ship model) will be examined in the following cases:

- without (w/o) WASP and using the 1-d.o.f. ship model,
- without (w/o) WASP and using the 3-d.o.f. ship model,
- with WASP and using the 3-d.o.f. ship model.

The main engine power along the route for the above mentioned scenarios are presented in Figure 56**Error! Reference source not found.**, whereas in Figure 57 the apparent wind speed and its direction is shown.

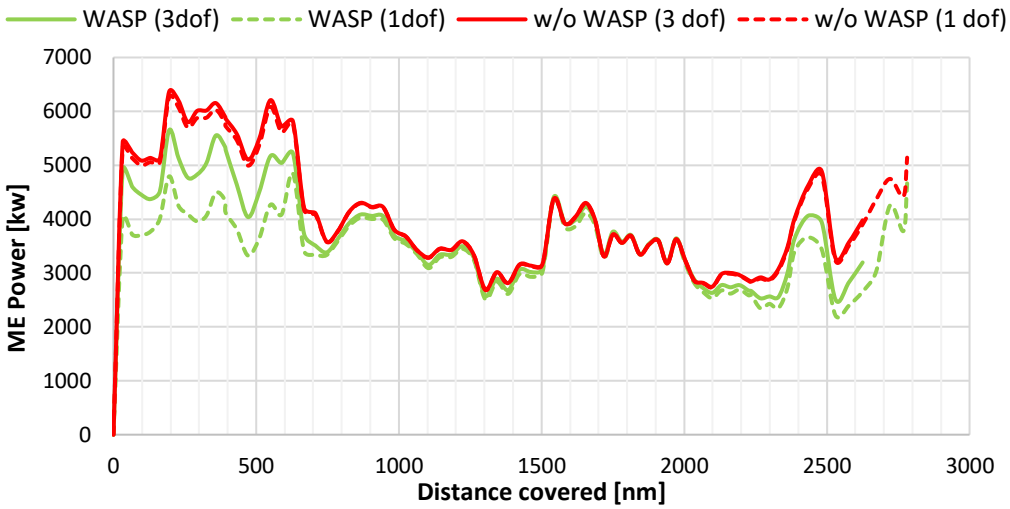

Figure 56: ME power with and w/o WASP for 1-d.o.f. and 3-d.o.f. for the optimal path.

It is evident that high wind speeds prevailing during the first 500 nautical miles, combined with quarter-to-bow wind angles, lead to decreased ME power demands when the WASP system is installed, particularly when the 1-d.o.f. model is considered. Under these conditions and when the 3-d.o.f. model is used the transverse forces generated by the wind and the WASP system are significant compared with all the longitudinal forces (Figure 58) In addition, the rudder resistance increases as well as the longitudinal force from the WASP system(Figure 59).

As illustrated in Figure 60, which presents data on induced drift and rudder angles, high rudder resistance values are also justified.

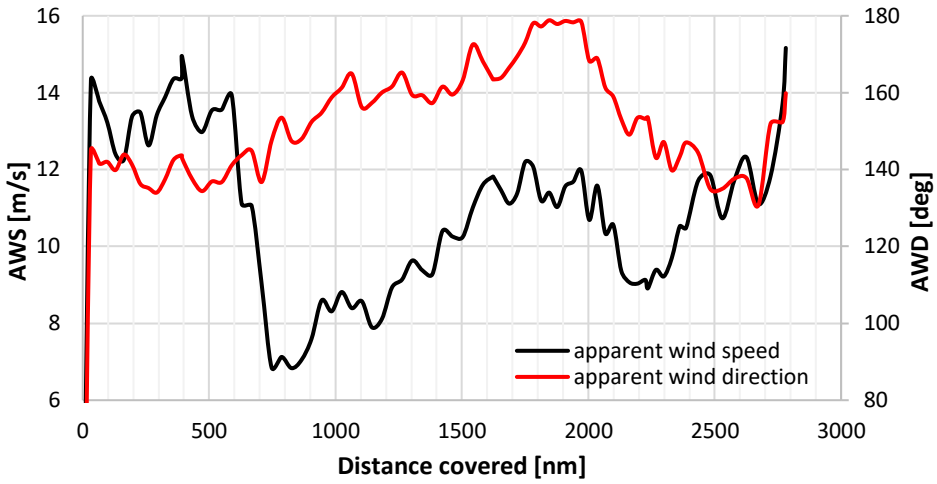

Figure 57: Prevailing wind conditions for the optimal path corresponding to 1-d.o.f. ship model.

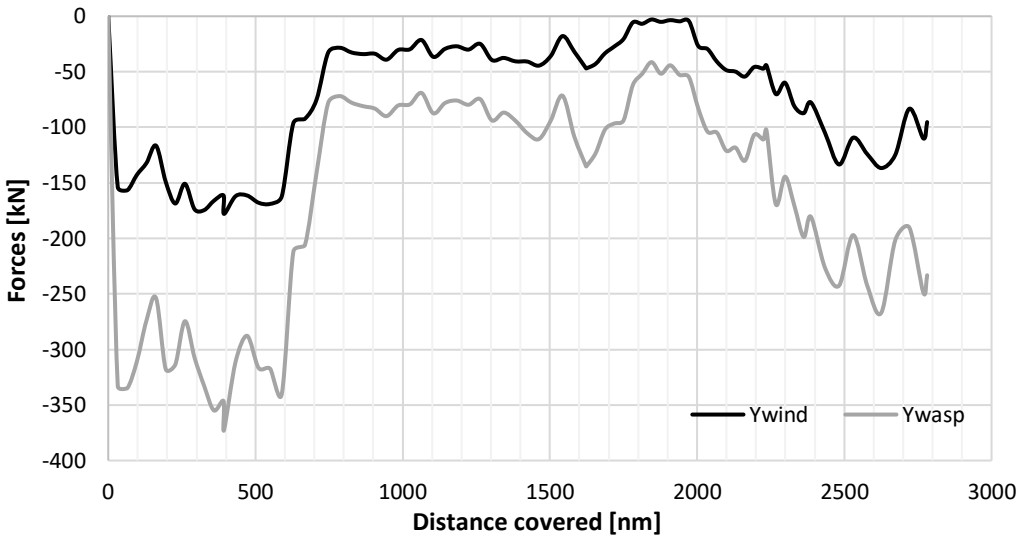

Figure 58: Transverse forces along the optimal path.

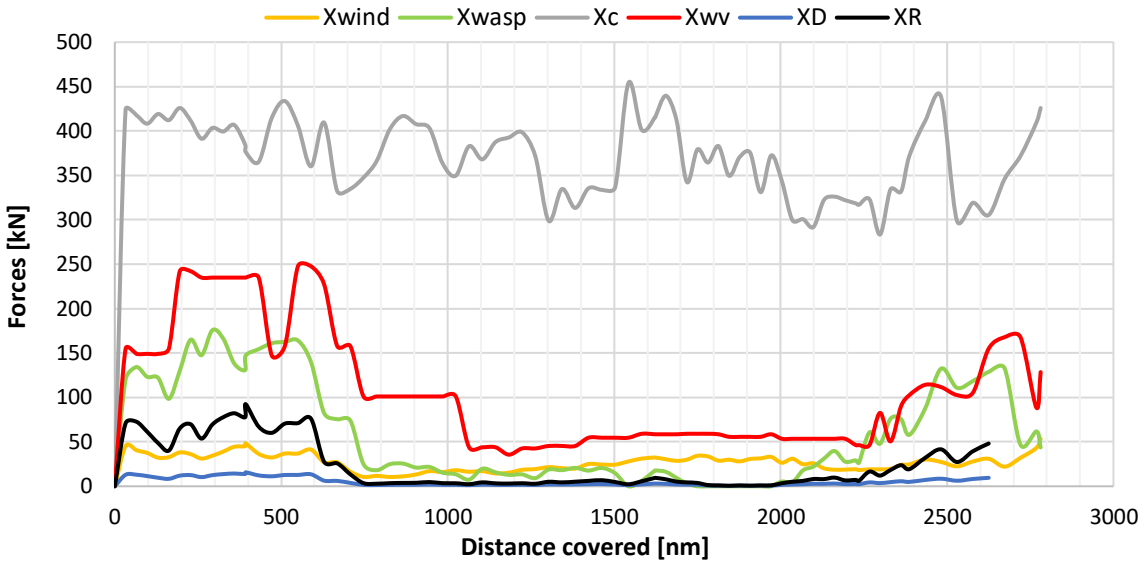

Figure 59: Longitudinal forces along the optimal path.

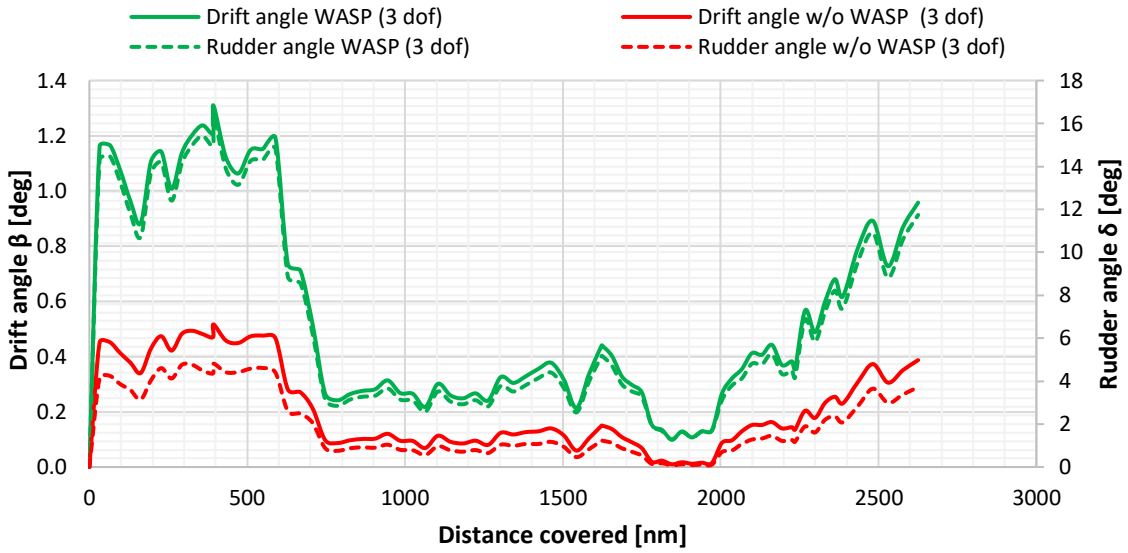

Figure 60: Drift and rudder angles along the optimal route considering different scenarios.

7.2 Comparison of previous results with the optimal route derived from the 3-d.o.f. ship model

A new optimization has been conducted using a genetic algorithm, considering the 3-d.o.f. Ship model, with 100 generations and a population size of 100 individuals per generation. The ship speed is constant at 11kn and a constraint for the rudder angle is applied, as mentioned in Section 4.3 and

Eq. 65. In Figure 61 the optimal route considering the 3-d.o.f. ship model is plotted on the map along with the real route and the 1-d.o.f. ship model optimal. In addition, in Figure 62 the apparent wind speed (AWS) and its direction (AWD) along the new optimal route is shown.

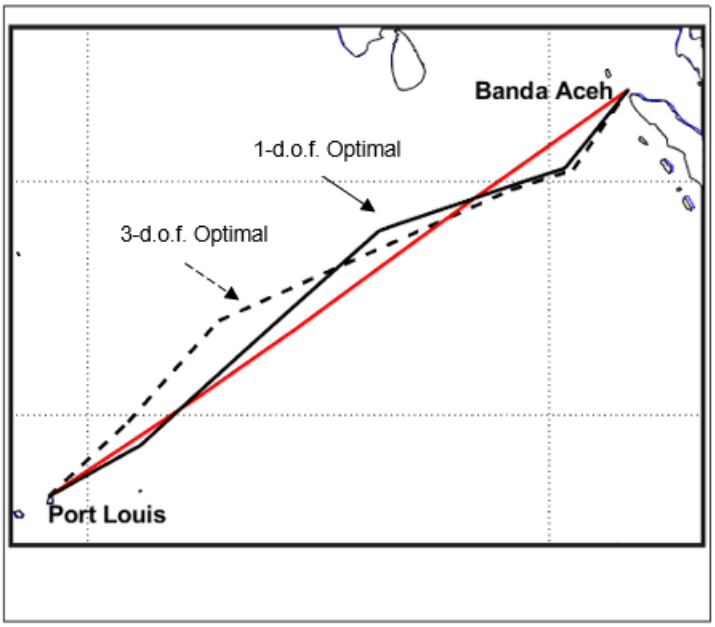

Figure 61: Real voyage (red) and the optimal routes found with 3-d.o.f. and 1-d.o.f. Ship Models when WASP is considered.

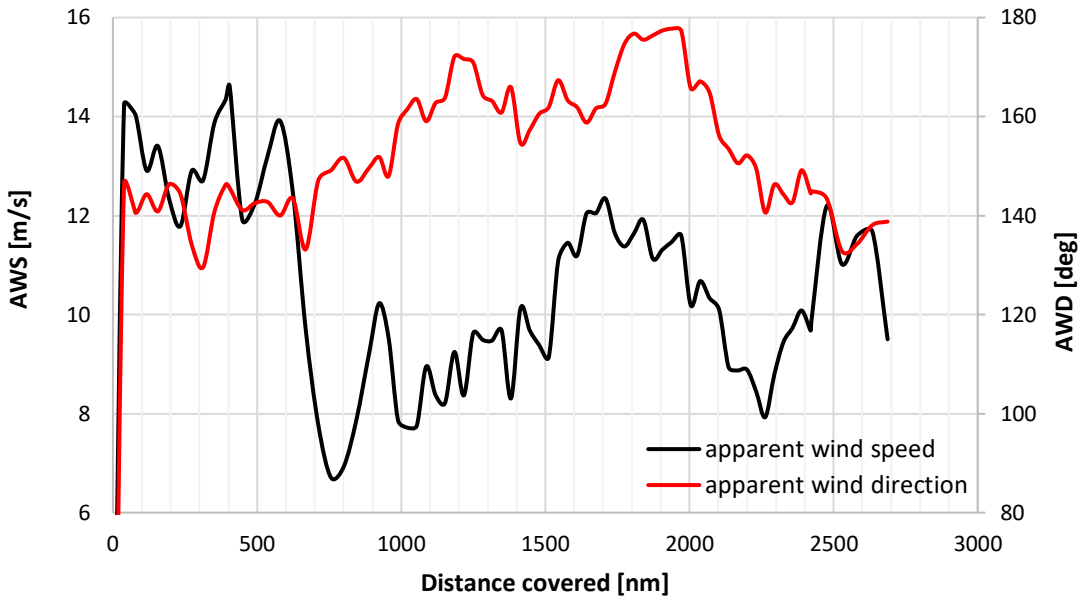

Figure 62: Apparent wind speed and direction along the 3-d.o.f. optimal route.

A notable point of comparison is between the newly obtained optimal solution (3-d.o.f. ship model optimal) and the one identified during the WASP optimisation (1-d.o.f. ship model optimal), which highlights the compromises required to achieve a new optimal solution when using the 3-d.o.f. ship model. The optimal obtained from the 3-d.o.f. ship model requires approximately 3[t] less fuel oil than the optimal obtained from the 1-d.o.f. ship model, as tested with the 3-d.o.f. ship model. However, it should be noted that the 3-d.o.f. model requires about two more hours of travel time. In Figure 63 , the drift and rudder angles are compared, showing that the algorithm seeks for paths to maintain low rudder angles , and consequently to keep the rudder resistance as low as possible (Figure 64).

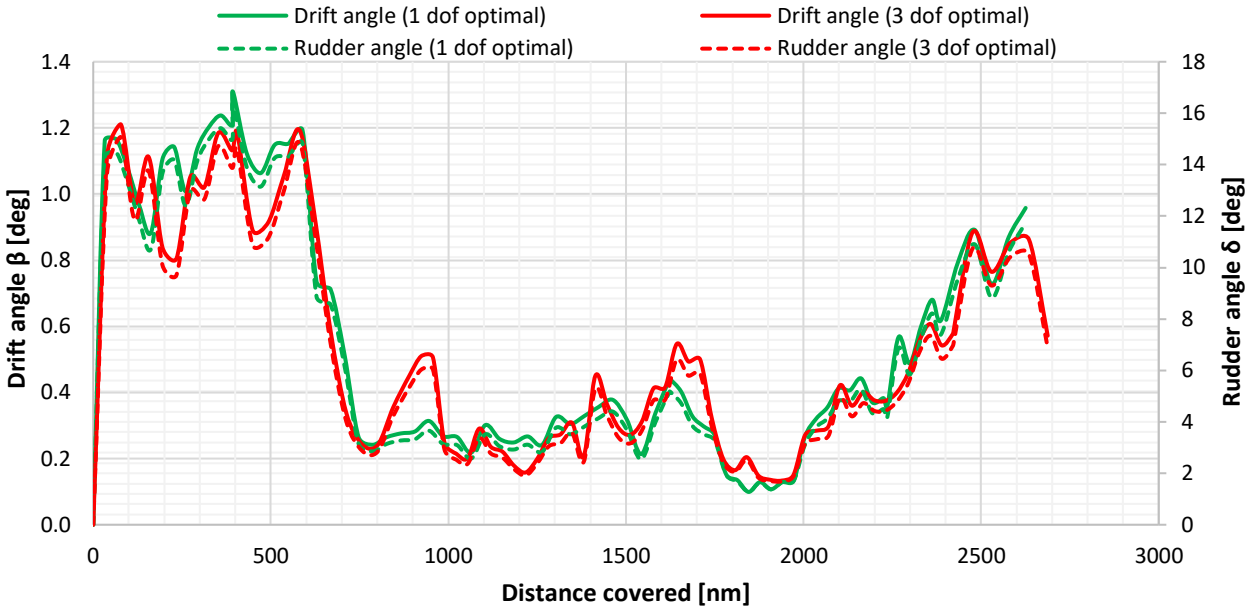

Figure 63: Drift and rudder angles along the 3-d.o.f. and the1-d.o.f. optimal paths.

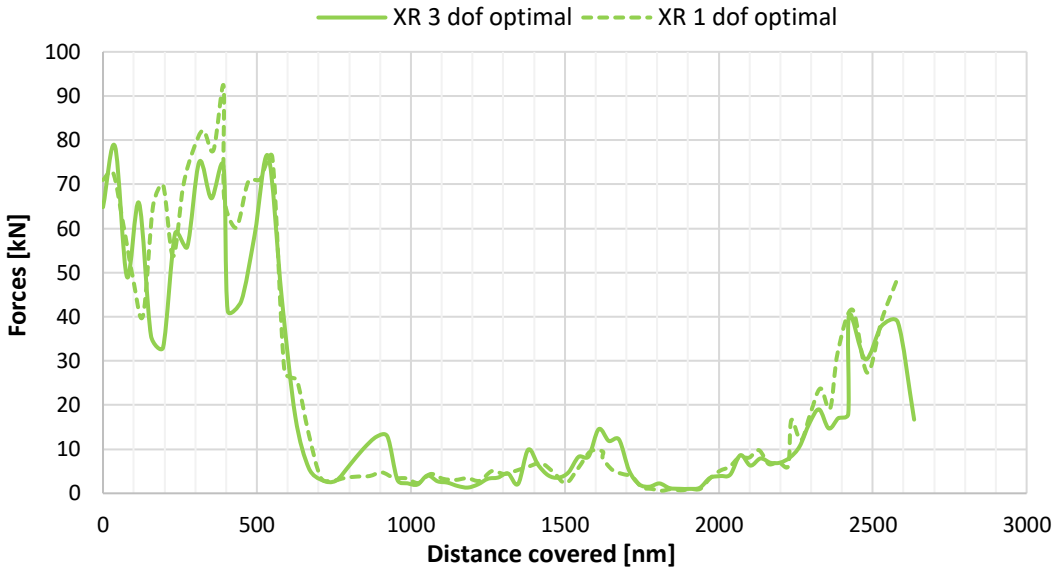

Figure 64: Longitudinal rudder forces along the 3-d.o.f. and 1-d.o.f. optimal paths.

In Figure 65 and Figure 66 the transverse and the longitudinal forces from the WASP system are presented, respectively. A trade-off between the longitudinal and transverse force developed by the WASP system is needed so the optimal path will maximize the first one while keep the second low to prevent the development of high rudder angles. The main engine FOC for both optimal routes are plotted in Figure 67, showing that the new optimal solution achieves a slight lower consumption in total. This reduction is also presented in Table 16, that summarizes all the information for the evaluation of all routes tested when using both the 1-d.o.f. and the 3-d.o.f. model. It is clear that,

when the 3-d.o.f. ship model is taken into consideration, FOC decreases for the real voyage when the WASP system is in use. That decrease is about 4.5%, highlighting the effectiveness of the WASP system for this specific route. Results are even more prominent when route optimization is performed, resulting to an additional improvement of about 5%. However, the optimal path requires 7.5 more hours of travel than the real voyage, when the same constant speed is considered.

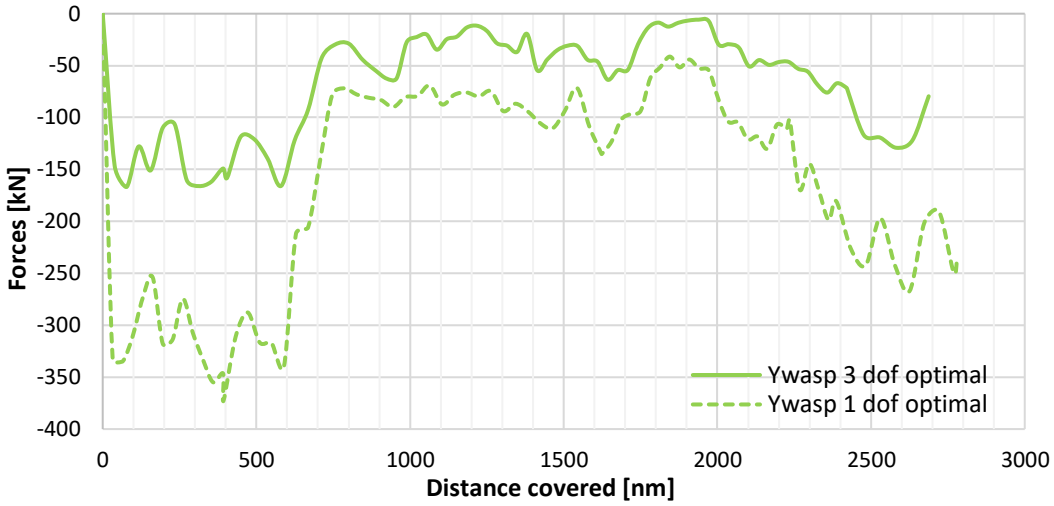

Figure 65: Transverse WASP forces for the 3-d.o.f. and 1-d.o.f. optimal paths.

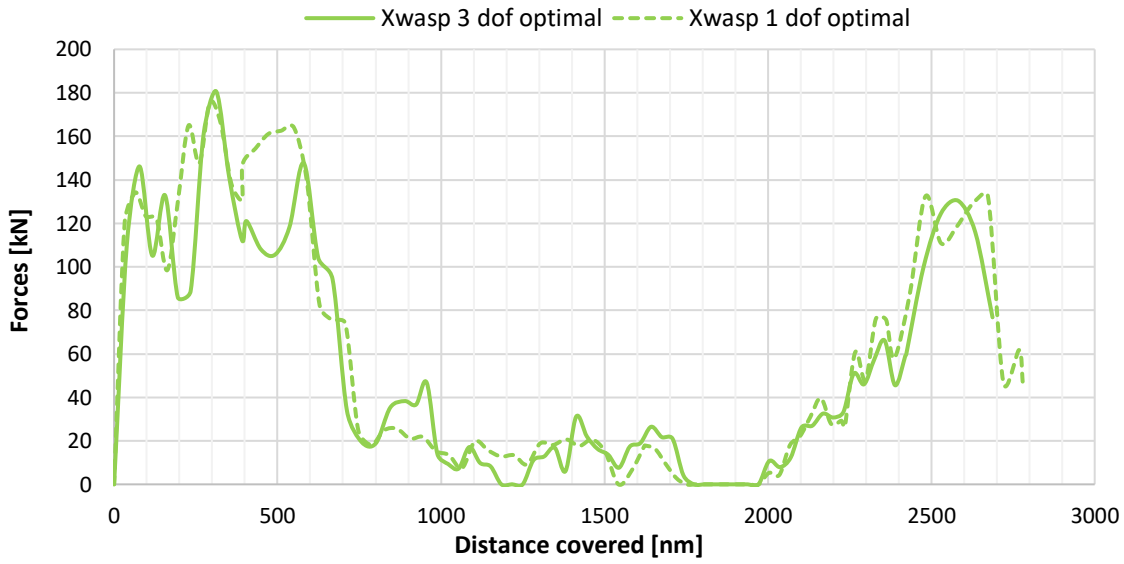

Figure 66: Longitudinal WASP forces for the 3-d.o.f. and 1-d.o.f. optimal paths.

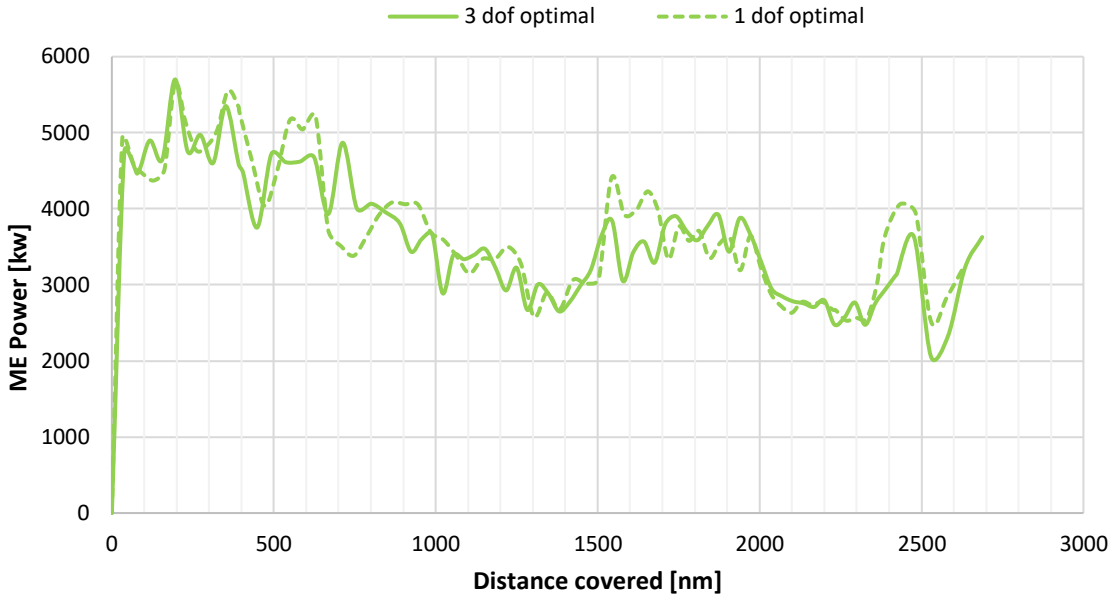

Figure 67: ME power along the 3-d.o.f. and 1-d.o.f. optimal paths.

In the following table (Table 16) a sum up of all routes tested with both the 1-d.o.f. and the 3-d.o.f. models is presented:

Table 16: Summary results for the examined routes using the 1d.o.f. and 3-d.o.f. models.

		Total FOC	ME FOC	DG FOC	Distance	Time	δTotal FOC	δME FOC	δDG FOC	Total FOC/Dist.
		[t]	[t]	[t]	[nm]	[days]	[%]	[%]	[%]	[t/nm]
Real Voyage										
w/o WASP	1-d.o.f.	201.41	181.19	20.22	2721.88	10.26	-	-	-	0.074
	3-d.o.f.	203.08	182.86	20.22	2721.88	10.26	0.82	0.09	0	0.075
with WASP	1-d.o.f.	181.14	155.01	26.12	2721.88	10.26	-10.06	-14.45	29.18	0.067
	3-d.o.f.	194.05	167.92	26.12	2721.88	10.26	-3.65	-7.32	29.18	0.071
Optimal with WASP [1-d.o.f.]										
w/o WASP	1-d.o.f.	194.48	173.82	20.66	2781.29	10.48	-3.44	-4.06	2.18	0.069
	3-d.o.f.	196.06	175.40	20.66	2781.29	10.48	-2.66	-3.19	2.18	0.070

with WASP	1-d.o.f.	175.33	148.93	26.40	2781.29	10.48	-12.95	-17.80	30.56	0.063
	3-d.o.f.	187.16	160.76	26.40	2781.29	10.48	-7.07	-11.27	30.56	0.067
Optimal [3-d.o.f.]										
with WASP	3-d.o.f.	184.64	158.87	26.90	2804.91	10.57	-8.32	-12.31	33.03	0.066

8 Conclusions

The enhancement of the ship model of NTUA's weather routing tool to account for retrofit measures is presented. The developed tool can be used for the assessment of retrofit measures along specific routes, with and without route optimization. The ship model is designed to calculate the shaft power and the main engine's fuel oil consumption, obtaining information from model tests, sea trials and shop tests provided for the examined bulk-carrier MV KASTOR. The model provides resistance estimation in calm water, as well as propeller and main engine characteristics modelling. In addition, semi-empirical methods available in ITTC are utilized to calculate the added resistance due to wind and waves. Due to the computational cost implications, regression techniques were also employed to develop suitable surrogate models for added resistance in waves, and a comparison for the goodness of fit was carried out. In addition, real operational measurements regarding the shaft power were available and compared with the respective predictions from the ship model for the initial design. Specifically, a real voyage of the vessel was simulated and compared with the available information from noon reports. Results showed good agreement between real fuel oil consumption and the calculated one from the ship model. Finally, optimization performed for the same voyage, resulting in the identification of optimal routes that achieved significant reductions in fuel oil consumption. These gains range between 2.3-8% fuel oil savings, depending on the length of the optimal route.

The ship model was enhanced also to incorporate retrofit options, such as the hydrodynamic optimization of the propeller and bulbous bow, as well as the use of an ALS and WASP, by appropriately modifying and introducing relevant parameters to the problem. Specifically, two ship models were developed: one accounting only for longitudinal forces (1-d.o.f.) and another incorporating transverse forces, yaw moments, as well as the corresponding hydrodynamic hull and rudder forces (3-d.o.f.). Firstly, fictitious hydrodynamic improvements related to propeller efficiency and calm water resistance reduction were examined using the 1-d.o.f. ship model along the above-mentioned route.

Next, the case of B4B's eSAILs system was examined, using a specific configuration for the examined bulk-carrier. A scenario of true wind and ship's speed corresponding to 7.5m/s and 11kn respectively, using the 1-d.o.f. ship model resulted in a fuel gain up to 27%, for a wide range of apparent wind heading. Nevertheless, the 3-d.o.f. ship model resulted in fuel reductions of up to 25% for a range of headings below 130°. The system was tested for the same voyage, calculating the fuel savings achieved by the WASP as well as a new optimal route. In this case, the auxiliary power needs for the usage of this WASP configuration were also considered. When using the 1-d.o.f. ship model, results show that, when WASP is in operation, fuel oil savings can reach up to 10% compared to the same voyage without the usage of WASP. When route optimization was enabled, this gain increased by about 3%. On the other hand, the 3-d.o.f. ship model reduced the WASP gains to 3.65% for the initial route considered, resulting thus to a 7.5% performance reduction of the WASP. Moreover, optimal routes are different depending on which model (1 or 3-d.o.f) is considered. For example, the optimal route corresponding to the 1-d.o.f. model achieves a total FOC reduction of 12.95%, whereas the respective reduction for the same route considering the 3-d.o.f. model is reduced to 7.07%. This reduction is improved to 8.32% when performing the optimization for the 3-d.o.f. model, however the voyage duration is increased by 7.5 hours compared to the initial one.

Except from fuel oil minimization, safety is also an aspect under consideration. Safety criteria were defined acting as constraints when examining optimal routes. The criteria are motion-based

(seakeeping) criteria, and specifically target the slamming of bulbous bow, the deck wetness, the propeller immersion as well as excessive accelerations in critical locations (e.g. at ship's bridge). The analysis was based on RAOs of heave, pitch and roll motions derived from strip theory. In addition, the captain is provided with a set of criteria based on IMO guidance, the aim of which is to prevent dangerous ship instability phenomena, including course-keeping.

References

[1] Bentin, M.; Zastrau, D.; Schlaak, M.; Freye, D.; Elsner, R.; Kotzur, S. (2016). A new routing optimization tool-influence of wind and waves on fuel consumption of ships with and without wind assisted ship propulsion systems. *Transportation Research Procedia,* 14, pp. 153 – 162.

[2] Lele, A.; Rao, K. V. S. (2017). Net Power Generated by Flettner Rotor for Different Values of Wind Speed and Ship Speed, International Conference on circuits Power and Computing Technologies [ICCPCT].

[3] Ma, R.; Wang, Z.; Wang, K.; Zhao, H.; Jiang, B.; Liu, Y.; Xing, H.; Huang L. (2023). Evaluation Method for Energy Saving of Sail-Assisted Ship Based on Wind Resource Analysis of Typical Route, Journal of Marine Science and Engineering, 11, 789.

[4] Ghorbani, M.; Slaets, P.; Lacely, J. (2023). A numerical simulation tool for a wind-assisted vessel verified with logged data at sea, *Ocean Engineering*, 290,116319.

[5] Tillig, F., & Ringsberg, J. (2019) A 4 DOF simulation model developed for fuel consumption prediction of ships at sea, Ships and Offshore Structures, 14:sup1, pp. 112-120, DOI: 10.1080/17445302.2018.1559912

[6] Elger, D.E.; Bentin, M.; Vahs, M. (2020). Comparison of different methods for predicting the drift angle and rudder resistance by wind propulsion systems on ships, *Ocean Engineering*, 217.

[7] Kytariolou, A.; Themelis, N.; (2022). Ship routing optimisation based on forecasted weather data and considering safety criteria, The Journal of Navigation, pp. 1-22.

[8] Matlab. (2022). Global optimisation toolbox user's guide, The MathWorks, Inc., Natick, Massachusetts, United States.

[9] Holtrop, J.; Mennen, G. G. J. (1982). An approximate power prediction method. *International Shipbuilding Progress, 29* (335), pp. 166–170.

[10] Liu, S.; Papanikolaou, A.; (2020). Regression analysis of experimental data for added resistance in waves of arbitrary heading and development of a semi-empirical formula, Ocean Engineering, 206, 107357.

[11] International Towing Tank Conference (ITTC). (2021). *Recommended Procedures and Guidelines: Resistance and Propulsion*. Proceedings of the 29th ITTC.

[12] Lloyd, A.R.J.M. (1989) Seakeeping: Ship Behavior in Rough Weather. Ellis Harwood Limited, Chichester.

[13] Blendermann, W. 1994. Parameter identification of wind loads on ships, *Journal of wind engineering and industrial aerodynamics*, 51, pp. 339-351.

[14] Skogman, A. (1985). The practical meaning of lateral balance for a sail-assisted research vessel, *Journal of Wind Engineering and Industrial Aerodynamics*, 20, pp. 201-226.

[15] Inoue, S; Hirano, M.; Kijima, K. (1981). Hydrodynamic derivatives on ship manoeuvring, *International Shipbuilding Progress*, pp. 112-125.

[16] Lewis, E.V. (1989). Motions in Waves and Controllability, *Principles of Naval Architecture*, vol. 3, Society of Naval Architects and Marine Engineers, Jersey City, NJ.

[17] Hirano, M. (1980). On calculation method of ship manoeuvring motion at initial design phase, *J. Soc. Nav. Archit. Japan*, 147, pp. 144-153.

[18] O'Hanlon, J. F.; & McCauley, M. E. (1974). Motion sickness incidence as a function of the frequency and acceleration of vertical sinusoidal motion. *Aerospace Medicine, 45*(4), pp. 366-369.

[19] Ghaemi, M.H.; Olszewski, H.; (2017). Total ship operability – Review, concept and criteria, *Polish Maritime Research*, Special Issue S1 93, vol. 24, pp. 74-81.

[20] International Maritime Organization (IMO). (2007). *Revised Guidelines for Formal Safety Assessment (FSA) for Use in the IMO Rule-Making Process*. MSC/Circ.1023-MEPC/Circ.392. London: IMO.

[21] Maxsurf (2023). Maxsurf Motions User Manual, Computer software, Bentley Systems. Available: https://www.bentley.com

Appendix A – Seakeeping

Maxsurf software [21] has been employed to calculate the RMS motions at center of gravity for different sea states and the respective results are presented in the next tables. Maxsurf Motions uses the strip theory method for seakeeping analysis [12], particularly for predicting Response Amplitude Operators (RAOs). This method involves dividing the vessel into a series of transverse sections along its length. Each section is treated as a two-dimensional slice, and its hydrodynamic properties are calculated individually. The coefficients for these sections are then integrated along the entire hull to derive the global hydrodynamic coefficients used in the vessel's equations of motion.

For RAO calculations, the software works in the frequency domain, which means it computes responses as a function of frequency. This allows for efficient prediction of motion behavior without high computational cost. Additionally, factors such as vessel speed can be included in the RAO computation, to account for the changes in frequency response due to forward motion. These RAOs are essential for evaluating safety criteria and determining relative velocities and accelerations under different sea conditions, making the strip theory method particularly useful for initial seakeeping assessments. Assuming that the response function (e.g. heave) is linear with respect to wave amplitude and the principle of superposition holds:

$$RAO_z = \frac{z_0(\omega_e)}{\zeta_a(\omega_e)} \quad \text{Eq. 66}$$

Where RAO_z is the heave Response Amplitude Operator and $z_0(\omega_e)$ is the heave motion amplitude at encountered frequency ω_e.

Then the motion response spectrum is:

$$S_z(\omega_e) = RAO_z(\omega_e)^2 S_\zeta(\omega_e) \quad \text{Eq. 67}$$

Where $S_\zeta(\omega_e)$ is the encountered wave energy spectrum and z indicates the heave motion.

Next, as the variances of the amplitude, velocity and acceleration of the motion at an appropriate location on the ship can be calculated by using the zero, second and fourth spectral moment (n=0,2,4 in Eq. 67) of the motion energy spectrum:

$$m_n = \int_0^\infty \omega^n S_z(\omega_e) d\omega_e \quad \text{Eq. 68}$$

And the respective RMS values are given by $\sqrt{m_n} \quad for\ n = 0,2\ and\ 4$.

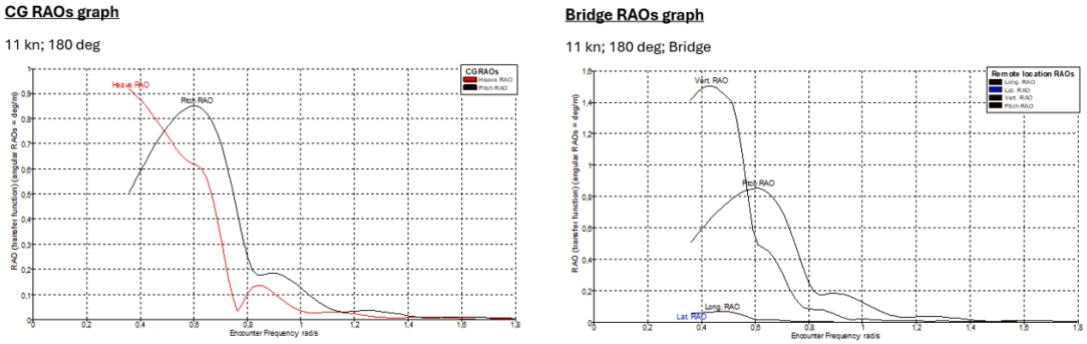

Figure 68: Typical RAO graphs with respect to centre of gravity and bridge.

All seakeeping criteria and safety constraints have been checked for the loading conditions mentioned in Table 17:

Table 17: Loading conditions considered for the safety criteria.

Loading condition	Mean draft [m]	VCG [m]	LCG [m]	Displacement [tn]
Full Load (No. 8)[3]	14.45	11.35	113.83	94796.20
Ballast (No. 01)[3]	6.37 [T_F=4.78; T_A=7.96]	10.40	111.23	38543.88

Maxsurf software has been employed to calculate the RMS motions at center of gravity for different sea states and the respective results are presented in the next tables (i.e., Table 18 to Table 20; Table 21 to Table 33).

Table 18: Heave and Pitch RMS (Heading 180 [deg], V=11[kn]).

Sea state	RMS Heave [m]		RMS Pitch [deg]	
	Ballast condition	Full Load	Ballast condition	Full Load
H_s=2m – T_p=8.85s	0.062	0.040	0.100	0.081
H_s=4m – T_p=12s	0.234	0.370	0.540	0.580
H_s=6m – T_p=16s	0.836	0.997	1.000	1.020

Table 19: Heave and Pitch RMS (Heading 180 [deg], V=14[kn]).

Sea state	RMS Heave [m]		RMS Pitch [deg]	
	Ballast condition	Full Load	Ballast condition	Full Load
H_s=2m – T_p=8.85s	0.053	0.038	0.092	0.072
H_s=4m – T_p=12s	0.244	0.414	0.540	0.590
H_s=6m – T_p=16s	0.858	1.105	1.020	1.060

Table 20: Heave, Pitch, and Roll RMS (Heading 150 [deg], V=11[kn]).

Sea state	RMS Heave [m]		RMS Pitch [deg]		RMS Roll [deg]	
	Ballast condition	Full Load	Ballast condition	Full Load	Ballast condition	Full Load
H_s=2m – T_p=8.85s	0.045	0.044	0.110	0.110	0.620	0.120

[3] Number of loading condition from Loading Manual.

H_s=4m – T_p=12s	0.285	0.393	0.590	0.600	2.920	0.370
H_s=6m – T_p=16s	0.941	1.043	0.950	0.940	2.840	1.180

As mentioned above, in the following tables, spectral moments m_0, m_2, m_4 are the variances of the amplitude, velocity and acceleration respectively, of the relative motion at the appropriate location on the ship.

CASE A: Propeller emergence

Table 21: Propeller emergence (Heading 180 [deg], V=11[kn]).

Sea state and loading conditions	**Relative r_3** [m]	**Absolute s_3** [m]	m_0 [m²]	m_2 [m²/s²]	m_4 [m²/s⁴]	P_{pe}	T_{p_av} [s]	N_{pe} per hour
	RMS	RMS						
H_s=2m – T_p=8.85s Full load	0.492	0.167	0.242	0.382	0.977	0	3.9	0
H_s=4m – T_p=12s Full load	0.862	1.038	0.742	0.692	1.371	0	4.5	0
H_s=6m – T_p=16s Full load	1.150	1.992	1.324	0.740	1.105	0	5.1	0
H_s=2m – T_p=8.85s Ballast condition	0.384	0.211	0.148	0.318	1.534	0	2.8	1.08
H_s=4m – T_p=12s Ballast condition	1.089	1.000	1.187	0.882	2.175	0.142	4.0	128.2
H_s=6m – T=16s Ballast condition	1.413	2.067	1.996	0.932	1.662	0.215	4.7	165.0

Table 22: Propeller emergence (Heading 180 [deg], V=14[kn]).

Sea state and loading conditions	**Relative r_3** [m]	**Absolute s_3** [m]	m_0 [m²]	m_2 [m²/s²]	m_4 [m²/s⁴]	P_{pe}	T_{p_av} [s]	N_{pe} per hour
	RMS	RMS						
H_s=2m – T_p=8.85s Full load	0.496	0.152	0.246	0.439	1.223	0	3.7	0
H_s=4m – T_p=12s Full load	0.876	1.155	0.768	0.809	1.763	0	4.7	0
H_s=6m – T_p=16s Full load	1.202	2.101	1.445	0.890	1.433	0	4.9	0
H_s=2m – T_p=8.85s Ballast condition	0.414	0.180	0.171	0.412	2.200	0.001	2.7	2.3
H_s=4m – T_p=12s Ballast condition	1.040	0.981	1.082	0.992	3.075	0.129	3.6	130.9
H_s=6m – T_p=16s Ballast condition	1.368	2.066	1.873	1.041	2.362	0.206	4.2	178.4

Table 23: Propeller emergence (Heading 150 [deg], V=11[kn]).

Sea state and loading conditions	**Relative r_3** [m]	**Absolute s_{33}** [m]	m_0 [m²]	m_2 [m²/s²]	m_4 [m²/s⁴]	P_{pe}	T_{p_av} [s]	N_{pe} per hour
	RMS	RMS						
H_s=2m – T_p=8.85s Full load	0.475	0.229	0.225	0.352	0.895	0	3.9	0
H_s=4m – T_p=12s Full load	0.836	1.237	0.698	0.625	1.240	0	4.4	0
H_s=6m – T_p=16s Full load	1.075	2.043	1.156	0.637	0.973	0	5.0	0
H_s=2m – T_p=8.85s Ballast condition	0.396	0.233	0.157	0.297	1.333	0.001	3.0	1.4
H_s=4m – T_p=12s Ballast condition	1.095	1.196	1.199	0.837	1.909	0.143	4.2	124.3
H_s=6m – T_p=16s Ballast condition	1.323	2.108	1.751	0.826	1.443	0.197	4.7	149.2

CASE B: Slamming occurrence

Table 24: Slamming occurrence (Heading 180 [deg], V=11[kn]).

Sea state and loading conditions	**Relative r_3** [m]	**Absolute s_{33}** [m]	m_0 [m²]	m_2 [m²/s²]	m_4 [m²/s⁴]	P_{sl}	N_{sl} per hour
	RMS	RMS					
H_s=2m – T_p=8.85s Ballast condition	0.649	0.220	0.766	0.421	0.587	1.787	0
H_s=4m – T_p=12s Ballast condition	1.722	1.163	1.375	2.964	1.889	2.812	0
H_s=6m – T_p=16s Ballast condition	2.061	5.029	1.389	4.247	1.930	2.223	0

Table 25: Slamming occurrence (Heading 180 [deg], V=14[kn]).

Sea state and loading conditions	**Relative r_3** [m]	**Absolute s_{33}** [m]	m_0 [m²]	m_2 [m²/s²]	m_4 [m²/s⁴]	P_{sl}	N_{sl} per hour
	RMS	RMS					
H_s=2m – T_p=8.85s Ballast condition	0.632	0.199	0.813	0.399	0.661	2.460	0
H_s=4m – T_p=12s Ballast condition	1.790	1.199	1.507	3.203	2.271	3.924	0
H_s=6m – T_p=16s Ballast condition	2.165	2.312	1.530	4.687	2.341	3.112	0.001

Table 26: Slamming occurrence (Heading 150 [deg], V=11[kn]).

Sea state and loading conditions	**Relative r_3** [m]	**Absolute s_{33}** [m]	m_0 [m²]	m_2 [m²/s²]	m_4 [m²/s⁴]	P_{sl}	N_{sl} per hour
	RMS	RMS					
H_s=2m – T_p=8.85s	0.559	0.204	0.656	0.312	0.430	1.433	0

Ballast condition							
H_s=4m – T_p=12s Ballast condition	1.593	1.206	1.247	2.537	1.554	2.310	0
H_s=6m – T_p=16s Ballast condition	1.702	2.087	1.182	2.897	1.398	1.759	0

CASE C: Deck wetness – Deck submergence

Table 27: Deck submergence (Heading 180 [deg], V=11[kn]).

Sea state and loading conditions	**Relative r_3** [m]	**Absolute s_3s_3** [m]	m_0 [m^2]	m_2 [m^2/s^2]	m_4 [m^2/s^4]	P_{ds}	N_{ds} per hour
	RMS	RMS					
H_s=2m – T_p=8.85s Ballast condition	0.513	0.173	0.263	0.453	1.866	0	0
H_s=4m – T_p=12s Ballast condition	1.142	0.914	1.304	1.057	2.591	0	0
H_s=6m – T_p=16s Ballast condition	1.235	1.807	1.524	0.936	1.947	0	0
H_s=2m – T=8.85s Full load	0.541	0.136	0.293	0.457	1.518	0	0
H_s=4m – T_p=12s Full load	1.592	1.075	2.534	1.607	2.426	0.045	32.0
H_s=6m – T_p=16s Full load	1.734	2.009	3.007	1.467	1.861	0.088	57.3

Table 28: Deck submergence (Heading 180 [deg], V=14[kn]).

Sea state and loading conditions	**Relative r_3** [m]	**Absolute s_3s_3** [m]	m_0 [m^2]	m_2 [m^2/s^2]	m_4 [m^2/s^4]	P_{ds}	N_{ds} per hour
	RMS	RMS					
H_s=2m – T_p=8.85s Ballast condition	0.509	0.152	0.259	0.530	2.574	0	0
H_s=4m – T_p=12s Ballast condition	1.159	0.915	1.343	1.245	3.599	0	0
H_s=6m – T_p=16s Ballast condition	1.240	1.812	1.539	1.088	2.713	0	0
H_s=2m – T_p=8.85s Full load	1.343	1.781	1.803	0.979	1.179	0.007	4.6
H_s=4m – T_p=12s Full load	1.604	1.016	2.571	1.733	2.290	0.048	31.8
H_s=6m – T_p=16s Full load	1.887	2.104	3.562	1.768	1.853	0.152	89.2

Table 29: Deck submergence (Heading 150 [deg], V=11[kn]).

Sea state and loading conditions	**Relative r_3** [m]	**Absolute s_3s_3** [m]	m_0 [m^2]	m_2 [m^2/s^2]	m_4 [m^2/s^4]	P_{ds}	N_{ds} per hour
	RMS	RMS					
H_s=2m – T_p=8.85s	0.527	0.224	0.277	0.425	1.740	0	0

Ballast condition							
H_s=4m – T_p=12s Ballast condition	1.471	1.327	2.165	1.377	2.591	0	0
H_s=6m – T_p=16s Ballast condition	1.411	2.167	1.990	1.118	1.923	0	0
H_s=2m – T_p=8.85s Full load	0.513	0.152	0.264	0.369	0.922	0	0
H_s=4m – T_p=12s Full load	1.342	0.951	1.800	1.183	1.558	0.007	4.8
H_s=6m – T_p=16s Full load	1.343	1.781	1.803	0.979	1.179	0.007	4.6

CASE D: Bridge accelerations

The appropriate location on the ship for this criterion, which is for the bulk-carrier case (measured from midship): x=-91m, y=6m, z=34.150m (from baseline).

Table 30: RMS values of bridge accelerations (Heading 180 [deg], V=11[kn]).

Sea state and loading conditions	**Vertical acceleration** [m/s^2]		**Lateral acceleration** [m/s^2]
	RMS		
	Relative $\ddot{r}_3$	**Absolute** $\ddot{s}_3$	(due to roll motion)
H_s=2m – T_p=8.85s Ballast condition	1.340	0.163	0
H_s=4m – T_p=12s Ballast condition	1.538	0.382	0
H_s=6m – T_p=16s Ballast condition	2.304	0.572	0
H_s=2m – T_p=8.85s Full load	1.038	0.104	0
H_s=4m – T_p=12s Full load	1.213	0.388	0
H_s=6m – T_p=16s Full load	1.827	0.582	0

Table 31: RMS values of bridge accelerations (Heading 150 [deg], V=11[kn]).

Sea state and loading conditions	**Vertical acceleration** [m/s^2]		**Lateral acceleration** [m/s^2]
	RMS		
	Relative $\ddot{r}_3$	**Absolute** $\ddot{s}_3$	(due to roll motion)
H_s=2m – T_p=8.85s Ballast condition	1.243	0.159	0.284
H_s=4m – T_p=12s	2.489	0.318	0.568

Ballast condition			
H_s=6m – T_p=16s Ballast condition	1.256	0.542	0.511
H_s=2m – T_p=8.85s Full load	0.979	0.134	0.070
H_s=4m – T_p=12s Full load	1.141	0.481	0.097
H_s=6m – T_p=16s Full load	1.008	0.550	0.121

Motion Sickness Incidence (MSI)

The appropriate location on the ship for this criterion, which is for the bulk-carrier case (measured from midship): x=-91m, y=6m, z=34.150m (from baseline).

Table 32: MSI (Heading 180 [deg], V=11[kn]).

Sea state and loading conditions	**MSI**
	(for 120 minutes)
H_s=2m – T_p=8.85s Ballast condition	0.402
H_s=4m – T_p=12s Ballast condition	3.060
H_s=6m – T_p=16s Ballast condition	3.680
H_s=2m – T_p=8.85s Full load	0.080
H_s=4m – T_p=12s Full load	3.089
H_s=6m – T_p=16s Full load	7.670

Table 33: MSI (Heading 150 [deg], V=11[kn]).

Sea state and loading conditions	**MSI**
	(for 120 minutes)
H_s=2m – T_p=8.85s Ballast condition	0.371
H_s=4m – T_p=12s Ballast condition	5.767
H_s=6m – T_p=16s Ballast condition	4.665
H_s=2m – T_p=8.85s Full load	0.192
H_s=4m – T_p=12s Full load	5.053
H_s=6m – T_p=16s Full load	4.509

Appendix B – Regression analysis for safety criteria

Except from all the results shown in the previous tables, a series of scenarios have been evaluated using the MaxSurf software, considering the draught from the real voyage presented in previous section (Section 6) of this report (13.1m). Specifically, systematical runs performed using the following parameters:

Table 34: Data used for safety regression analysis.

Parameter	Range
V_s	11-14 per 1kn
a	0-180 per 20 deg
H_s	2-5 per 1m
T_p	7-14 per 1 s

Combing all the above-mentioned information, 1280 scenarios resulted and used to train regression models regarding:

- Heave RMS (Figure 69**Error! Reference source not found.**)
- Pitch RMS (Figure 69)
- r_3
- S_3
- m_0
- m_2
- m_4

  Different model for each criterion (propeller emergence, slamming, deck wetness, etc.)
- Relative velocity (for slamming criterion)
- Bridge acceleration vertical (**Error! Reference source not found.Error! Reference source not found.**)

  The exact location of the calculations has been defined previously.
- Bridge acceleration lateral (**Error! Reference source not found.Error! Reference source not found.**)
- MSI

Validation metrics for evaluating the performance of the regression models are presented in Table 35.

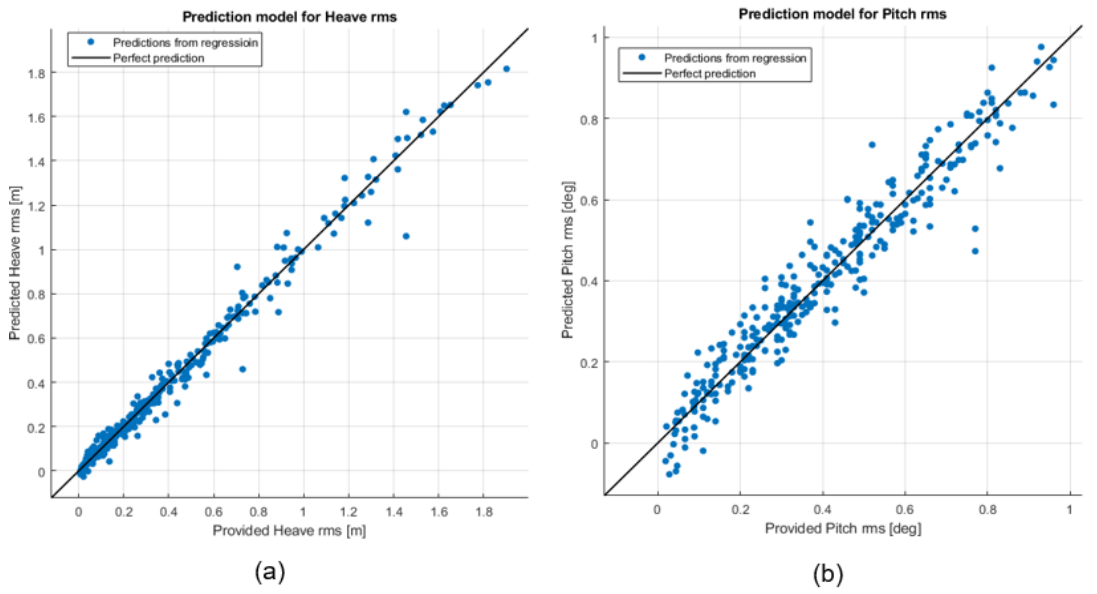

Figure 69: Regression model for Heave (a) and Pitch (b) RMS.

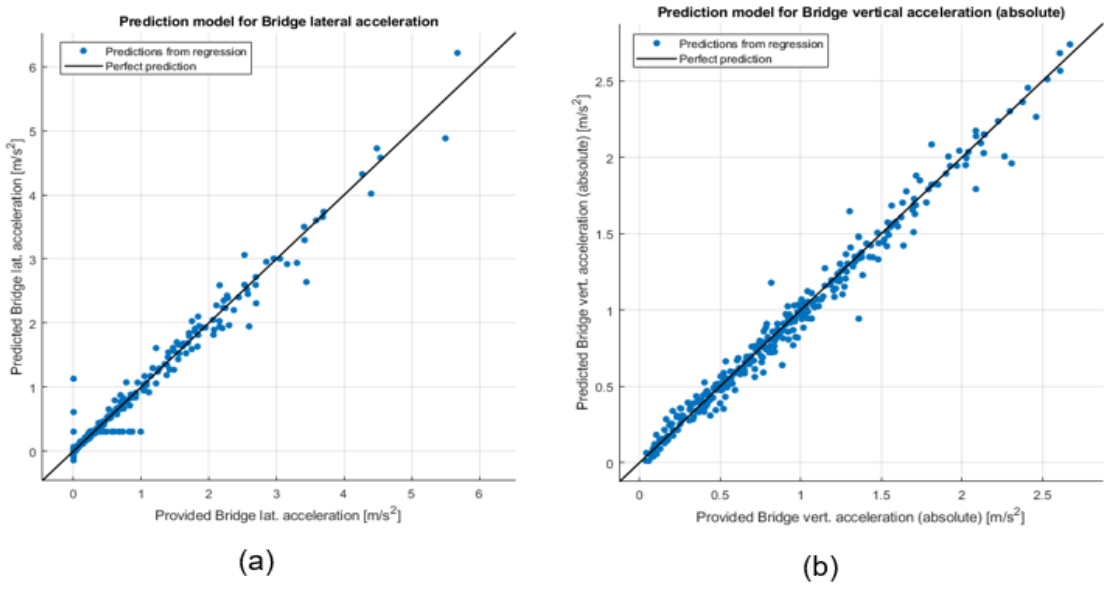

Figure 70: Regression model for Bridge lateral (a) and vertical acceleration (b).

Table 35: Neural network validation for all regression models used for safety calculations.

	RMSE	MSE	RSquared	MAE
Heave RMS	0.050	0.002	0.984	0.030
Pitch RMS	0.059	0.003	0.934	0.045
Bridge acc. Vert. abs.	0.080	0.006	0.980	0.054
Bridge acc. Lat.	0.159	0.025	0.976	0.077

Deck Wetness	r_3	0.105	0.011	0.972	0.066
	m_0	0.597	0.357	0.931	0.256
	m_2	0.143	0.020	0.968	0.083
	m_4	0.195	0.038	0.990	0.811

Appendix C – Regression analysis for added wave resistance

A regression model to estimate the added wave resistance has been developed, using a dataset derived by applying the semi-empirical method found in [10] using the data shown on Table 36**Error! Reference source not found.**. These scenarios correspond to different combinations among significant wave heights, peak periods, relative wave headings and ship speeds.

Table 36: Data for added resistance regression analysis.

Parameter	Range value
H_s	1-5 m per 1m
T_p	2-16 s per 1s
a	0-180 deg per 20deg
V_s	11-15 kn per 0.5kn

The regression model was created in MATLAB using the regression learner application (**Error! Reference source not found.**Figure 71). More specifically, a fine tree regression model has been selected resulting in an R^2 validation of 0.98673.

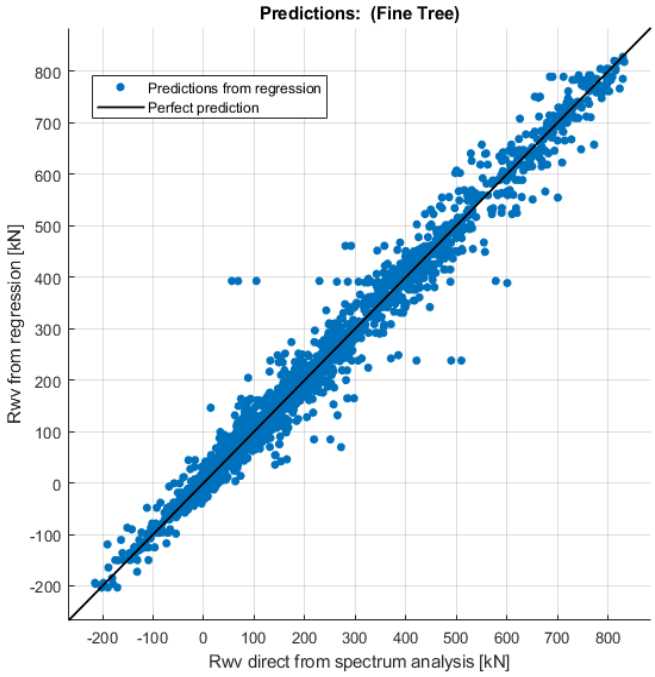

Figure 71: Regression model for added wave resistance at mean draft=13.1m.

The training range for the SWHs and the peak periods values (Table 36) were selected based on an analysis of the wave data of the real voyage of MV KASTOR that examined in Section 6, along with the sea state in the surrounding area during the same period. The ship's mean draft for this regression analysis is selected at 13.1m (same as noon reports). This means that for other mean draft values, new models need to be trained accordingly. It should be also noted that some combinations of SWHs and peak periods have a low probability of occurrence, although they have been included for the convenience of the regression model. As far as the ship speed values are concerned, they have been selected according to the available noon reports data. In total, 6300

different scenarios have been considered to develop the regression model for the added wave resistance.

In **Error! Reference source not found.**Figure 72 a comparison between results from the regression model and the respective ones calculated directly from the spectrum analysis for the assumed range of SWH is presented. Differentiations are identified at higher values of added wave resistance, where consequently the significant wave height values are also higher.

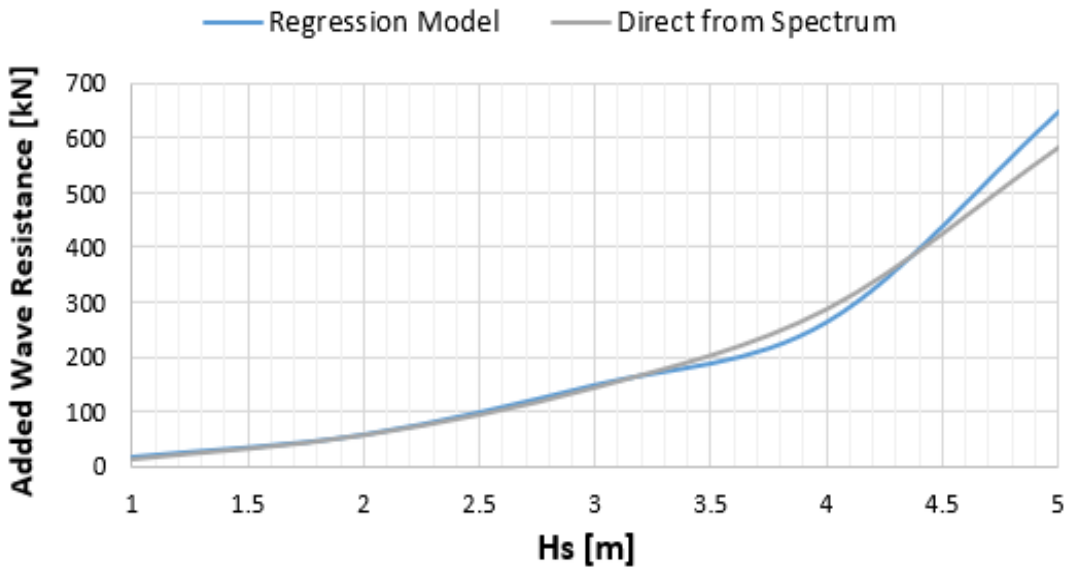

Figure 72: Comparison between regression and direct from spectrum data.

Appendix D – Hydrodynamic transverse force and yaw moment

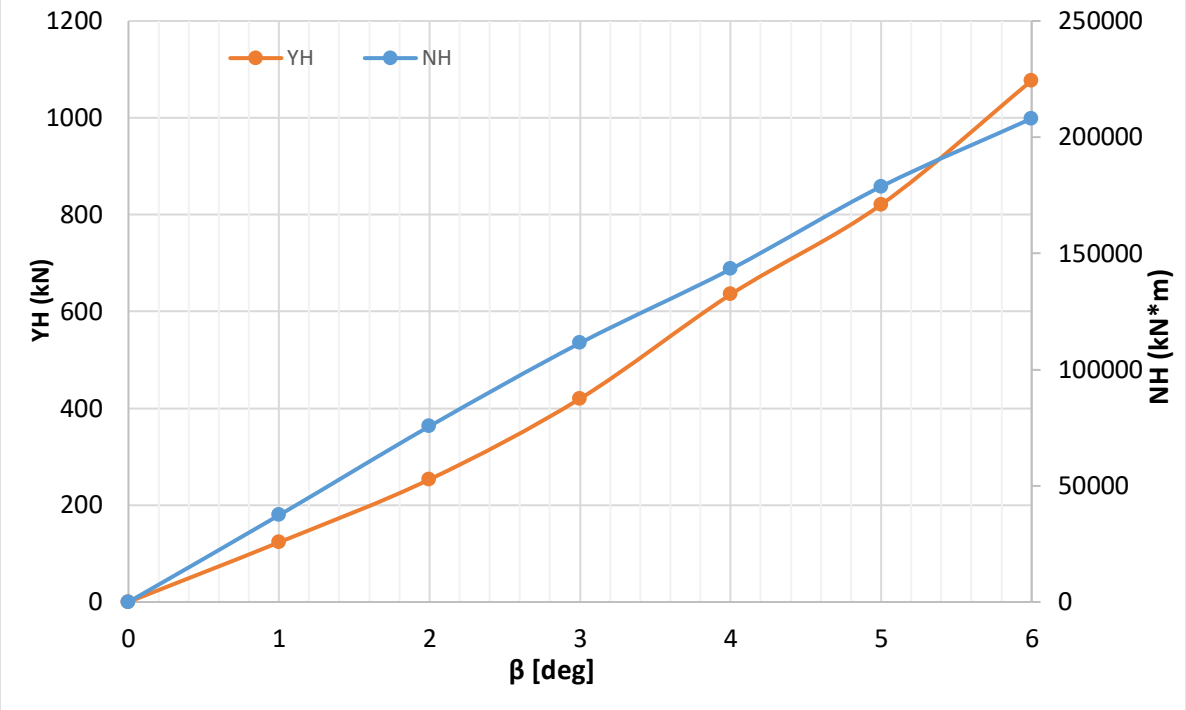

Figure 73: Transverse force and yaw moment based on CFD results carried out in D2.2.